Dalton Transactions

ROYAL SOCIETY OF CHEMISTRY

PERSPECTIVE

View Article Online
View Journal | View Issue

Cite this: *Dalton Trans.*, 2025, **54**, 10504

Reactive main group metal complexes of the neutral *NNNN* macrocycle, Me_4TACD

Priyabrata Ghana, [a] Louis J. Morris [b] and Jun Okuda *[c]

Received 24th April 2025,
Accepted 28th May 2025

DOI: 10.1039/d4dt03357d

rsc.li/dalton

Currently, there is considerable interest in introducing molecularly defined main group metal compounds as precursors and model complexes of homogeneous catalysts for various bond cleavage and forming transformations. With a focus on the *NNNN* macrocyclic ligand Me_4TACD (*N*,*N*′,*N*″,*N*‴-tetramethyl-1,4,7,10-tetraazacyclododecane), this review summarizes the versatility of the ligand Me_4TACD for the stabilization of reactive main group s- and p-block (group 1, 2, 12–14) metals. Metal hydrides, hydrocarbyls and silyls are often monomeric and catalyze alkene hydrofunctionalisations. In contrast to the rich coordination chemistry of d- and f-block transition metals using a plethora of ligands, main group metals still leave room for new structures and reactivities, aligning with the current efforts to develop a systematic understanding in s- and p-block metal–ligand combinations.

1. Introduction

Commonly, reactive main group metal fragments are stabilized by anionic ligands of the general type $[L_lX_x]$ (L = two-electron ligand, l = 0–4; X = one-electron ligand, x = 1–4), which exhibit sterically bulky substituents.[1–10] N-Heterocyclic carbene derivatives are often employed in this regard as neutral L-type ligands.[11–15] Neutral multidentate N- and O-donor ligands of the general type L_n can provide access to soluble and reactive molecular s-block complexes.[16–20] Macrocyclic N-donor ligands have seen less widespread use in the main group chemistry.

The macrocyclic tetraamine ligand, Me_4TACD (*N*,*N*′,*N*″,*N*‴-tetramethyl-1,4,7,10-tetraazacyclododecane, also called 12-TMC or Me_4cyclen) has been used in the coordination chemistry of 3d metals as a redox innocent supporting ligand. It was first developed in 1982 to study the effect of *N*-methylation of cyclic polyamines on the coordination number of late transition metals such as Ni and Cu and extensively to study reactive (di)oxygen species during O_2 activation at Cr, Mn, Fe, Co, Ni, and Cu centers.[21,22] This review summarizes the use of Me_4TACD as a versatile supporting ligand for the study of main group metal centers featuring reactive ligands such as hydride and organyls, mostly as cations. Such species are often of low-nuclearity, often monomeric and allow to study the inherent property of main group metal–ligand interaction. Since some group 1 and 2 metals are abundant, inexpensive and non-toxic, reactions and catalysis based on molecularly defined complexes could eventually substitute some reactivity patterns so far dominated by transition metals.

2. Synthesis and properties of Me_4TACD

The commonly used method for preparing the Me_4TACD ligand consists of three steps. First, the Richman–Atkins cyclization assembles the macrocycle by reacting *N*,*N*′,*N*″-tris(*p*-tolysulfonyl) diethylenetriamine-*N*,*N*″-disodium salt (**A**) with tosylbis[2-(tosyloxy)ethyl]amine (**B**) (Scheme 1).[23,24] This cyclization can also be done using diethylamine **B** with mesyloxy or halides (Cl–I) as the leaving group.[24] The highest yield of ~80% was obtained when the tosyloxy (OTs) group was used as a leaving group.[24] This cyclization works best when carried out in *N*,*N*-dimethylformamide. The second step is the detosylation of tetra(tosyl)cyclen using concentrated sulphuric acid. Finally, the *N*-methylation (Eschweiler–Clarke reaction) of the parent macrocycle H_4TACD employing a mixture of formic acid and formaldehyde provides Me_4TACD in 45–55% yield.[21,25] The main drawback of this route is its low atom economy, as it requires both tosylation and detosylation steps. Additionally, the cyclization step requires a large quantity of dry DMF. A more efficient alternative produces the parent cyclen in two steps with an overall yield up to 57% (route 2).[26] The first step of this route involves the *S*-alkylation of dithiooxamide using excess bromoethane and subsequent reaction of the resulting bis-thioimido ester salt with triethylenetetraamine to afford the tricyclic bis-amidine (Scheme 1). The reduction of the bis-amidine with DIBALH in refluxing toluene, followed by treatment with NaF in water, resulted in the parent

[a]*Department of Chemistry, Indian Institute of Technology, Gandhinagar, Gujarat-382355, India*
[b]*Department of Chemistry, University of Bath, Bath, BA2 7AY, UK*
[c]*Institute of Inorganic Chemistry, RWTH Aachen University, Landoltweg 1, 52056 Aachen, Germany. E-mail: jun.okuda@ac.rwth-aachen.de*

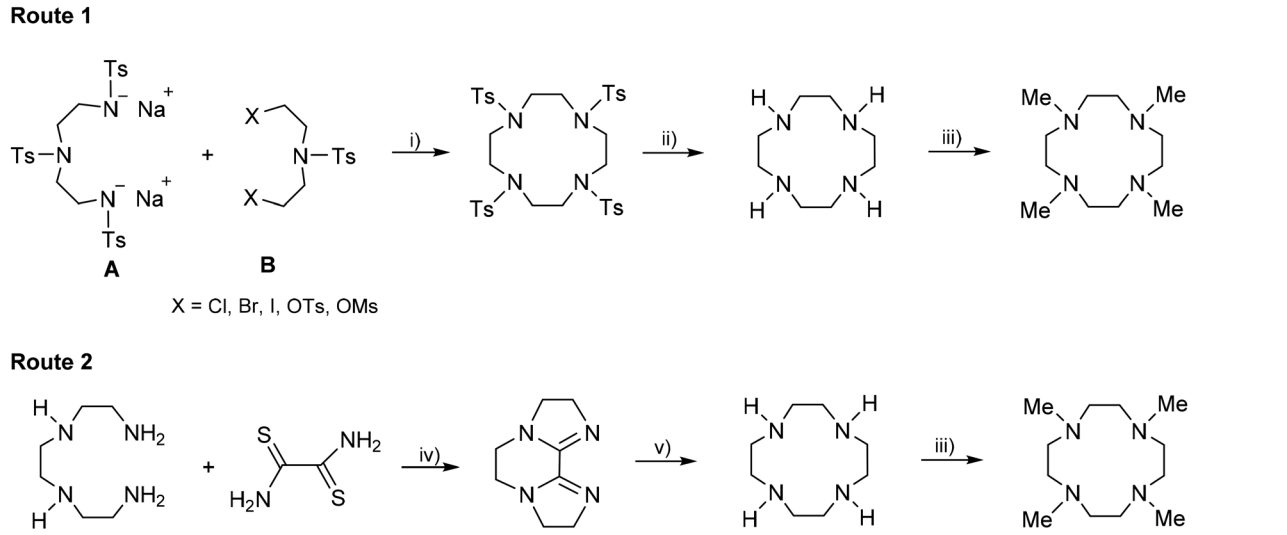

Scheme 1 Synthetic methods of the ligand Me_4TACD. (i) DMF, 100 °C. (ii) H_2SO_4 (conc.), NaOH. (iii) HCO_2H/CH_2O, 100 °C, NaOH. (iv) DIBAL-H, refluxing toluene. (v) NaF, H_2O.

cyclen. Finally, *N*-methylation of cyclen using the Eschweiler–Clarke reaction provides Me_4TACD.[21,25,26]

As a ligand, Me_4TACD generally binds to a metal fragment MLX in a κ^4-fashion and adopts a C_4-symmetric, boat-like conformation (Fig. 1a). The four nitrogen atoms of the ligand form a square planar core with the coordinated metal residing above the plane and all four NMe groups pointing towards the metal. In the solid state, the four CH_2CH_2 groups adopt a staggered conformation to avoid steric congestion, giving rise to two enantiomers (δδδδ, λλλλ) for an achiral metal center. The CH_2 protons of the ligand are magnetically inequivalent, leading to AA′XX′-type signal sets for CH_2CH_2 groups in the ^{1}H NMR spectrum. Depending on the size of the coordinated metal ion, lability of N–M bonds, and remaining coordination sphere, the AA′XX′-spin system can appear resolved, unresolved AB spin system, or collapsed broad singlet on the NMR timescale. AB-multiplets indicate rapid ring flipping between the two enantiomers but persistent macrocycle coordination with two disparate faces, whilst complete collapse can indicate fluxional ligand coordination. In two examples shown below,[27,28] the Me_4TACD ligand has been observed to adopt a folded conformation where one of the four methyl groups is orientated away from the metal centre (Fig. 1b). This highly strained conformation appears to relieve steric congestion for small metal cations with two strongly-bound ancillary X-type ligands (Al–H, Mg–O); weakly bound X-type ligands (*e.g.* Zn–I) are readily displaced by the chelating macrocycle to give auto-ionised products of the type $[(\kappa^4\text{-}Me_4TACD)MX]^+X^-$. The folded conformation in solution is diagnosed with ^{1}H NMR spectroscopy by the presence of three methyl environments in a 1 : 2 : 1 integral ratio and 8-sets of magnetically inequivalent CH_2 protons in the ^{1}H NMR spectrum.[28]

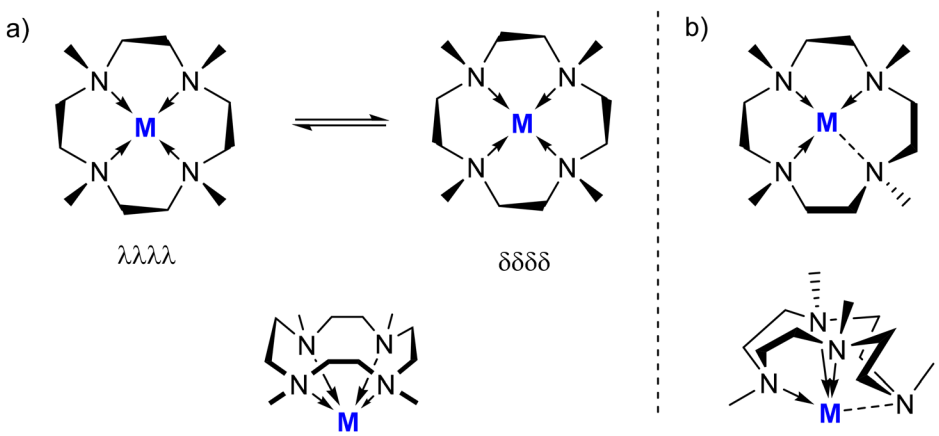

Fig. 1 Coordination behaviour of Me_4TACD ligand: (a) κ^4*NNNN*-bonding with boat-like conformation; (b) κ^3*NNN*-bonding with folded conformation.

3. Group 1 metals

Alkali metal compounds typically exist as saline or aggregated species, but neutral polydentate ligands help to stabilize well-defined low-nuclearity molecular species. Polyamines offer advantages over crown-ethers due to stronger N → M bonds and being less prone to nucleophilic attacks. Indeed, large aza-crowns have been used to stabilise highly reducing sodide compounds.[29] A renewed interest in organoalkali compounds as useful reagents in synthetic organic chemistry[17,20,30] has highlighted the impact of different chelating donor ligands on reactivity and chemoselectivity.[18,19,31] While the use of Me_4TACD remains limited to the examples described herein, the steric and coordinative demand and strong chelate effect (especially for lithium and sodium) make it a promising candidate for the future development of organoalkali metal chemistry.

Trends in alkali metal coordination chemistry of Me_4TACD complexes depend on the ionic radius and strength of M–N bonds. While lithium forms strong, monomeric complexes with 12-membered aza-crown with appreciable covalency in Li–N bonds, the heavier alkali metals exhibit more labile bonding, leading to dimeric or polymeric structures. Me_4TACD has been employed to provide well-defined molecular hydridotriphenylborates, which were employed as catalysts in the hydroboration of unsaturated organic substrates. Low-nuclearity triphenyl- and trihydridosilanide complexes have also been structurally characterised.

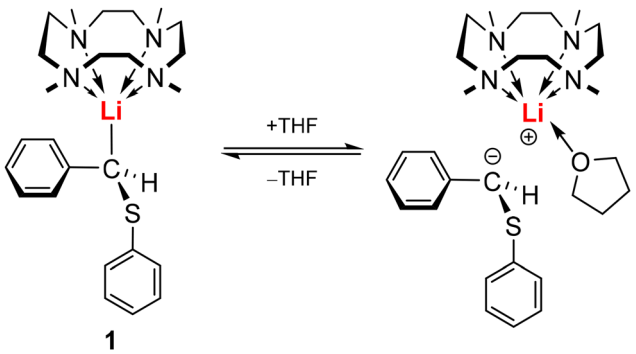

Scheme 2 Equilibrium between the contact ion pair and the solvent-separated ion pair of **1** in THF.

3.1. Charge-separated lithium and sodium complexes

The first lithium complex of Me_4TACD ligand, $[(Me_4TACD)^6Li][CH(C_6H_5)(S\text{-}C_6H_5)]$ (**1**), which was obtained upon treatment of [^{6}Li]-α-(phenylthio)benzyllithium with one equiv. of Me_4TACD in THF/THF-d_8, was prepared to study its structure in solution by NMR spectroscopy.[32] Based on ^{6}Li-HOESY, ^{1}H, and ^{13}C NMR spectroscopy, the study revealed an equilibrium between contact ion pairs and solvent-separated ion pairs at ambient temperature and with an increased proportion of solvent-separated ion pairs at lower temperatures (Scheme 2).

Me_4TACD ligated lithium and sodium complexes $[(Me_4TACD)M(L)][BAr_4]$ (M = Li (**2**), Na (**3**); L = H_2O, THF; Ar = C_6H_3-3,5-$(CF_3)_2$) were prepared from their respective borate salts $[Li(H_2O)_4][BAr_4]$ and $[Na(THF)_2][BAr_4]$ (Scheme 3).[33,34] Attempts to isolate the heavier homologues resulted in $[(Me_4TACD)H][BAr_4]$, likely due to hydrolysis from traces of water present in the solvent. Unlike the sandwich structure of [12]-crown-4 complexes of group 1 metals, these complexes exhibit half-sandwich structures with five-coordinate alkali metal cations of square pyramidal geometry (Scheme 3). The Me_4TACD ligand adopts a distorted boat-like conformation, positioning all four nitrogen atoms in a square planar arrangement. The metal cations are located below this N_4 plane, with all NMe groups oriented toward the metal centre. In solution, the Me_4TACD ligand binds the alkali metals more strongly than the corresponding crown ethers, as evidenced by a significant downfield shift of the ^{23}Na NMR signal ($\delta(^{23}Na)$ +12.7 ppm (**3**) *vs.* ~0 ppm for $[Na([12]\text{-crown-}4)_2]^+$).[33] In fact, the coordination of alkali metals to the aza-macrocycle is not just an electrostatic interaction but also involves a significant donation of electron density from the nitrogen's 2p-nonbonding orbitals to the alkali metal center.[34]

3.2. Alkali metal hydridotriphenylborates

Me_4TACD-supported alkali metal hydridotriphenylborates $[(Me_4TACD)M][HBPh_3]$ (M = Li (**4**), Na (**5**), K (**6**)) were syn-

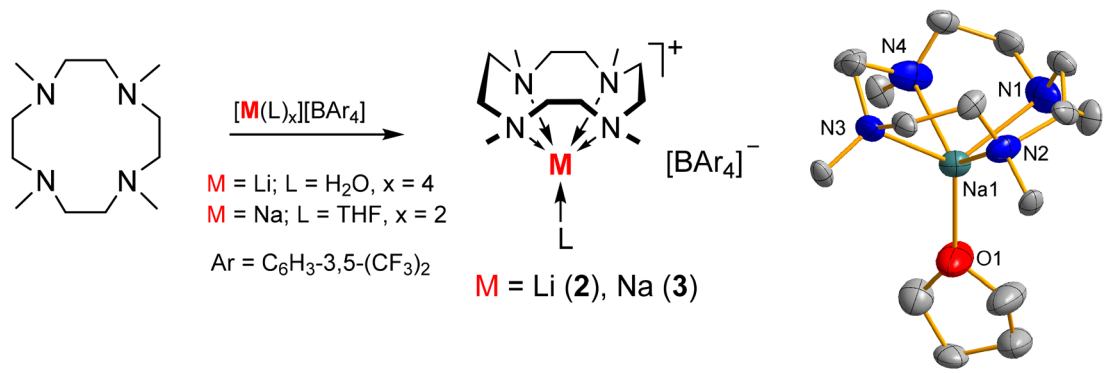

Scheme 3 Synthesis of the Li and Na borate complexes of Me_4TACD; molecular structure of the cationic part of **3**.

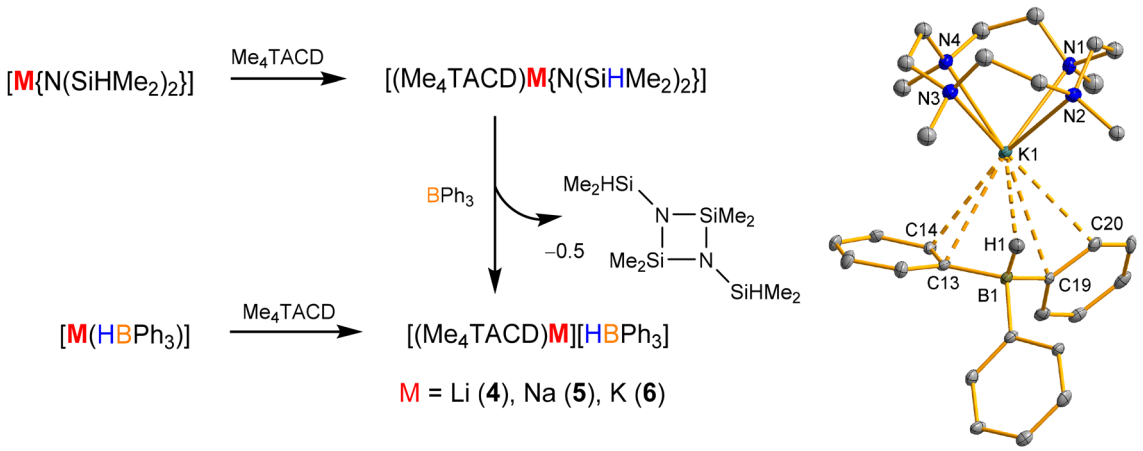

Scheme 4 Synthesis of Me_4TACD ligated alkali metal hydridotriphenylborates and the molecular structure of **6**.

thesized *via* two pathways.[35] One approach involves a two-step, one-pot reaction where Me_4TACD reacts with tetramethyldisilazides $[M\{N(SiHMe_2)_2\}]$ (M = Li, Na, K) in THF, followed by BPh_3 to obtain compounds **4–6** after elimination of $(Me_2HSiN–SiMe_2)_2$ (Scheme 4). The other method involves mixing Me_4TACD with the alkali metal hydridotriphenylborates $[M(HBPh_3)]$ in THF (Scheme 4, left). The structural analysis of **4–6** revealed distinct bonding geometries: while the lithium complex **4** forms a separated ion pair with a THF molecule at the lithium, the sodium (**5**) and the potassium (**6**) homologues exist as contact ion pairs due to the non-covalent $M^+\cdots C_\pi$ (M = Na, K) interactions along with a 3-centered-2-electron M···H–B bonding interaction (Scheme 4). The five-coordinate lithium cation in compound **4** adopts a distorted square-pyramidal geometry. For compounds **5** and **6**, the sodium and the potassium cations are formally eight and nine coordinated and exist in a distorted square anti-prismatic and monocapped square anti-prismatic geometry, respectively. Compounds **4–6** serve as chemoselective catalysts for carbonyls and CO_2 hydroboration, with the lithium complex exhibiting the highest activity.[35] While the hydridoborate provides the hydride in catalysis, the alkali metals and supporting ligand play an important role in activating the substrate by its Lewis-acidic properties. Lower denticity acyclic polyamines *N*,*N*,*N*′,*N*′-tetramethylethylenediamine (TMEDA) and *N*,*N*,*N*′,*N*″,*N*″-pentamethyldiethylenetriamine (PMDTA) provide higher activity than Me_4TACD derivatives due to easier access to the metal centre. The tetradentate, yet hemilabile ligand *N*,*N*,*N*′,*N*′,*N*″,*N*″-hexamethyltriethylenetetraamine (Me_6TREN) provided further improved activity.[36]

3.3. Alkali metal silanides

Given the current interest in hydrogen storage materials, the alkali metal silanides $[MSiH_3]_\infty$ (M = Li–Cs) have been widely studied recently.[37–40] Normally, alkali metal silanides are thermodynamically unstable and exist as polymeric clusters. Employing the Me_4TACD ligand, a series of molecular alkali metal silanides $[(Me_4TACD)M(SiH_3)]_n$ (M = Li (**12**), Na (**13**), K (**14**) and Rb (**15**); n = 1–2) were isolated, and exist as monomer or dimer in the solid-state.[41] Compounds **12–15** were prepared from triphenylsilanides $[(Me_4TACD)M(SiPh_3)]_n$ (M = Li (**7**), Na (**8**), K (**9a**), Rb (**10**); n = 1 (Li–K), 2 (Rb)) and H_2 or $PhSiH_3$ (Scheme 5). Hydrogenolysis or hydrosilylation is chemoselective for the Si–C bonds to eliminate benzene or diphenylsilane, rather than heterolyzing the M–Si bond to provide the corresponding alkali metal hydride and hydrosilane. While the hydrogenolysis of **7–10** with H_2 takes several days to complete, the reaction with $PhSiH_3$ finishes within 5 min and proceeds with redistribution of the organosilane to give Ph_2SiH_2 and SiH_4. The triphenylsilanides **7–10**, along with the caesium analogue $[(Me_4TACD)Cs(SiPh_3)]_\infty$ (**11**), were synthesized from the reaction of Me_4TACD, $Ph_3SiSiMe_3$, and $LiCH_2SiMe_3$ or MO^tBu (M = Na–Cs). Alternatively, compounds **7** and **9–10** were prepared through the ligand exchange reaction from isolated THF adducts $[M(SiPh_3)(thf)_n]$ with Me_4TACD. Lithium (**7**) and sodium (**8**) triphenylsilanides exist as monomers with a direct M–Si σ-bond. The potassium complex was crystallised as a monomeric THF-adduct, $[(Me_4TACD)K(SiPh_3)(thf)]$ (**9b**), which contains a K–Si σ-bond, but rapidly loses THF under vacuum to provide **9a**, where the silanide is alternatively bound to potassium *via* an η^6–π-facial interaction.[41,42] The stability of the triphenylsilanides decreases down the group (Li: $t_{1/2}$ = 14 d; Cs: $t_{1/2} \approx$ 12 h). In contrast, the trihydridosilanide **12–15** shows a reverse trend; the Na, K, and Rb homologues are stable for weeks both in solution and solid state, but the Li homologue decomposes in two days. While the light alkali metal analogues **7–9** exist as a monomer in the solid state, the heavier analogues show a more extended coordination sphere (**10**: dimer with bridging $[SiPh_3]^-$; **11**: one-dimensional chain-like structure through $Cs–C_{Ph}$ interactions). Similarly, trihydridosilanide **13** exists in monomeric form with square pyramidal coordination geometry around the sodium atom. The potassium (**14**) and rubidium (**15**) homologues form dimers in the solid state, with SiH_3 anions bridging the two $[(Me_4TACD)M]$ fragments.

The complete series of alkali metal triphenylsilanide derivatives enabled comparative NMR spectroscopic analysis of the

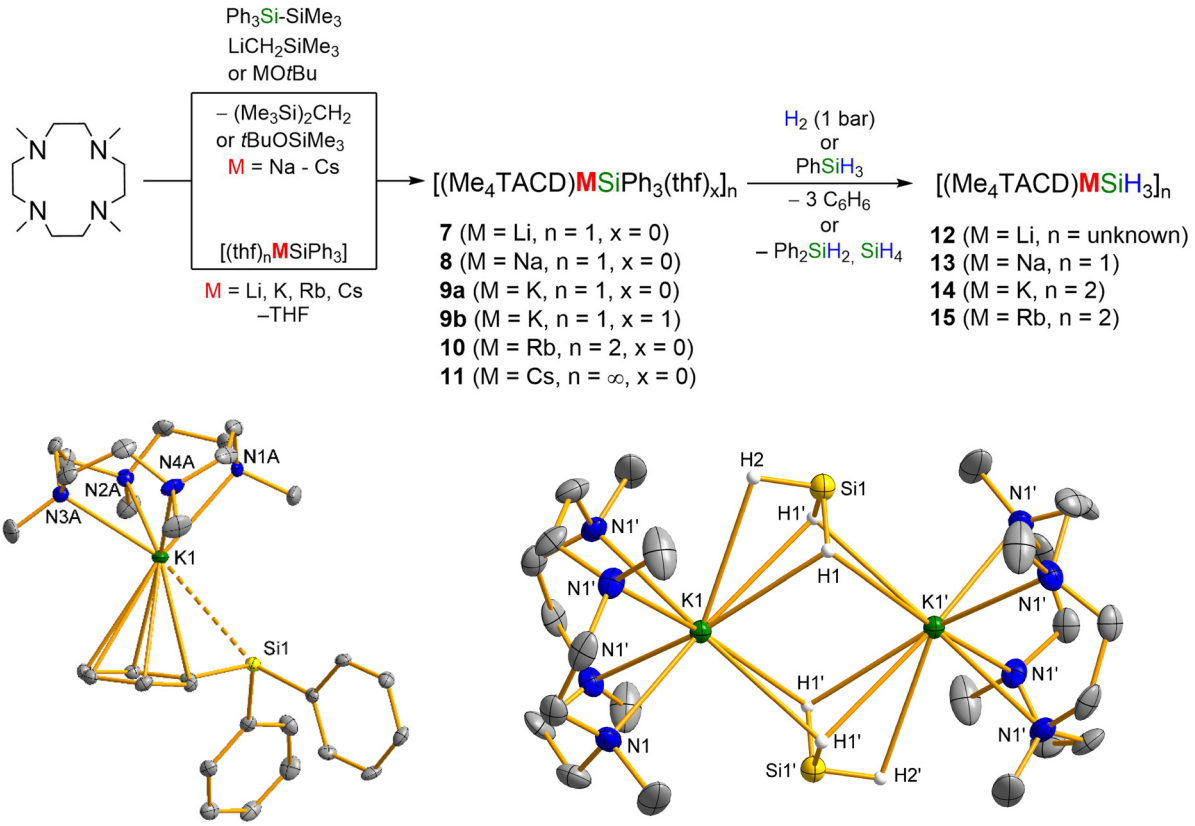

Scheme 5 Synthesis of Me_4TACD stabilized alkali metal silanides (top) and molecular structure of potassium silanide complexes **9a** and **14**.

binding of the Me_4TACD ligand to metal cations with increasing ionic radius. The lithium (**7**) and sodium (**8**) complexes show two multiplets for the methylene protons in their ^1H NMR spectrum (THF-d_8, 25 °C), consistent with time-averaged C_{4v}-symmetry and persistent ligand coordination. In contrast, compounds **9–11** show a broad signal for the methylene environment, which is also notably sharper for Cs (**11**) than for K (**10**), indicating increasingly faster ligand dynamics for the larger metal cations. The similarity of the methylene chemical shift (δ 2.4 ppm) to that of the free ligand suggests partial ligand dissociation.

3.4. Molecular alkali metal organoperoxides

Alkali metal organoperoxides [MOOR] (M = Li, Na, K; R = hydrocarbyl), which form as unstable intermediates in the oxidation of organometallics by O_2, exist in oligomeric forms. The Me_4TACD ligand is suitable for stabilizing such highly reactive peroxide intermediates. The addition of Me_4TACD to an *n*-pentane solution of LiN^iPr_2 and ROOH (R = ^{t}Bu, CMe_2Ph) at ambient temperature and subsequent cooling gave the molecular organoperoxides [$(Me_4TACD)Li(OOR)(ROOH)$] [R = ^{t}Bu (**16**), CMe_2Ph (**17**)] (Fig. 2, left).[43] The same reactions without the Me_4TACD ligand gave the dodecameric clusters $[LiOOR]_{12}$. When Me_4TACD was treated with $[MN(SiMe_3)_2]$ (M = Na, K) and ^{t}BuOOH in a 1 : 1 : 5 ratio in *n*-pentane, corresponding molecular organoperoxides [$(Me_4TACD)M(OO^tBu)(^tBuOOH)_3$] (M = Na (**18**), K (**19**); Fig. 2, right) were obtained in good yields. In all the syntheses, an excess of organoperoxides was necessary to maintain the homogeneity of the reaction mixtures. Single-crystal X-ray diffraction studies confirmed the mononuclear nature of compounds **17**, **18**, and **19**, with lithium in a hexa-coordinate environment, while sodium and potassium adopt an eight-coordinate, distorted square-antiprismatic geometry. The O–H···O hydrogen bonding between the metal-coordinated organoperoxides and neutral peroxides plays an important role in the stability of the complexes.

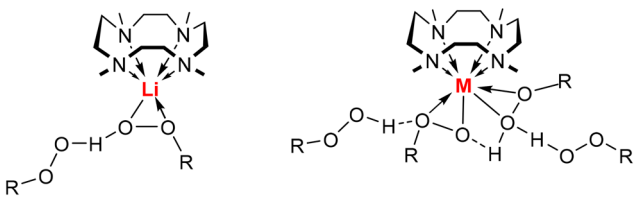

Fig. 2 Light alkali metal organoperoxides stabilized by Me_4TACD.

4. Group 2 metals

The Me_4TACD ligand was utilized to stabilize molecular hydrides of group 2 metals, suppressing aggregation into saline MH_2.

Hydride complexes were synthesised *via* hydrogenolysis or hydrosilanolysis of organo- and silanido-alkaline earth precursors. Structural trends reflect decreasing electronegativity and increasing ionic radius and polarizability, with increasing atomic number. While discrete dimeric (di)cations $[(Me_4TACD)M_2H_n]^{(4-n)+}$ (n = 2, 3) were structurally characterised for M = Mg, Ca, Ba, only a trimeric $[(Me_4TACD)_3Sr_3H_4(thf)]^{2+}$ cluster was isolated for the Sr^{2+} ion. $[(Me_4TACD)Mg_2H_2]^{2+}$ exhibits hydridic reactivity towards Lewis-acidic and polar unsaturated small molecules. The larger calcium congener can access a coordinatively unsaturated state; combined with highly nucleophilic hydride ligands, this enables H/D exchange under D_2 and catalytic hydrogenation/hydrosilylation of unactivated *n*-alkenes. The extreme nucleophilicity of Sr–H bonds led to the isolation of a rare hexahydridosilicate complex. Calcium and strontium hydrides are highly labile and undergo dynamic hydride-exchange equilibria. Neutral and cationic allyl, benzyl, and silyl derivatives of calcium, strontium, and barium have also been described as molecular Me_4TACD complexes. The Me_4TACD ligand has also used to stabilize related dinuclear polyhydride complexes of lanthanides, including yttrium, ytterbium and lutetium, highlighting its broad application in molecular hydride chemistry.[44–46]

4.1. Magnesium

4.1.1. Synthesis of molecular magnesium hydride complexes. The neutral magnesium hydride $[(Me_4TACD)Mg(\mu\text{-}H)_2Mg\{N(SiMe_3)_2\}_2]$ (**20**) was synthesized in 82% yield by reacting a mixture of $[Mg\{N(SiMe_3)_2\}_2(thf)_2]$ and Me_4TACD with $PhSiH_3$ in aromatic solvents (Scheme 6).[47] Alternatively, compound **20** was also obtained directly by reacting magnesium dihydride $[MgH_2(thf)_{0.23}]$ with $[Mg\{N(SiMe_3)_2\}_2(thf)_2]$ and Me_4TACD, but in lower yield (54%). The dinuclear structure of **20** observed in the solid state can be viewed as a monomeric $[(Me_4TACD)MgH_2]$ stabilized by magnesium bis(amide) $[Mg\{N(SiMe_3)_2\}_2]$. The ^1H NMR spectrum in THF-d_8 showed a characteristic MgH resonance at δ 3.61 ppm. Partial protonolysis of **20** with $[NEt_3H][B(C_6H_3\text{-}3,5\text{-}Me_2)_4]$ afforded the cationic magnesium hydride $[(Me_4TACD)Mg(\mu\text{-}H)]_2[B(C_6H_3\text{-}3,5\text{-}Me_2)_4]_2$ (**21**) in 43% yield after elimination of H_2, NEt_3, and $[Mg\{N(SiMe_3)_2\}_2]$ (Scheme 6). The deuterium analogue of $[(Me_4TACD)_2Mg_2(\mu\text{-}D)_2][B(C_6H_3\text{-}3,5\text{-}Me_2)_4]_2$ (**21-d$_2$**) was synthesized using $PhSiD_3$ or in an exchange reaction of **21** with D_2 over 54 h. In the D_{2h}-symmetric structure of **21**, two macrocyclic ligands bind the $[Mg_2(\mu\text{-}H)_2]^{2+}$ core in a κ^4-coordination mode and in a staggered conformation, which differs from the eclipsed conformation observed in its calcium analogue **42a**.

4.1.2. Reactivity of molecular magnesium hydride complexes. Hydridic nature of the Mg–H functionality in **21** was exploited in the reaction with the weak Brønsted acids $[NEt_3H]Cl$ and PhC≡CH, affording the monomeric magnesium complexes $[(Me_4TACD)MgX][B(C_6H_3\text{-}3,5\text{-}Me_2)_4]$ (X = Cl (**22**), C≡CPh (**23**)) (Scheme 7).[48] Lewis acids, such as BH_3(thf), HBpin and DIBAL(H) gave the hydride-bridged mononuclear adducts $[(Me_4TACD)Mg(\mu\text{-}H)_3BH][B(C_6H_3\text{-}3,5\text{-}Me_2)_4]$ (**24**), $[(Me_4TACD)Mg(\mu\text{-}H)BHpin][B(C_6H_3\text{-}3,5\text{-}Me_2)_4]$ (**25**) and $[(Me_4TACD)Mg(\mu\text{-}H)_2Al^iBu_2][B(C_6H_3\text{-}3,5\text{-}Me_2)_4]$ (**26**), respectively (Scheme 7).[47] While insertion of CO_2 into the Mg–H bond gave the dimeric formate complex $[(Me_4TACD)_2Mg_2(\mu\text{-}O_2CH)_2][B(C_6H_3\text{-}3,5\text{-}Me_2)_4]_2$ (**27**), the reactions with PhN=C=O and (Dipp)N=C=N(Dipp) (Dipp = 2,6-^{i}Pr$_2$-C$_6$H$_3$) afforded the monomeric compounds $[(Me_4TACD)Mg(OCHNPh)][B(C_6H_3\text{-}3,5\text{-}Me_2)_4]$ (**28**) and $[(Me_4TACD)Mg\{(DippN)_2\text{-}CH\}_2][B(C_6H_3\text{-}3,5\text{-}Me_2)_4]$ (**29**), respectively (Scheme 7).[48] Similarly, benzaldehyde and benzophenone both insert into the Mg–H bond to afford the monomeric alkoxides $[(Me_4TACD)Mg(OCH(R)Ph)][B(C_6H_3\text{-}3,5\text{-}Me_2)_4]$ (R = Me (**30**); Ph (**31**)).[47] Magnesium hydride **21** also reduces pyridine to give the 1,2-dihydridopyridyl (DHP) complex $[(Me_4TACD)Mg(1,2\text{-}DHP)][B(C_6H_3\text{-}3,5\text{-}Me_2)_4]$ (**32a**; Fig. 3),

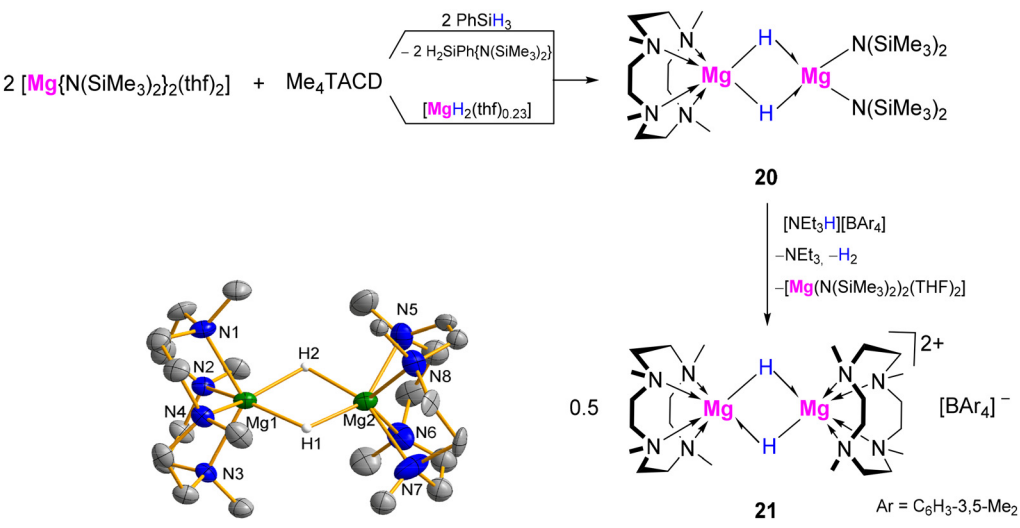

Scheme 6 Me_4TACD-supported magnesium hydrides **20** and **21** and the molecular structure of the dicationic part of **21**. Ar = C_6H_3-3,5-Me_2.

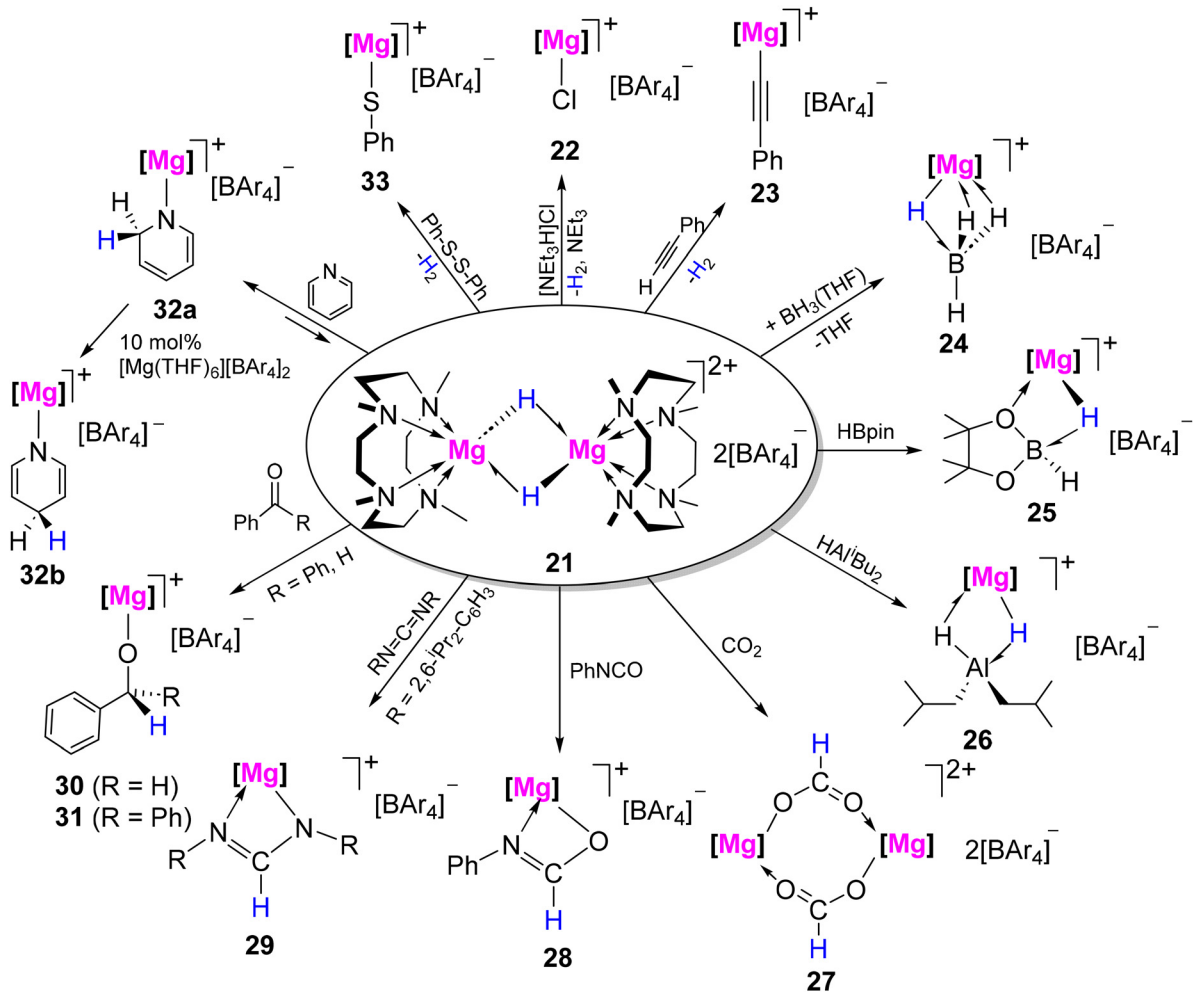

Scheme 7 Reactivity of magnesium hydride **21**; [**Mg**] = $[(Me_4TCD)Mg]^{2+}$; Ar = C_6H_3-3,5-Me_2.

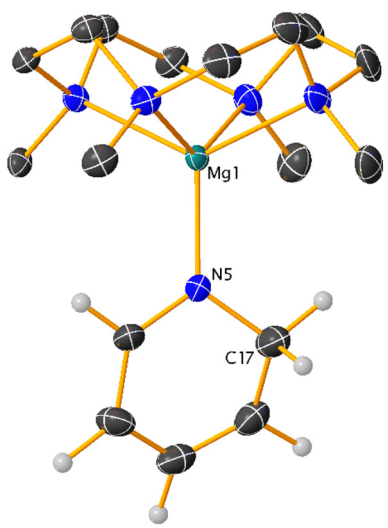

Fig. 3 Molecular structure of the cationic part of 1,2-dihydropyridyl complex **32a**.[47]

which isomerises to the 1,4-dihyridopyridyl isomer $[(Me_4TACD)Mg(1,4\text{-}DHP)][B(C_6H_3\text{-}3,5\text{-}Me_2)_4]$ (**32b**) in the presence of catalytic amount of $[Mg(thf)_6][B(C_6H_3\text{-}3,5\text{-}Me_2)_4]_2$.[47]

Dihydridopyridyl complexes **32a** and **32b** undergo slow exchange with pyridine-d_5 at 70 °C to give fully deuterated species **32a**-d_6 and **32b**-d_6 *via* partially deuterated species **32a**-d_5 and **32b**-d_5. Due to the reversibility of the 1,2-insertion, gradual generation of the deuteride **21**-*d* accounts for the fully deuterated species. Compounds **32a** and **32b** catalysed the hydroboration of pyridine using pinacolborane, providing a mixture of regioisomers.[47] Compound **21** reacts with diphenyl disulfide to give the thiophenolate complex $[(Me_4TACD)Mg(SPh)][B(C_6H_3\text{-}3,5\text{-}Me_2)_4]$ (**33**) after H_2 elimination.[48]

The dimeric formate complex **27** crystallized as a co-crystalline mixture of two conformers. The minor conformer displayed a rare folded conformation of the Me_4TACD ligands (Fig. 1b), with one of the NMe groups pointing away from the metal.[48] However, according to NMR spectroscopy, the ligand in solution adopts its usual C_4-symmetric, boat-like conformation.

4.2. Calcium

4.2.1. Organo- and silanido-calcium complexes. Neutral dibenzyl- and bis(triphenylsilyl)calcium complexes [(Me$_4$TACD)Ca(CH$_2$Ph)$_2$] (**34**) and [(Me$_4$TACD)Ca(SiPh$_3$)$_2$] (**35**) were synthesised by treating THF solutions of the corresponding THF-solvates [Ca(CH$_2$Ph)$_2$(thf)$_4$] and [Ca(SiPh$_3$)$_2$(thf)$_2$] with Me$_4$TACD (Scheme 8).[49,50] The orange dibenzyl complex is insoluble in THF and precipitates directly from the reaction mixture, whilst the bis(silyl) derivative is somewhat soluble in this solvent and was precipitated from a THF/*n*-pentane mixture. Single crystals of **34** were grown by layering THF solutions of [Ca(CH$_2$Ph)$_2$(thf)$_4$] and Me$_4$TACD.[49] The six-coordinate metal centre adopts a distorted trigonal prismatic geometry with each benzyl ligand bound in an η^1-manner through the formally sp^3-hybridised carbanionic methylene carbon. The Ca–C(1) distances (2.6392(19) Å) are significantly longer than those of the tetrakis(THF)-solvate (2.568(5)–2.595(5) Å).[51] The crystal structure of yellow [(Me$_4$TACD)Ca(SiPh$_3$)$_2$] similarly adopts a distorted trigonal prismatic geometry, with a Ca–Si distance (3.1654(15) Å) comparable to that of the precursor.[50]

Dibenzyl **34** reacts with the weak Brønsted acid [NEt$_3$H][BAr$_4$] (Ar = C$_6$H$_4$-4-^{t}Bu, C$_6$H$_3$-3,5-Me$_2$, C$_6$H$_4$-4-^{n}Bu) to yield the cationic benzyl complex [(Me$_4$TACD)Ca(CH$_2$Ph)(thf)][BAr$_4$] (**36a**, Ar = C$_6$H$_4$-4-^{t}Bu; **36b**, Ar = C$_6$H$_3$-3,5-Me$_2$; **36c**, Ar = C$_6$H$_4$-4-^{n}Bu) (Scheme 8). Loss of THF provides access to the η^6-benzyl complex [(Me$_4$TACD)Ca(CH$_2$Ph)][B(C$_6$H$_3$-3,5-Me$_2$)$_4$] (**36d**).[42] The related red ytterbium(II) analogues [(Me$_4$TACD)Yb(CH$_2$Ph)$_2$] (**34-Yb**) and [(Me$_4$TACD)Yb(CH$_2$Ph)][B(C$_6$H$_3$-3,5-Me$_2$)$_4$] (**36d-Yb**) have also been synthesised and crystallographically characterised; similar to calcium, both benzyl moieties are η^1-bonded for **34-Yb**, but purple **36d-Yb** crystallises as an η^6-benzyl complex without coordinated THF.[44] Addition of two equiv. of [NEt$_3$H][BAr$_4$] to **34** provided the dicationic bis(borate) salt [(Me$_4$TACD)Ca(thf)$_2$][BAr$_4$] (**37a**, Ar = C$_6$H$_4$-4-^{t}Bu;[49] **37b**, Ar = C$_6$H$_3$-3,5-Me$_2$).[52] In THF-solution, **36b** was found to exist in equilibrium with the zwitterionic compound [(Me$_4$TACD)Ca{CH$_2$(C$_6$H$_3$-3-BAr$_3$-5-Me)}] (**38**, Ar = C$_6$H$_3$-3,5-Me$_2$) *via* deprotonation of one of the *meta*-methyl groups of the borate anion and elimination of toluene.[49] Notably, in contrast to **34**, the putative neutral dibenzyl complex of the pentadentate aza-macrocycle Me$_5$PACP (Me$_5$PACP = *N*,*N*′,*N*″,*N*‴,*N*⁗-pentamethyl-1,4,7,10,13-pentaazacyclopentadecane) is unstable to ligand decomposition.[53]

Cationic calcium derivatives can be accessed by protonolysis of neutral bis(organo)calcium or bis(silanido)calcium precursors using cationic conjugate acid of Me$_4$TACD (Scheme 9).[42,53–55] Reaction of [(Me$_4$TACD)H][B(C$_6$H$_3$-3,5-Me$_2$)$_4$] with a THP slurry of THF-free dibenzylcalcium [Ca(CH$_2$Ph)$_2$], provided direct access to the η^6-benzyl complex **36d**.[42] Similarly, bis(allyl)calcium reacts with [(Me$_4$TACD)H][B(C$_6$H$_3$-3,5-Me$_2$)$_4$] in THF to yield the cationic allyl complex [(Me$_4$TACD)Ca(η^3-C$_3$H$_5$)(thf)][B(C$_6$H$_3$-3,5-Me$_2$)$_4$] (**39**) under elimination of propene.[54] **39** adopts a distorted pseudo-trigonal prismatic geometry with the allyl ligand coordinating in an η^3-manner. Protonolysis of bis(triphenylsilanido)calcium with [(Me$_4$TACD)H][B(C$_6$H$_3$-3,5-Me$_2$)$_4$] yielded a cationic silanide complex, **40**, characterised by NMR spectroscopy.[42]

4.2.2. Synthesis of molecular calcium hydride complexes. Unlike alkali metal triphenylsilanides **7**–**11**, which form parent silanides **12**–**15** upon hydrogenolysis, (Scheme 5)[41] **35** reacts with H$_2$ by heterolysis across the Ca–Si bonds to provide a dimeric trihydride cation as its charge-separated triphenylsilanide salt [(Me$_4$TACD)$_2$Ca$_2$(μ-H)$_3$][SiPh$_3$] (**41a**) and triphenylsilane (Scheme 10).[50] Closely related Yb(II) silanide complex

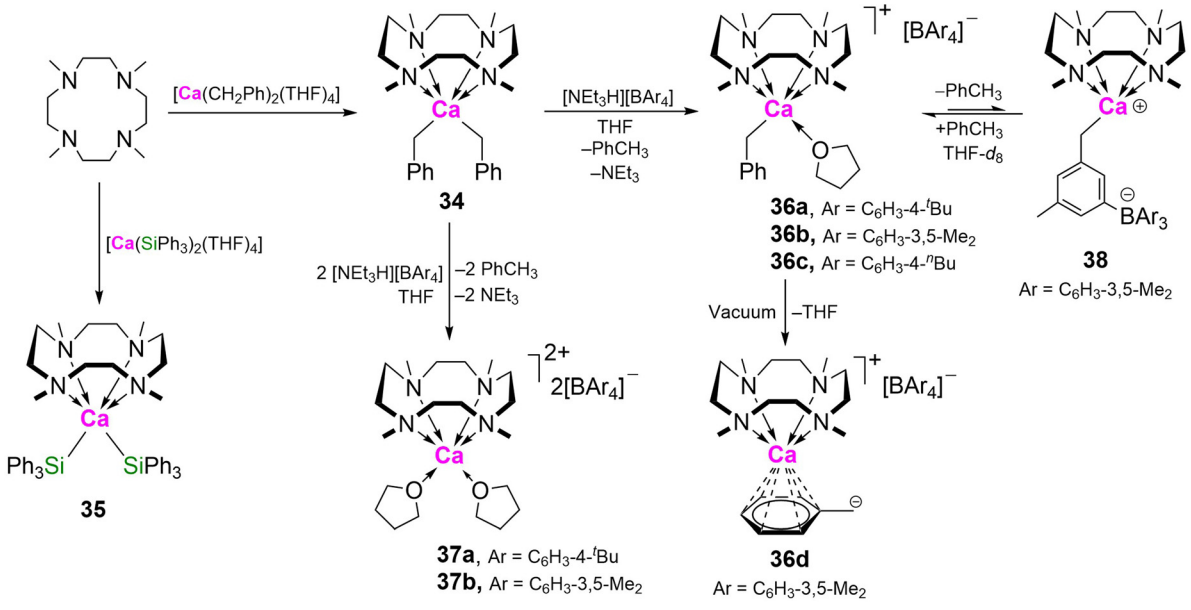

Scheme 8 Synthesis of Me$_4$TACD ligated calcium benzyl and silanide complexes **34**–**38**.

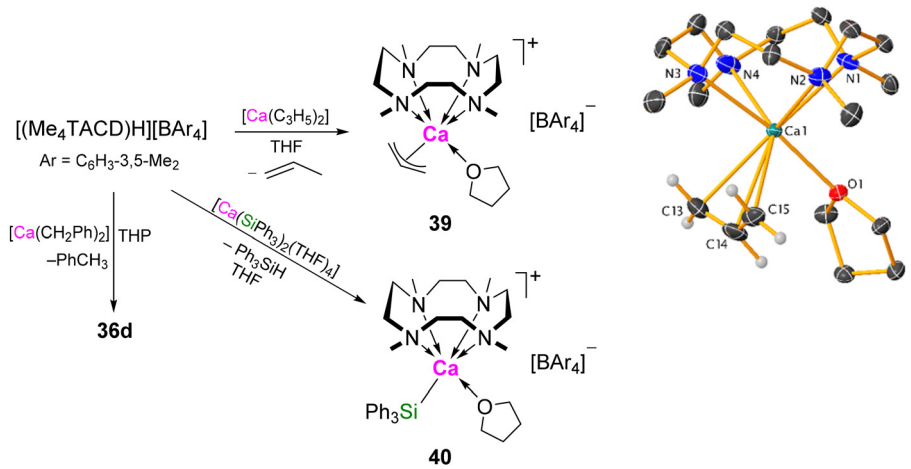

Scheme 9 Direct access to cationic calcium η^6-benzyl (**36d**), η^3-allyl (**39**), and triphenylsilanide (**40**) complexes by protonolysis using [(Me_4TACD)H][BAr_4]. The cationic part of the crystal structure of compound **39**.

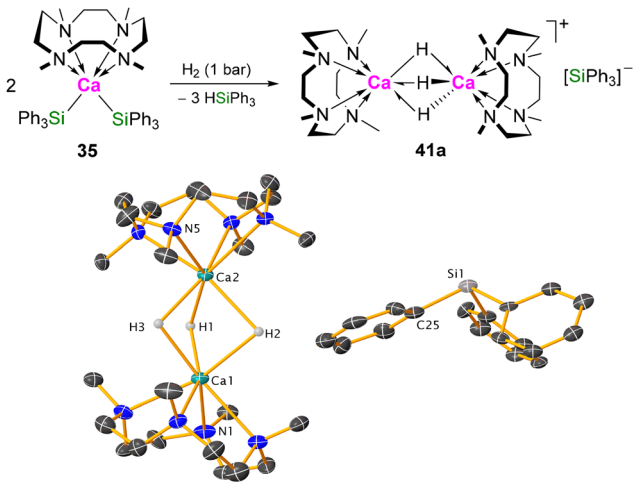

Scheme 10 Hydrogenolysis of compound **35** and molecular structure of dicalcium trihydride silanide salt **41a**.

[(Me_4TACD)Yb($SiPh_3$)$_2$] is similarly hydrogenated to provide the congeneric black Yb(II) trihydride dimer [(Me_4TACD)$_2$Yb$_2$(μ-H)$_3$][$SiPh_3$].[44]

Hydrogenolysis of **34** provided an insoluble precipitate, likely CaH_2, along with free Me_4TACD and decomposition products. However, using triphenylsilane as a hydride source produced a dimeric dicalcium dihydride cation, which crystallised as its triphenylsilylbenzyl salt [(Me_4TACD)$_2$Ca$_2$(μ-H)$_2$][PhCHSiPh_3]$_2$ (**42a**) (Scheme 11).[49] The crystal structure of **42a** consists of a dicationic C_i-symmetric dimer with two six-coordinate calcium centres bridged by two μ-hydride ligands. **42a** decomposes in THF-d_8 ($t_{1/2}$ = 6 h) *via* ligand degradation with formation of $PhCH_2SiPh_3$ amongst other species. Due to the reactive silylbenzyl anion, **42a** activates H_2 in an FLP-like manner to yield the dimeric trihydride cation [(Me_4TACD)$_2$Ca$_2$(μ-H)$_3$][PhCHSiPh_3] (**41b**) under elimination of $PhCH_2SiPh_3$. **41b** can also be formed directly by hydrogenolysis of **34** in the presence of $PhCH_2SiPh_3$.

Molecular calcium di- and trihydride dimers can be accessed as relatively robust tetraarylborate salts *via* hydrogenolysis of **36** or a 1 : 1 mixture of **36** and **34** (Scheme 12), respectively providing [(Me_4TACD)Ca$_2$(μ-H)$_2$][BAr_4]$_2$ (**42b**, Ar = C_6H_4-4-^{t}Bu; **42c**, Ar = C_6H_3-3,5-Me_2) or [(Me_4TACD)Ca$_2$(μ-H)$_3$][BAr_4] (**41c**, Ar = C_6H_4-4-^{t}Bu; **41d**, Ar = C_6H_3-3,5-Me_2).[49] **41c** can be converted to **42c** *via* protonolysis by addition of [NEt_3H][B(C_6H_4-4-^{t}Bu)$_4$], or through hydride-redistribution by combining with calcium bis(borate) **37a**. Hydrogenolysis of **36** [42,53] or silanolysis of either **36** [42,53] or **39** [54] with $RSiH_3$ (R = *n*-octyl or Ph), followed by crystallisation from THF/*n*-pentane provides reliable access to the dimeric dihydride dication as a THF-solvate [(Me_4TACD)$_2$Ca$_2$(μ-H)$_2$(thf)][BAr_4]$_2$ (**42d**, Ar = C_6H_3-3,5-Me_2;[54] **42e**, Ar = C_6H_3-4-^{n}Bu).[53]

The crystal structures of **42d** (Fig. 4),[54] and **42e** [53] reveal a dimeric dication with six- and seven-coordinate calcium centres bridged by two μ-hydrides. Compared to **42a**, the seven-coordinate calcium centre exhibits longer Ca–H distances, leading to an elongated Ca–Ca separation (3.6306(11) Å *vs.* 3.4650(10) Å). The red Yb(II) congener [(Me_4TACD)$_2$Yb$_2$(μ-H)$_2$(thf)][B(C_6H_3-3,5-Me_2)$_4$]$_2$ is isostructural to **42d**, and was prepared similarly by hydrogenolysis of the corresponding cationic Yb(II) benzyl complex.[44]

In THF-d_8 solution, the anions have minimal effect on the hydride resonances of trihydride complexes **41a–d**, with silanide, silylbenzyl, and tetraarylborate salts all displaying a singlet at δ 4.71–4.73 ppm in their ^{1}H NMR spectra.[49,50] However, the dihydride silylbenzyl salt **42a** exhibits a significantly downfield-shifted hydride resonance (δ 4.70 ppm)[49] compared to borate salts **42b–e** (δ 4.49–4.54 ppm).[42,49,53,54] This indicates that whilst compounds **41a–d** and **42b–e** exist as charge-separated species in THF, a significant anion–cation interaction may exist for **42a**. THF coordination to the dicationic core in **42** is highly labile, as **42c** and **42d** exhibit identical

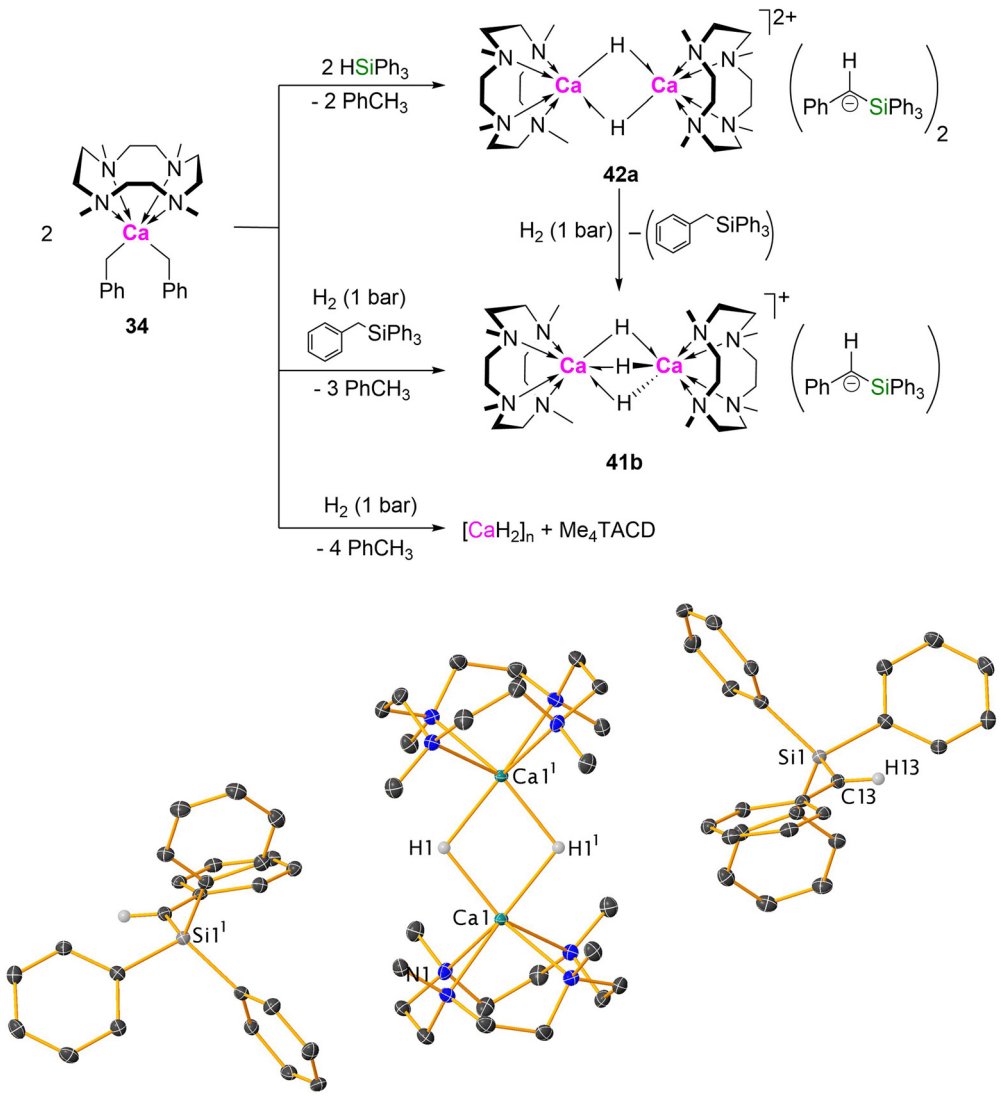

Scheme 11 Synthesis of dicalcium di- and trihydrides **42a** and **41b** *via* hydrogenolysis and silanolysis of benzyl precursors in THF. Molecular structure of compound **42a** with selected hydrogen atoms shown.

NMR spectra with time-averaged C_i-symmetry, and THF resonates at the same shift as free solvent. Coordination of THF to the unsolvated dimer $[(Me_4TACD)_2Ca_2H_2]^{2+}$ is mildly exothermic (*ca.* 33 kJ mol^{-1}),[54] consistent with Lewis acidity of the relatively large and coordinatively unsaturated metal cation.

Molecular calcium hydrides commonly adopt a dimeric dihydride structure when supported by bulky or highly coordinating ligands to suppress further aggregation. The dimeric trihydride motif $[(L)_2M_2H_3]^+$, however, is unique in alkaline-earth chemistry to cationic complexes supported by neutral macrocycles, observed only in compounds **41a–d** and the related strontium hydride $[(Me_5PACP)_2Sr_2(\mu\text{-}H)_3][B(C_6H_3\text{-}3,5\text{-}Me_2)_4]$.[52] The ability to accept a third hydride reflects the electrophilic and coordinatively unsaturated nature of the metal cations in the dimeric dihydride. The combination of nucleophilic hydride and electrophilic metal centre is crucial to the observed reactivity of such complexes towards kinetically inert substrates such as ethylene and carbon monoxide (*vida infra*), and in the catalytic hydrogenation and hydrosilylation of olefins. The kinetic stabilisation of low-nuclearity calcium hydrides is dependent on ligand bulk and coordination strength. Employing the smaller Me_3TACN (*N*,*N*′,*N*″-trimethyl-1,4,7-triazacyclononane) ligand results in the isolation of tetranuclear $[(Me_3TACN)_4Ca_4(\mu\text{-}H)_6][B(C_6H_3\text{-}3,5\text{-}Me_2)_4]_2$.[55] Discrete calcium hydride clusters can be isolated *via* silanolysis of amide precursors.[56,57] Cluster nuclearity can be controlled by the size of supporting amine and/or amide ligands, with smaller clusters exhibiting higher activity as hydrogenation catalysts.[58,59]

4.2.3. Reactivity of molecular calcium hydride complexes

Dihydrogen and hydrosilanes. The silanide salt of dicalcium trihydride **41a** exchanges with D_2 forming **41a**-d_3 and HD *via* mixed isotopomers (Scheme 13). This was proposed to involve

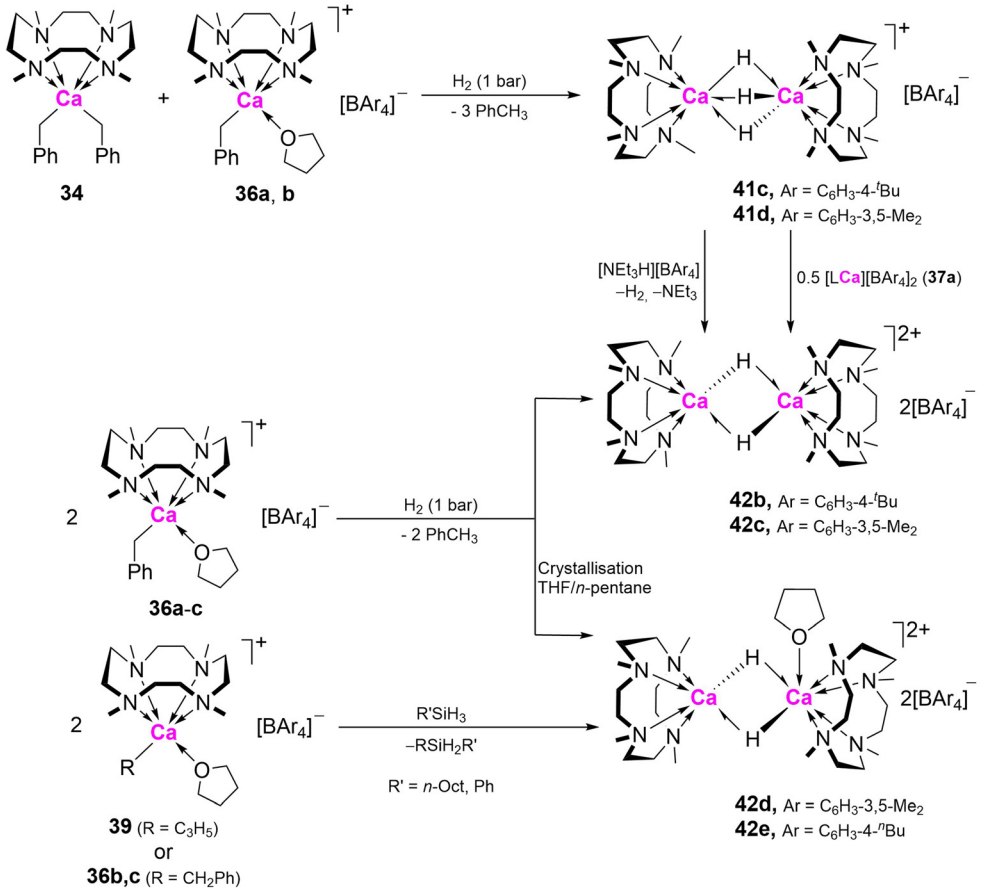

Scheme 12 Synthesis of dimeric calcium hydrides **41c,d**, and **42b–e** in THF.

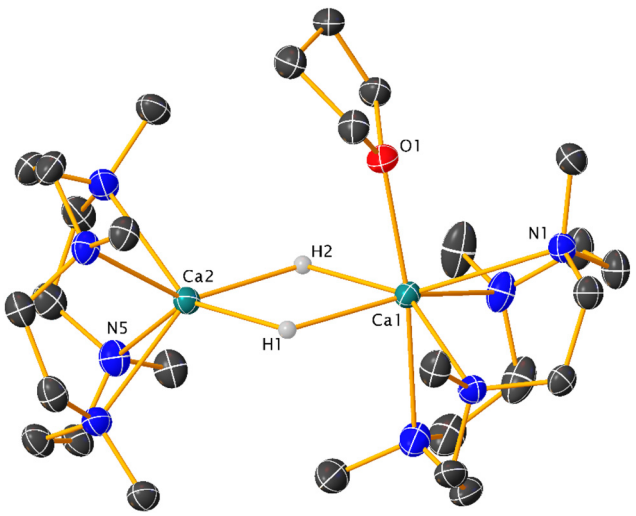

Fig. 4 Molecular structure of the dicationic part of compound **42d**.

the silyl anion, as carrying out the reaction with D_2 in the presence of $HSiPh_3$ also resulted in H/D exchange to give $DSiPh_3$. Dimer-dissociation is implied by the rapid equilibration of **41a** and **41a**-d_3 to a mixture of isotopomers.[50] **42b** also exchanges with D_2; formation of HD was observed by NMR spectroscopy, and complete deuteration occurred after 8 h (1 bar pressure), *via* intermediate formation of the monodeutero isotopomer (Scheme 13). Exposing **42b** to an equimolar mixture of D_2 and H_2 or HD resulted in rapid equilibration to a mixture of isotopomers after 5 min with respective formation of HD or H_2 and D_2.[49]

42d catalyses organosilane redistribution, converting $PhSiH_3$ into Ph_2SiH_2 and SiH_4 (Scheme 14). Exposing a solution of **42d** and $RSiH_3$ (R = *n*-octyl, Ph) to D_2 produces HD, **42d**-d_n, and an isotopomeric mixture of hydrosilanes.[54] Broad SiH and CaH resonances in the ^1H NMR spectrum suggest mutual exchange according to EXSY NMR experiments, while NOESY NMR reveals NOE correlations between the silicon hydrides and NCH_3 resonances. The reaction likely involves hypervalent silicates formed *via* nucleophilic hydride attack on silane. Similar propositions have been made for $[(BDI^{dipp})Ca(\mu\text{-}H)]_2$ (BDI^{dipp} = $HC\{C(CH_3)N(C_6H_3\text{-}2,6\text{-}^iPr_2)\}_2$) synthesis using $PhSiH_3$ as a hydride source.[3] Hypervalent silicates have been experimentally and computationally implicated as intermediates in alkaline-earth catalysed Si–E dehydrocoupling (E = N, O) reactions, in preference to concerted σ-bond metathesis.[60–62] Further, crystallographically characterised calcium and strontium hydridosilicate complexes derived from

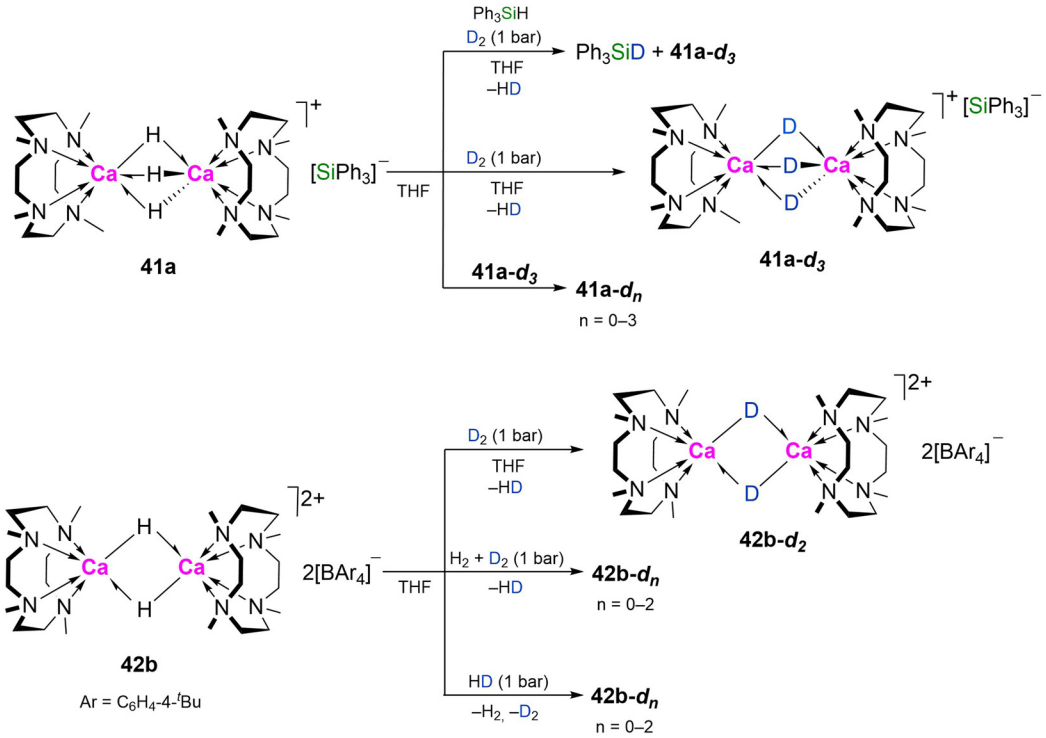

Scheme 13 Isotopic exchange of **41a** and **42b**.

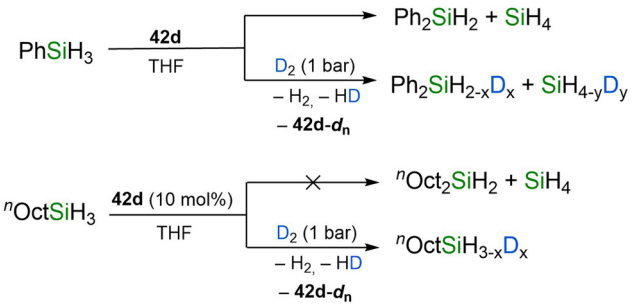

Scheme 14 Calcium-mediated redistribution and deuteration of organosilanes.

the reaction of organo- and amido-alkaline earth complexes with hydrosilanes have also been isolated (*vide infra*).[63,64]

Insertion of unsaturated C–X multiple bonds. The nucleophilic hydrides of **42d** readily insert CO_2, forming the dimeric formate complex $[(Me_4TACD)_2Ca_2(\mu\text{-}OCHO)_2(thf)_2][B(C_6H_3\text{-}3,5\text{-}Me_2)_4]_2$ (**43**, Scheme 15),[65] and react with CO to yield the *cis*-ethenediolate complex $[(Me_4TACD)_2Ca_2(OC(H)C(H)O)_2][B(C_6H_3\text{-}3,5\text{-}Me_2)_4]_2$ (**44**, Scheme 15). Monomerization of **42d** was calculated to be only slightly endothermic; DFT calculations suggest that CO insertion occurs at the monomeric hydride $[(Me_4TACD)Ca(H)(thf)_x]^+$, providing a formyl intermediate that subsequently dimerizes into **44** (Scheme 15).[65] The relative ease by which **42d** can monomerize in THF solution carries important mechanistic implications in hydrofunctionalisation catalysis. Dimeric β-diketiminato magnesium and calcium hydrides $[(BDI^{dipp})M(\mu\text{-}H)(thf)_n]_2$ (M = Mg, n = 0; M = Ca, n = 1) also react with CO to form *cis*-enediolates.[66–68] In these cases, however, the dimer is proposed to remain intact throughout the reaction, with a calculated mechanism involving initial two-fold hydride insertion to give an oxomethylene intermediate, followed by insertion of a second CO molecule and subsequent 1,2-hydride shift.

Ethylene readily inserts into the Ca–H bonds of **42d**, forming the unstable ethyl-calcium complex $[(Me_4TACD)CaEt(thf)_x]^+$ (**45**), observed *via* ^{1}H NMR spectroscopy. This species decomposes rapidly ($t_{1/2}$ = 10 min) into an intractable mixture.[54] Similar to $[(BDI^{dipp})Ca(\mu\text{-}H)]_2$ and $[(BDI^{dipp})Sr(\mu\text{-}H)]_2$ (BDI^{dipep} = $HC\{C(CH_3)N(C_6H_3\text{-}2,6\text{-}(C(H)Et_2)_2)\}_2$),[3,69] **45** also reacts further with ethylene to generate labile calcium *n*-alkyl species. The nuclearity of **45** remains unclear; given the low energy barrier to hydride monomerization, which is proposed to occur during hydrogenation and hydrosilylation catalysis,[49,53,65,70] and the isolation of a related mononuclear seven-coordinate calcium ethyl cation $[(Me_5PACP)CaEt(thf)][B(C_6H_3\text{-}3,5\text{-}Me_2)_4]$,[53] it is plausible that Me_4TACD-supported calcium *n*-alkyl complexes also exist as monomers in THF solution.

Nucleophilic and Brønsted-basic reactivity. The nucleophilic hydride of **42d** reacts with alkynyl silanes $Me_3SiC{\equiv}CSiMe_3$ and $HMe_2SiC{\equiv}CSiMe_3$ *via* nucleophilic substitution, forming dimeric alkynyl calcium complex $[(Me_4TACD)_2Ca_2(\mu\text{-}C{\equiv}CSiMe_3)_2][B(C_6H_3\text{-}3,5\text{-}Me_2)_4]_2$ (**46a**) after elimination of Me_3SiH or Me_2SiH_2, respectively (Scheme 16).[65] Similarly, reaction with $N(SiMe_2H)_3$, $MeSiH(OMe)_2$, or $O(SiMe_2H)_2$ resulted

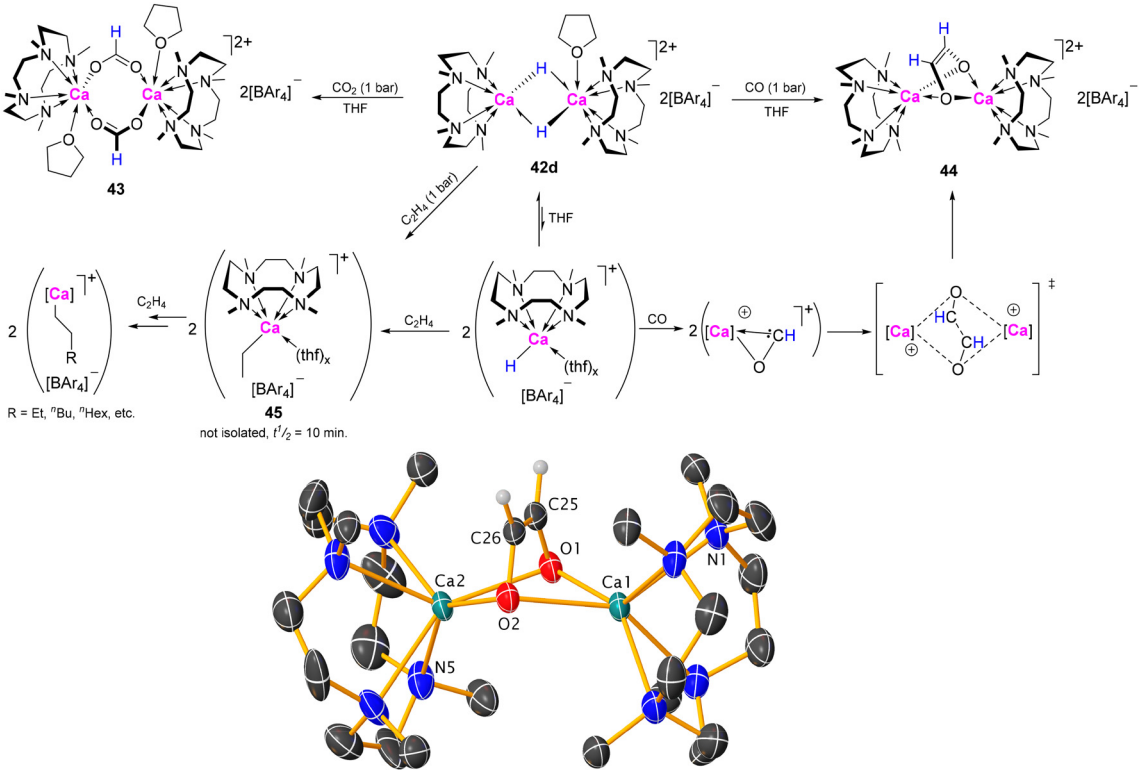

Scheme 15 Reactivity of compound **42d** towards small molecules, and molecular structure of *cis*-enediolate **44**. Ar = C_6H_3-3,5-Me_2.

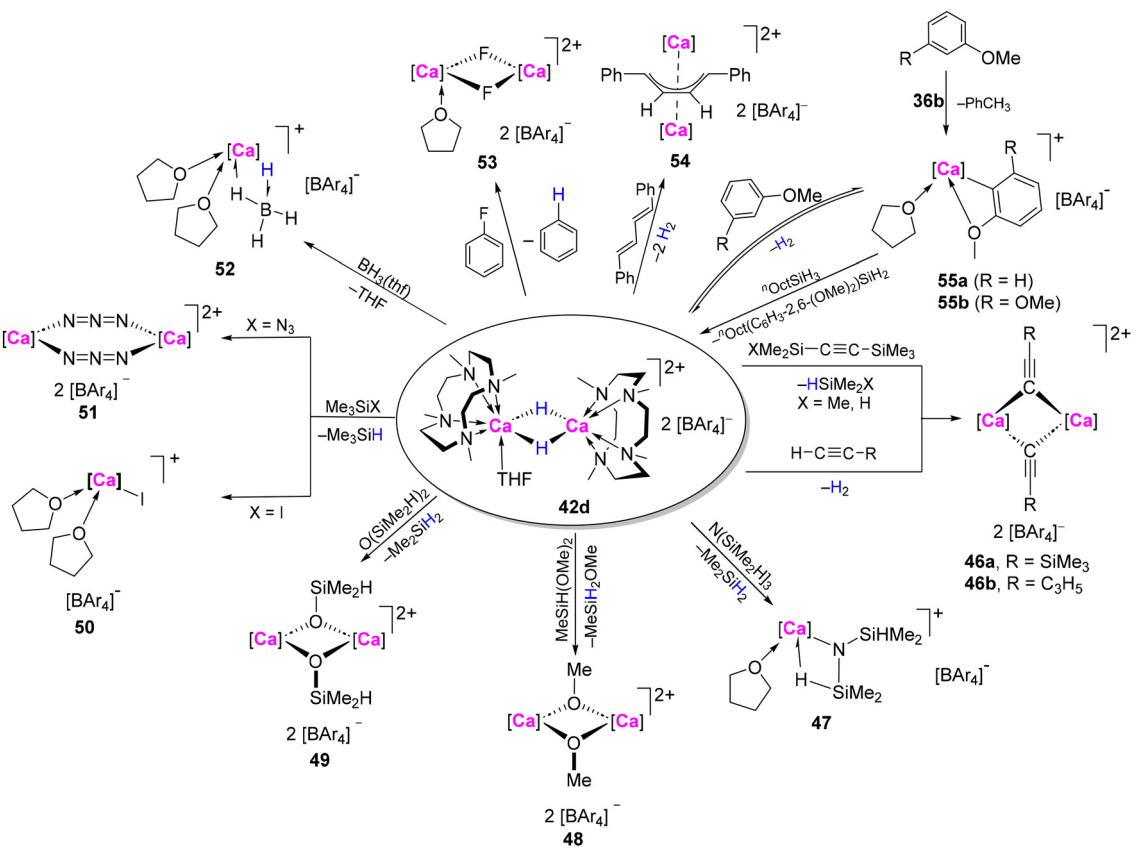

Scheme 16 Reactivity of calcium hydride **42d**. [Ca] = $[(Me_4TACD)Ca]^{2+}$; Ar = C_6H_3-3,5-Me_2.

in nucleophilic substitution to form [(Me$_4$TACD)Ca(N(SiHMe$_2$)$_2$)][B(C$_6$H$_3$-3,5-Me$_2$)$_4$] (**47**), [(Me$_4$TACD)$_2$Ca$_2$(μ-OMe)$_2$][B(C$_6$H$_3$-3,5-Me$_2$)$_4$]$_2$ (**48**), or [(Me$_4$TACD)Ca(OSiMe$_2$H)][B(C$_6$H$_3$-3,5-Me$_2$)$_4$] (**49**) with elimination of Me$_2$SiH$_2$ or MeSiH$_2$OMe.[54,65] Whereas **48** crystallises as a dimer with bridging methoxide ligands, **47** is monomeric with an anagostic interaction between calcium and one of the Si–H bonds. Similarly, reactions with Me$_3$SiI and Me$_3$SiN$_3$ provide monomeric iodide, and dimeric azide complexes, [(Me$_4$TACD)CaI(thf)$_2$][B(C$_6$H$_3$-3,5-Me$_2$)$_4$] (**50**) and [(Me$_4$TACD)$_2$Ca$_2$(μ-N$_3$)$_2$][B(C$_6$H$_3$-3,5-Me$_2$)$_4$]$_2$ (**51**) after eliminating Me$_3$SiH.[65] Hydridic reactivity of **42d** is also observed in the reaction with BH$_3$·THF leading to tetrahydridoborate complex [(Me$_4$TACD)Ca(BH$_4$)(thf)$_2$][B(C$_6$H$_3$-3,5-Me$_2$)$_4$] (**52**).[65] The strong nucleophilicity of **42d** enables nucleophilic aromatic substitution with fluorobenzene, cleaving the C$_{sp^2}$–F bond to form the dimeric fluoride complex [(Me$_4$TACD)$_2$Ca$_2$(μ-F)$_2$(thf)][B(C$_6$H$_3$-3,5-Me$_2$)$_4$]$_2$ (**53**) with benzene elimination.[65] Structurally, **53** resembles the parent hydride, with two fluoride ligands bridging six- and seven-coordinate calcium centres. As a strong Brønsted base, **42d** deprotonates RC≡CH (R = SiMe$_3$, C$_3$H$_5$) to yield dimeric acetylides, **46a** and [(Me$_4$TACD)$_2$Ca$_2$(μ-C≡CC$_3$H$_5$)$_2$][B(C$_6$H$_3$-3,5-Me$_2$)$_4$]$_2$ (**46b**), and reacts with *trans*,*trans*-1,4-diphenylbutadiene to provide the dinuclear butadienyl complex [(Me$_4$TACD)$_2$Ca$_2$(μ$_2$–η^4-1,4-Ph$_2$C$_4$H$_2$)][B(C$_6$H$_3$-3,5-Me$_2$)$_4$]$_2$ (**54**) (Fig. 5). Anisole and 1,3-dimethoxybenzene are deprotonated, forming aryl-calcium complexes [(Me$_4$TACD)Ca(κ^2-O,C-C$_6$H$_4$-6-OMe)(thf)][B(C$_6$H$_3$-3,5-Me$_2$)$_4$] (**55a**) and [(Me$_4$TACD)Ca(κ^2-O,C-C$_6$H$_4$-2,6-(OMe)$_2$)(thf)][B(C$_6$H$_3$-3,5-Me$_2$)$_4$] (**55b**).[42] Compound **55b** undergoes σ-bond metathesis with ^{n}OctSiH$_3$ to regenerate **42d** under elimination of ^{n}Oct(C$_6$H$_3$-2,6-(OMe)$_2$)SiH$_2$.

4.2.4. Catalysis mediated by molecular calcium hydride complexes. The dinuclear trihydride-silanide salt **41a** reacts with 1,1-diphenylethylene by silicon-centred nucleophilic addition to give {(triphenylsilyl)methyl}diphenylmethanide salt **41e** (Scheme 17).[50]

The calcium complex **41e** catalyses the hydrogenation of 1,1′-diphenylethylene at 60 °C within 24 h under 1 bar H$_2$, likely *via* Ca–H insertion and subsequent σ-bond metathesis (Scheme 18a). The borate-salt **41c** catalysed the same reaction in 12 h at 25 °C, whilst the dicationic dihydride **42b** is more active, achieving 98% conversion in 6 h under ambient conditions.[49] **42b** also catalyses the hydrogenation of styrene (10 h, 25 °C), 1,2-diphenylethylene (24 h, 60 °C), triphenyl- (16 h, 60 °C) and (trimethyl)vinylsilane (36 h, 60 °C). Catalytic activity was not restricted to activated alkenes; 1-hexene, 1-octene, 3-vinylcyclohexene, 1,5-hexadiene, and 1,9-decadiene were also hydrogenated (Scheme 18b). Dihydride **42b** displayed higher activity than trihydride **41c**. No hydrogenation of internal double bonds (3-vinylcyclohexene, cyclohexene) was observed. For 1-hexene, 1-octene, 1,5-hexadiene, and 1,9-decadiene, 5% 2-alkene was observed in the product mixture; for 1,5-hexadiene, 4% of the cyclisation product methylcyclopentane was also formed.

The activity of compounds **41c,e**, and especially **42b** in alkene hydrogenation compares well with other alkaline-earth catalysts. Bulky cyclopentadienyl-derivatives [(η^5-C$_5$R$_5$)$_2$M$_2$(μ-H)$_2$(L)] (M = Ca, Sr, Ba; R = C$_6$H$_3$-3,5-^{i}Pr; L = THF or DABCO) also catalyse alkene hydrogenation, including unactivated *n*-alkenes at 30 °C under 6 bar H$_2$, with activity increasing with metal size.[71] By comparison, a magnesium PNP pincer complex [{C$_5$H$_3$N(C(H)P^{t}Bu$_2$)(CH$_2$P^{t}Bu$_2$)}$_2$Mg$_2$Et$_2$(μ-1,4-dioxane)] was reported to catalyse the hydrogenation of alkenes including unactivated 1-dodecene, 1-octene, 3-(*ortho*-methoxy)phenyl-prop-1-ene, 4-phenyl-but-1-ene, and 3-(trimethylsilyl)-prop-1-ene, but requires harsh conditions (120 °C, 5 bar).[72] A related calcium-based system was limited to activated substrates like 1,1′-diphenylethene and styrene.[73] The β-diketiminato derivative [(BDI^{dipp})Ca(μ-H)(thf)]$_2$ catalyses the

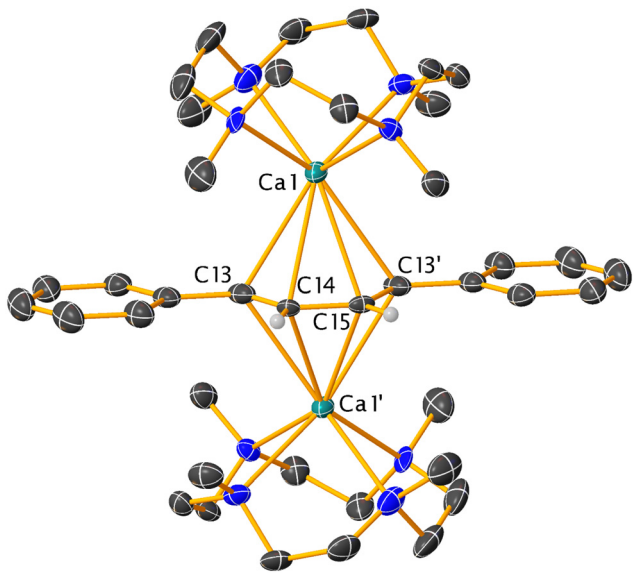

Fig. 5 Molecular structure of the dicationic part of the butadienyl calcium complex **54**.[65]

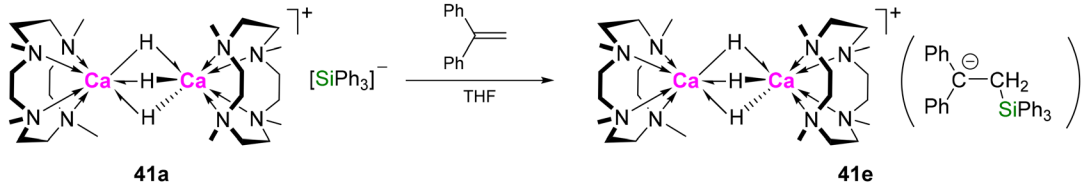

41a **41e**

Scheme 17 Silanide-centred reactivity of **41a** towards 1,1′-diphenylethene.

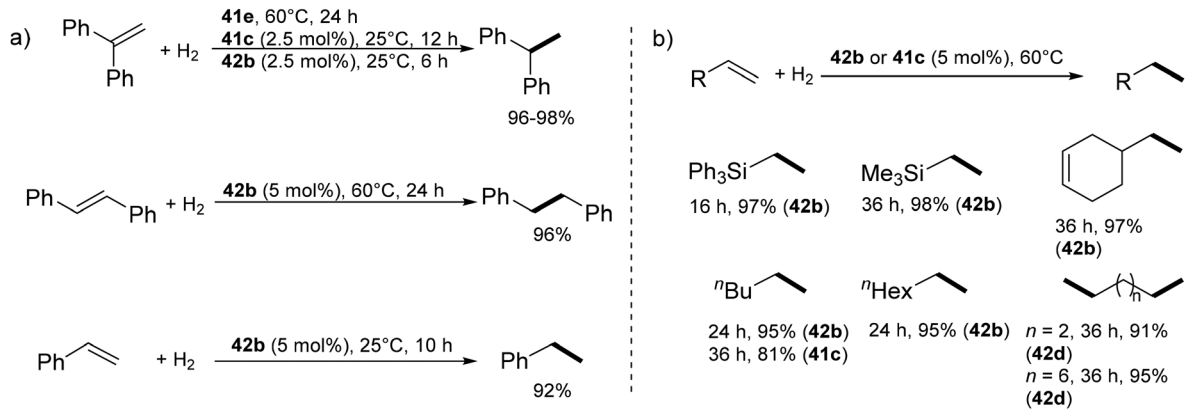

Scheme 18 Hydrogenation of (a) activated, (b) unactivated alkenes catalysed by calcium hydrides **41c,e**, and **42b**.

hydrogenation of 1,1′-DPE and styrene derivatives at 60 °C under 20 bar H_2 pressure.[74] In contrast, the unsolvated analogue $[(BDI^{dipp})Ca(\mu\text{-}H)]_2$ catalyses the hydrogenation of unactivated *n*-alkenes at ambient conditions,[75] although catalysis was limited to room temperature with slow conversion (21 d), due to competitive nucleophilic alkylation of benzene at elevated temperature.[3,75] The Me_4TACD-based systems are thermally robust, permitting mildly elevated temperatures and appreciable rates. High activity compared to $[(BDI^{dipp})Ca(\mu\text{-}H)(thf)]_2$ [74] was attributed to a high degree of Lewis acidity and facile monomerization due to cationic charge. Notably, heavier alkaline-earth amides $[Ae(NRR')_2]_n$ (R = $SiMe_3$, Si^iPr_3; R′ = $SiMe_3$, Si^iPr_3, C_6H_3-2,6-$^iPr_2$) act as pre-catalysts for the efficient hydrogenation and transfer hydrogenation of challenging unactivated *n*-alkenes, as well as internal secondary alkenes and aromatic rings under relatively mild conditions (up to 120 °C, 1–6 bar H_2).[58,59,76,77] Here, multinuclear (amido)alkaline-earth hydride clusters are proposed as active species, with bulkier amides leading to lower nuclearity and higher activity.

Hydride **42d** also catalysed alkene hydrosilylation.[54] Ethylene was hydrosilylated by various aromatic and aliphatic hydrosilanes at 70 °C in under 60 min (Scheme 19a). Primary and secondary hydrosilanes yielded di- and monoethylated silanes. Longer-chain aliphatic *n*-alkenes were hydrosilylated more slowly (24 h, 70 °C, conversion 70–96%) with anti-Markovnikov regioselectivity (Scheme 19b). Markovnikov products were observed for aryl-substituted olefins (Scheme 19c), as the result of a π-interaction of the phenyl group with the Lewis-acidic Ca centre. A mixture of Markovnikov and anti-Markovnikov products was obtained for the hydrosilylation of triphenyl(vinyl)silane with *n*-octylsilane. Internal double bonds were not hydrosilylated. Arylsilanes undergo scrambling reactions promoted by the electrophilic calcium hydride (Scheme 14), providing SiH_4 and Ph_2SiH_2 in the case of phenylsilane, and alkoxy and siloxy calcium derivatives (*e.g.*, **48**, **49**, Scheme 16)[54,65] from alkoxy- and siloxy-substituted hydrosilanes, thus making aliphatic hydrosilanes preferable. Attempted hydrosilylation of terminal alkyne $HC{\equiv}CSiMe_3$ with $^nOctSiH_3$ using 5 mol% **42d** instead provided dehydrocoupling products $(Me_3SiC{\equiv}C)(^nOct)SiH_2$ and $(Me_3SiC{\equiv}C)_2(^nOct)SiH$ in a 2 : 1 ratio (Scheme 19e).[42]

Monomerization of $[(Me_4TACD)_2Ca_2(\mu\text{-}H)_2(thf)_x]^{2+}$ to give a reactive terminal hydride species $[(Me_4TACD)Ca(H)(thf)_y]^+$ was suggested to precede alkene insertion and catalytic turnover (Scheme 20). While monomeric hydride or alkyl-derivatives were not isolated for Me_4TACD, a mononuclear terminal ethyl complex $[(Me_5PACP)CaEt(thf)][B(C_6H_3\text{-}3,5\text{-}Me_2)_4]$, was crystallised for the larger 15-membered macrocycle, Me_5PACP.[53] Further, kinetic studies on the hydrosilylation of 1-octene by *n*-octylsilane showed a 1/2-order dependence on dimeric hydride pre-catalyst for both **42d** and $[(Me_5PACP)_2Ca_2(\mu\text{-}H)_2][B(C_6H_4\text{-}4\text{-}^nBu)_4]_2$, implying a monomeric active species in both cases.[53] Despite increased steric and coordinative demand, the Me_5PACP derivative was more active than **42d**, likely due to easier access to mononuclear species for the larger ligand. Catalysis is first-order in 1-octene and pseudo-zeroth order in *n*-octylsilane, suggesting rate-limiting alkene insertion and rapid σ-bond metathesis of the *n*-alkyl intermediate with hydrosilane.

When compared with the similarly dimeric pre-catalyst $[(BDI^{dipp})Ca(\mu\text{-}H)]_2$ (Scheme 20), dimeric alkyl-hydride species $[(BDI^{dipp})_2Ca_2(\mu\text{-}H)(\mu\text{-}R)]$ (R = *n*-alkyl) were observed by *in situ* NMR spectroscopy as a resting-state in the catalytic run, indicating a persistent dimeric active species, slow insertion of alkene into the second μ-H, and rate-limiting σ-bond metathesis with H_2.[75] Dimeric dialkyl insertion products $[(BDI^{dipp})Ca(\mu\text{-}R)]_2$ could be isolated in the absence of H_2.[3,75,78] Conversely, the hydride resonance in the ^1H NMR spectrum of **42b**-mediated *n*-alkene hydrogenation remained unchanged in catalysis, and attempts to isolate insertion products of 1-hexene or 3-vinylcyclohexane failed, suggesting reversible and rate-limiting alkene insertion/β-hydride elimination and rapid σ-bond metathesis with H_2.[49,53]

The hydrosilylation of unactivated *n*-alkenes using phenylsilane has also been reported for the dimeric magnesium pre-catalyst $[(BDI^{dipp})Mg(\mu\text{-}H)]_2$.[79] Near-quantitative conversion was achieved in over 4 d at 60 °C, with bulkier or aryl alkenes like styrene showing reduced activity. Similar to the calcium analogue, *n*-alkene insertion was calculated to occur at the

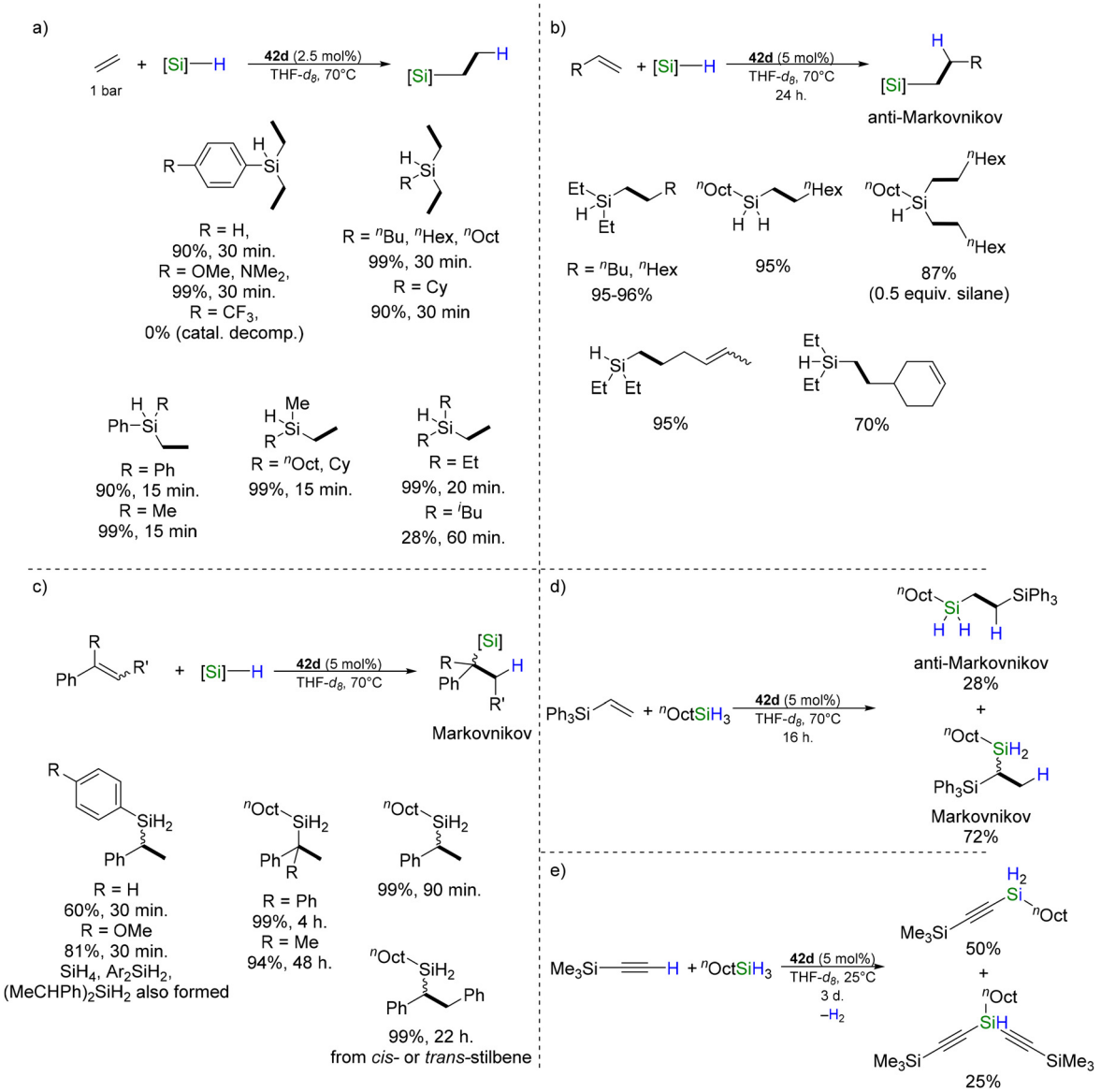

Scheme 19 Hydrosilylation of olefins catalysed by **42b**: (a) hydrosilylation of ethylene; (b) anti-Markovnikov selective hydrosilylation of aliphatic 1-alkenes; (c) Markovnikov selective hydrosilylation of styrene derivatives; (d) hydrosilylation of triphenyl(vinyl)silane with mixed selectivity; (e) dehydrocoupling of trimethylsilylacetylene and *n*-octyl silane.

intact dimeric μ-hydride complex rather than through mononuclear species, although ready dissociation of the resultant mixed hydride-alkyl species $[(BDI^{dipp})_2Mg_2(\mu\text{-}H)(\mu\text{-}R)]$ implicates mononuclear on-cycle intermediates during catalysis (Scheme 20). The faster reaction rates observed for **42b** compared to $[(BDI^{dipp})Mg(\mu\text{-}H)]_2$ are likely due to calcium's lower electronegativity, stronger polarization, and lower steric hindrance at the metal centre, facilitating more efficient alkene activation and hydrosilylation. The cationic charge of the active species may also play a role in promoting the coordination and polarisation of alkene and silane during catalysis.

The mechanism of the hydrogenation of 1-alkenes mediated by $[(Me_4TACD)_2Ca_2(\mu\text{-}H)_2]^{2+}$ as pre-catalyst was studied computationally.[70] A mechanism involving an intact μ-H bridged dimer was computed to be more energetically favourable for H_2 isotope exchange than with a mononuclear terminal hydride. Anti-Markovnikov addition of aliphatic 1-alkenes was competitive for either hydride-bridged dimer or mononuclear terminal hydride $[(Me_4TACD)Ca(H)(thf)]^+$, whilst Markovnikov addition of styrene was observed for the mononuclear hydride, influenced by Ca^+–Ph cation–π interactions, which directed regioselectivity.

In summary, it appears that the ability for chelating polydentate aza-macrocycles to infer relatively high stability towards highly Lewis acidic mononuclear calcium cations may play an important role in the comparatively high activity of calcium hydride complexes **42b,d** as pre-catalysts for hydrogenation and hydrosilylation of unactivated alkenes.

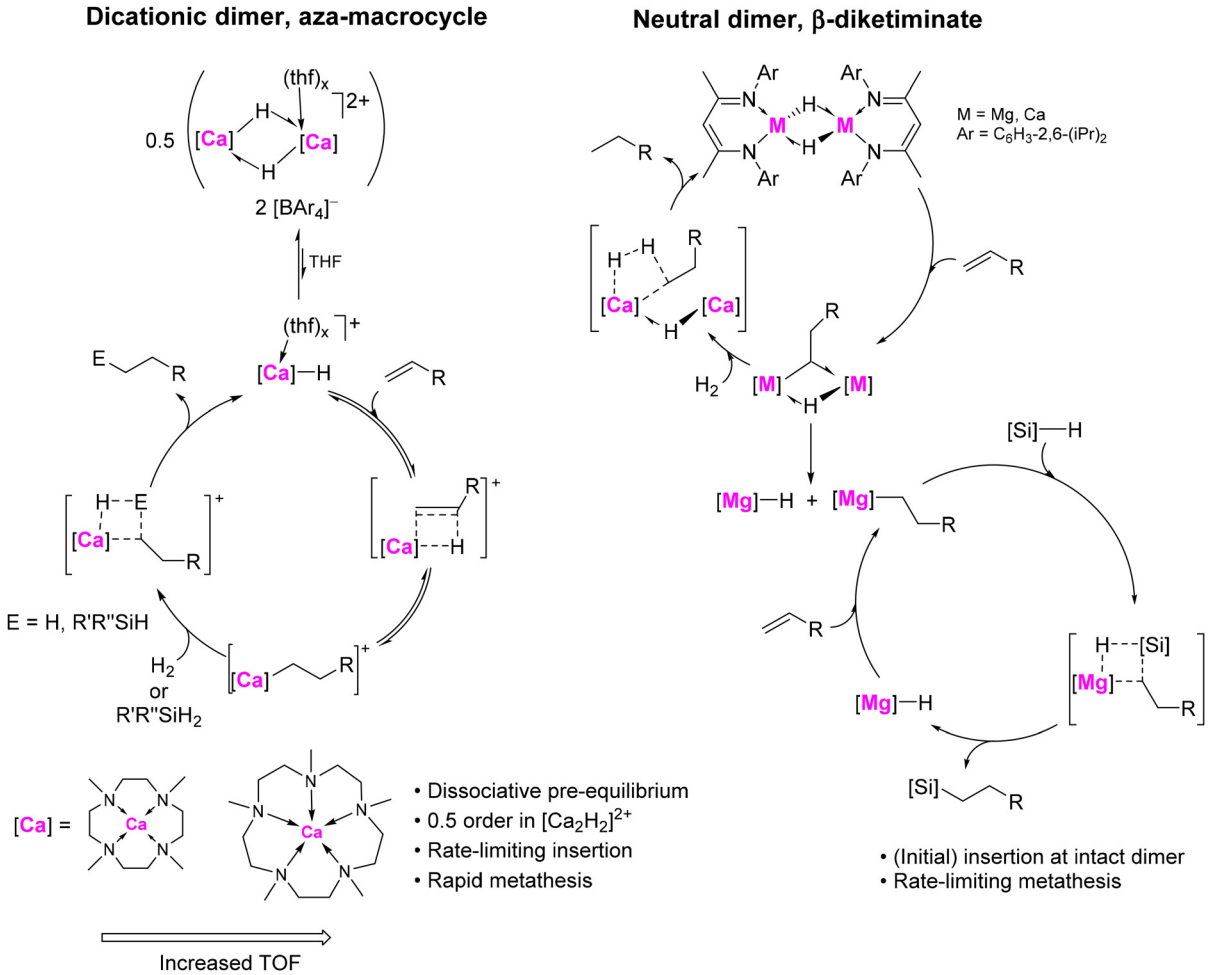

Scheme 20 Contrast in proposed mechanisms for olefin hydrogenation and hydrosilylation mediated by Me_4TACD/Me_5PACP-calcium and BDI^{dipp}-calcium/magnesium catalysts.

4.3. Strontium

4.3.1. Organostrontium complexes. The dibenzyl strontium complex, [(Me_4TACD)Sr(CH_2Ph)$_2$(thf)] (**56a**) was synthesised by combining Me_4TACD and [Sr(CH_2Ph)$_2$(thf)] in THF (Scheme 21).[80] The crystal structure of **56a** consists of a seven-coordinate metal centre with two η^1-coordinated benzyl ligands and one coordinated THF. Coordinated THF was found to be labile, giving the six-coordinate dibenzyl complex [(Me_4TACD)Sr(CH_2Ph)$_2$] (**56b**) under vacuum. Protonation of **56b** with the Brønsted acid [NEt_3H][BAr_4] (1 or 2 equiv.) produced the respective benzyl strontium cation [(Me_4TACD)Sr(CH_2Ph)(thf)][BAr_4] (**57a**, Ar = C_6H_3-3,5-Me_2; **57b**, Ar = C_6H_4-4-^{n}Bu) and bis-borate dication [(Me_4TACD)Sr(thf)$_2$][B(C_6H_3-3,5-Me_2)$_4$]$_2$ (**58**).[80] The coordination sphere of the {(Me_4TACD)Sr} unit appears rather flexible, adopting coordination numbers of either six or seven. Further, η^1-benzyl cation **57a** loses THF under vacuum to provide the slipped η^6-benzyl complex [(Me_4TACD)Sr(CH_2Ph)][B(C_6H_3-3,5-Me_2)$_4$] (**57c**), which could also be synthesised by protonolysis of **56b** with [NEt_3H][B(C_6H_3-3,5-Me_2)$_4$] in THP. The crystal structure of **57c** closely resembles the THF-free η^6-benzyl calcium complex **36d** (Scheme 8).[42] Unlike **36b**, **57a** did not deprotonate the borate anion to form a zwitterionic complex similar to **38**.

4.3.2. Strontium hydride complexes. Me_4TACD appears less effective at stabilizing low-nuclearity strontium hydride complexes compared to calcium due to the larger ionic radius, lower charge density, and more ionic Sr–H bonds. Indeed, structurally characterised molecular strontium hydride complexes are less common compared to the lighter group 2 elements. Whilst simple amides and chelating amines can stabilise strontium hydride clusters,[56,57] extremely bulky ligands are generally necessary to isolate di- and trinuclear complexes.[69,71,81,82]

Whilst hydrogenolysis or silanolysis of **36** provides access to dimeric calcium dihydride, hydrogenolysis of **57a** in THF leads to a complex mixture.[80] A single species repeatedly crystallised from these solutions, and was structurally characterised as the trinuclear cluster dication, [(Me_4TACD)$_3$Sr$_3$(μ-H)$_4$(thf)][B(C_6H_3-3,5-Me_2)$_4$]$_2$ (**59**), which can be rationally synthesised by hydrogenating a 2 : 1 mixture of **57a** and **56b** (Scheme 22).

The trinuclear dication of **59** (Fig. 6) consists of three seven-coordinate strontium centres and can be described as an

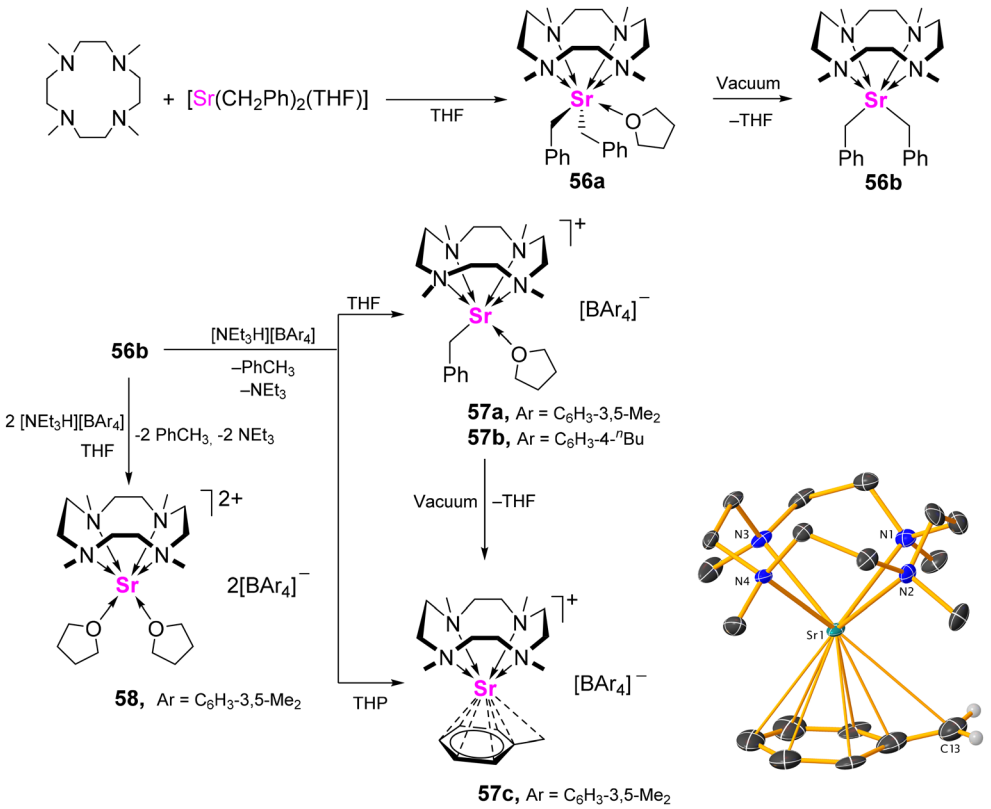

Scheme 21 Synthesis of dibenzyl strontium complexes **56a,b**, cationic benzyl complexes **57a–c**, and strontium bis(borate) salt **58**. Molecular structure of the cationic part of **57c**, with benzylic hydrogen atoms shown.

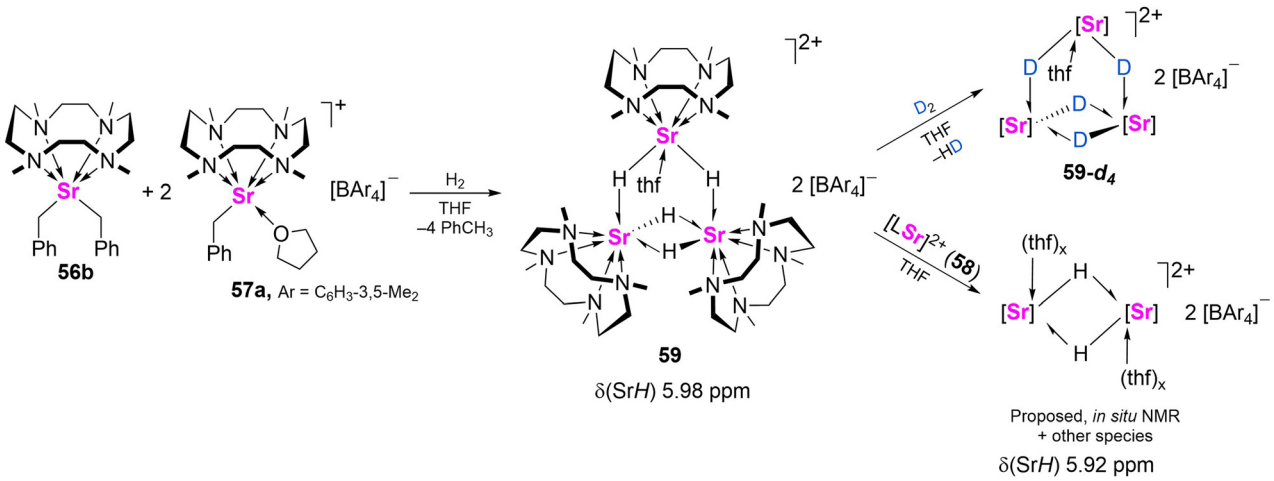

Scheme 22 Synthesis of trinuclear strontium hydride **59**, isotopic exchange with D_2, and proposed formation of dimeric $[L_2Sr_2H_2]^{2+}$ species in solution.

adduct of $[(Me_4TACD)SrH_2(thf)]$, and $[(Me_4TACD)_2Sr_2(\mu\text{-}H)_2]^{2+}$ units, or of two $[(Me_4TACD)SrH_2]$ units and a $[(Me_4TACD)Sr(thf)]^{2+}$ dication. Sr1 bridges Sr2 and Sr3 *via* a hydride ligand and coordinates to a THF ligand, while Sr2 and Sr3 share two bridging hydrides. The ^{1}H NMR spectrum reveals two distinct {(Me$_4$TACD)Sr} environments, with a single hydride resonance at δ 5.98 ppm, indicating rapid hydride exchange between the distinct strontium centres even at −60 °C. Complex **59** rapidly exchanges with D_2, providing the fully deuterated isotopologue after 30 min at room temperature (Scheme 22). Combining **59** and **58** resulted in an additional hydride resonance at δ 5.92 ppm in the ^{1}H NMR spectrum, which was tentatively

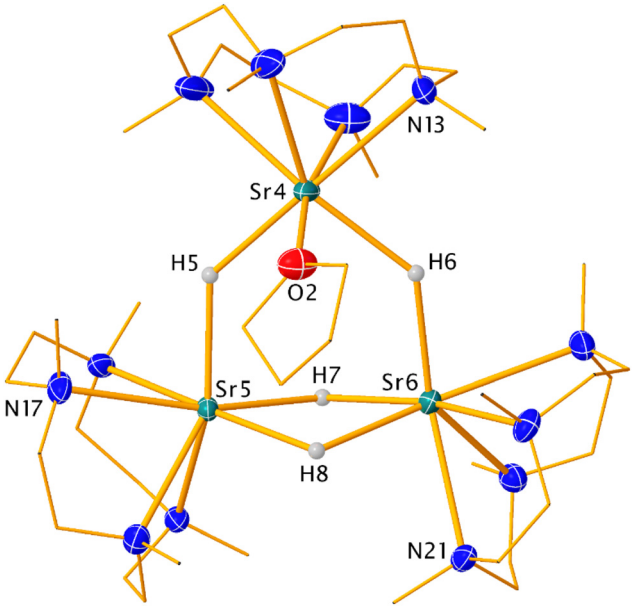

Fig. 6 Molecular structure of the cationic part of trinuclear strontium hydride **59**.[80]

assigned to the elusive $[(Me_4TACD)_2Sr_2(\mu\text{-}H)_2(thf)_x]^{2+}$, although attempts to isolate it remained unsuccessful. Me_4TACD lacks sufficient steric and coordinative demand to prevent redistribution. A stable $[Sr_2H_2]^{2+}$ dication, $[(Me_5PACP)_2Sr_2(\mu\text{-}H)_2][B(C_6H_3\text{-}3,5\text{-}Me_2)_4]_2$, was isolated using the larger 15-membered macrocycle Me_5PACP.[52]

Hydrogenation of an equimolar THF solution of **57a** and **36b** provided the heterobimetallic hydride complex $[(Me_4TACD)_2CaSr(\mu\text{-}H)_2(thf)][B(C_6H_3\text{-}3,5\text{-}Me_2)_4]_2$ (**60**; Scheme 23), which is isostructural to **42d**.[54] The crystal structure of **60** revealed a $Ca(\mu\text{-}H)_2Sr$ core, where the calcium is six-coordinate and the strontium is seven-coordinate with an additional THF ligand. The ^1H NMR analysis of **60** in THF-d_8 showed a major hydride resonance at δ 5.10 ppm, intermediate between homometallic Sr hydride **59** (δ 5.98 ppm) and Ca hydrides **41** (δ 4.72 ppm) and **42** (δ 4.45 ppm).[80] Notably, resonances corresponding to calcium hydride dimers **41** and **42**, and several broad resonances between δ 5.98 and 5.92 ppm for strontium hydrides, were also observed in the spectrum. ^1H–^1H EXSY experiments confirmed rapid exchange between these species, suggesting facile dissociation and recombination of **60** in solution. Thermodynamic studies indicated that Ca–H bonds are more favourable than Sr–H bonds, as excess $[(L)Ca]^{2+}$ shifted the equilibrium toward calcium hydrides. Mixing calcium bis-borate **37b** with calcium–strontium hydride **60** resulted in the selective formation of calcium hydride dimer **41** and strontium bis-borate **58**. Conversely, combining **58** and **60** resulted in the persistence of **60** as the major species, with minor quantities of **41** and **42** and traces of postulated $[(Me_4TACD)_2Sr_2(\mu\text{-}H)_2(thf)_x][B(C_6H_3\text{-}3,5\text{-}Me_2)_4]_2$. Complexes **59** and **60** catalyse *n*-alkene hydrogenation,[80] but quantitative activity comparison with homometallic calcium hydride dimers **41** and **42** is not appropriate due to the aforementioned hydride lability and poorly-defined solution-state speciation.

4.3.3. Strontium hydridosilicate and silanide complexes. Me_4TACD-ligated organocalcium complexes can be converted to molecular hydrides *via* hydrogenation or hydridosilanes. However, reacting **57** with $RSiH_3$ (R = Ph, ^{n}Oct) led to a different outcome compared to hydrogenolysis.[63] When $PhSiH_3$ was employed, $Ph(PhCH_2)SiH_2$, $Ph_2(PhCH_2)SiH$, and SiH_4 were observed in the *in situ* ^1H NMR spectrum, indicating σ-bond metathesis with the benzyl precursor and subsequent organosilane scrambling. The dinuclear hexahydridosilicate complex $[(Me_4TACD)_2Sr_2(\mu\text{-}\kappa^3\text{:}\kappa^3\text{-}SiH_6)(thf)_4][BAr_4]_2$ (**61a**, Ar = C_6H_3-3,5-Me_2; **61b**, Ar = C_6H_4-4-^{n}Bu) was isolated in high yields (91%, **a**; 69%, **b**) (Scheme 24). Compounds **61** are thermola-

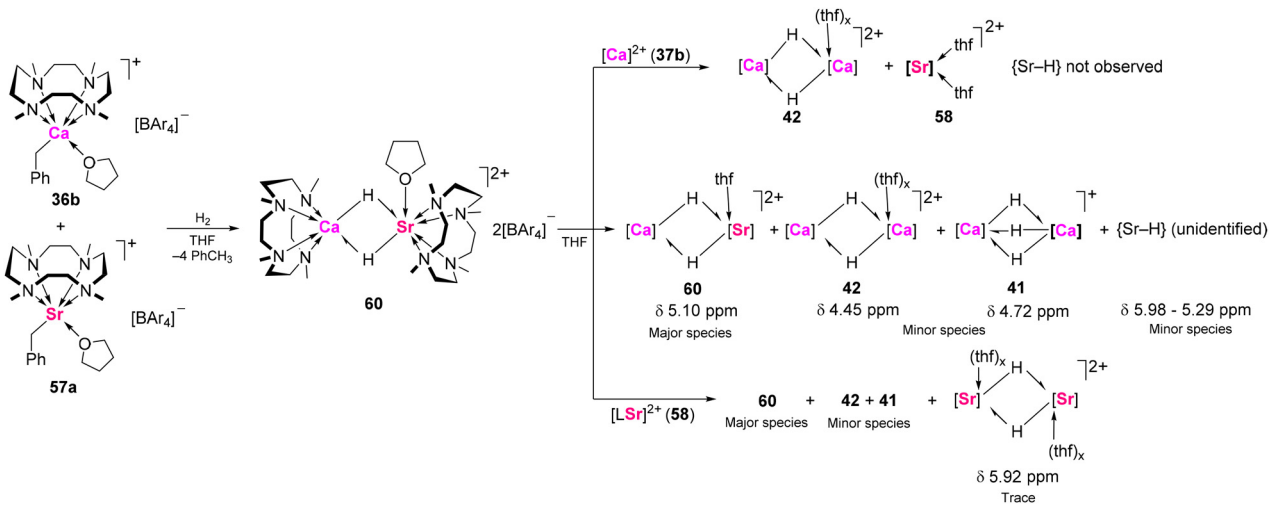

Scheme 23 Synthesis of Sr/Ca hydride **60** and hydride exchange reactions with **37b** and **58** in solution. ^1H NMR chemical shifts are shown for diagnostic hydride resonances. Ar = C_6H_3-3,5-Me_2.

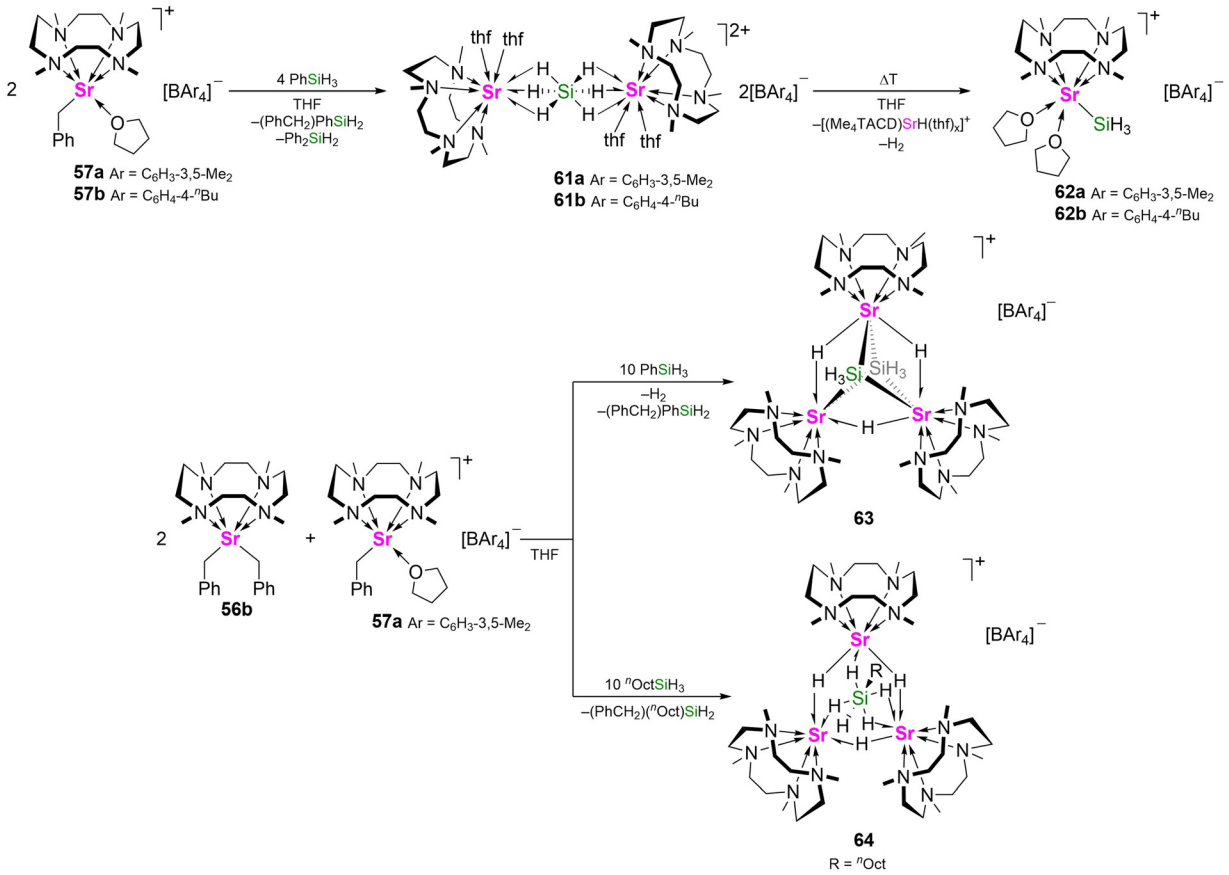

Scheme 24 Synthesis of strontium hydridosilicate complexes **61a,b** and **64**, and silanide complexes **62a,b** and **63**.

bile, decomposing at room temperature with dihydrogen release (also detected by ^{1}H NMR spectroscopy), forming the mononuclear parent silanide complex, [(Me$_4$TACD)Sr(SiH$_3$)(thf)$_2$][BAr$_4$] (**62a**, Ar = C$_6$H$_3$-3,5-Me$_2$; **62b**, Ar = C$_6$H$_4$-4-^{n}Bu).[63] The reaction can be formally considered as the net-reductive elimination of dihydrogen from the hypervalent Si(IV) centre, and dissociation of the putative strontium hydride cation [(Me$_4$TACD)SrH(thf)$_x$]$^+$. A 2 : 1 mixture of **57a** and **57b** with excess phenylsilane at room temperature produced the trinuclear hydride-silanide cluster, [(Me$_4$TACD)$_3$Sr$_3$(μ-H)$_3$(μ$_3$-SiH$_3$)$_2$][B(C$_6$H$_3$-3,5-Me$_2$)$_4$] (**63**). The observed evolution of H$_2$ in this reaction also suggests the dehydrogenation of a hypervalent silicate species.

Similarly, the synthesis and isolation of a carbozolido barium silanide complex *via* metathesis of a hexamethyldisilazide precursor with PhSiH$_3$ has been reported; the {SiH$_3$}$^-$ moiety was found to act either as nucleophilic silanide, or as a hydride surrogate.[83] Heavy alkaline-earth elements facilitate hydrido(aryl)silanes redistribution, but using ^{n}OctSiH$_3$ as hydride source suppresses such redistribution reactions, yielding the trinuclear hydride-hydridosilicate cluster, [(Me$_4$TACD)$_3$Sr$_3$(μ-H)$_3$(μ$_3$-SiH$_5$(^{n}Oct))][B(C$_6$H$_3$-3,5-Me$_2$)$_4$] (**64**) with the *n*-alkyl group intact. Compound **64** was rationally synthesised in 65% yield by reacting a 2 : 1 mixture of **56b** and **57a** with a ten-fold excess of ^{n}OctSiH$_3$ (Scheme 24). These complexes likely result from two-fold nucleophilic addition of highly reactive [(Me$_4$TACD)SrH]$^+$ units to either SiH$_4$ (derived from [(Me$_4$TACD)SrH]$^+$ mediated organosilane scrambling), or ^{n}OctSiH$_3$. This interpretation corroborates with the broadened and exchanging hydride resonances observed for calcium hydride **42d** and PhSiH$_3$ mixture, where Ph$_2$SiH$_2$ and SiH$_4$ are also observed, implicating hydridosilicate species.[54]

Similar hydridosilicate complexes were not isolated for the analogous reaction of either **36**, **39**,[42,54] or [(Me$_5$PACP)Sr(CH$_2$Ph)(thf)][BAr$_4$] (Ar = C$_6$H$_3$-3,5-Me$_2$ or C$_6$H$_4$-4-^{n}Bu)[52] with RSiH$_3$, suggesting that the kinetic stability of **61** depends on the high nucleophilic character of the Sr–H bonds, and the moderate size of the Me$_4$TACD ligand relative to the ionic radius of Sr^{2+}. Previously, a dinuclear ruthenium hexahydridosilicate complex [{(PhB(CH$_2$PPh$_2$)$_3$)Ru}$_2${μ–η^4,η^4-SiH$_6$}] was reported.[84] In this case, the {SiH$_6$} unit binds to the ruthenium centres *via* covalent 3-centre-2-electron bonding interactions. By contrast, the interaction between Sr and {SiH$_6$} in **61** is predominantly electrostatic, as indicated by NMR and vibrational spectroscopy, as well as DFT calculations. Recently, a comparable calcium–potassium hexahydridosilicate complex [(NON)$_2$Ca$_2$K$_2$(μ$_4$–κ^3:κ^3:κ^2:κ^2-SiH$_6$)(thf)$_2$] (NON = 4,5-bis(2,6-diisopropylanilido)-2,7-di-*tert*-butyl-9,9-dimethyl-xanthene) was

reported, and similarly reacts as a masked metal hydride under SiH_4 elimination.[64] Unlike **61**, $[(NON)_2Ca_2(\mu_4\text{–}\kappa^3\text{:}\kappa^3\text{:}\kappa^2\text{:}\kappa^2\text{-}SiH_6)(thf)_2]$ is stable in benzene at room temperature, probably due to a more robust binding cavity offered by the tetranuclear Ca_2K_2 assembly compared to the labile dinuclear structure of **61**. A strontium–potassium pentahydrido(aryl)silicate complex $[(NON)_2Sr_2K_2(\mu_4\text{–}\kappa^3\text{:}\kappa^3\text{:}\kappa^2\text{:}\kappa^2\text{-}PhSiH_5)(thf)_2]$ reminiscent of **64** was also reported.[64]

Single crystal X-ray diffraction revealed the cationic part of **61** to formally contain an $[SiH_6]^{2-}$ dianion sandwiched in a $\mu\text{–}\kappa^3\text{:}\kappa^3$-fashion between two $[(Me_4TACD)Sr(thf)_2]^{2+}$ dications (Fig. 7). The dinuclear core exhibits flexibility around the Sr–Sr axis. In the solid-state, **61a** contains a non-centrosymmetric dication with a *gauche* arrangement of the neutral ligands on each Sr, whilst **61b** is crystallographically centrosymmetric, with an anti-periplanar arrangement.

Compound **61** was characterised by NMR spectroscopy at low temperatures due to its instability in THF above 0 °C. In the ^{1}H NMR spectrum, the hydrides appeared as a singlet at δ 5.39 ppm, sharpening when cooled to −40 °C. Direct ^{29}Si NMR measurement of **61** was unsuccessful, but at −40 °C, a signal was observed by ^{29}Si–^{1}H HSQC and HMBC experiments at δ_{Si} −172.6 ppm, appearing as a doublet with a coupling constant $J(^{29}Si\text{–}^1H)$ = 118 Hz. These spectroscopic features indicate largely ionic Sr–H bonding interactions and thus a relatively unperturbed $[SiH_6]^{2-}$ dianion compared to $[\{(PhB(CH_2PPh_2)_3)Ru\}_2\{\mu\text{–}\eta^4,\eta^4\text{-}SiH_6\}]$, whose more covalent Ru–H bonding results in smaller ^{29}Si–^{1}H coupling constant, upfield shifted ^{29}Si resonance in the NMR spectrum, and longer Si–H distances.[84] Similarly, $[(NON)_2Ca_2(\mu_4\text{–}\kappa^3\text{:}\kappa^3\text{:}\kappa^2\text{:}\kappa^2\text{-}SiH_6)(thf)_2]$ exhibited hydride resonances at δ 5.38 ppm, and a ^{29}Si signal at δ −261.2 ppm.[64] A Si–H stretching absorption was observed in the ATR-IR spectrum of **61a** at ν = 1717 cm^{-1}, similar to previously reported values for K_2SiH_6 and $[\{(PhB(CH_2PPh_2)_3)Ru\}_2\{\mu\text{–}\eta^4,\eta^4\text{-}SiH_6\}]$. In contrast, the ATR-FTIR spectrum of $[(NON)_2Ca_2(\mu_4\text{–}\kappa^3\text{:}\kappa^3\text{:}\kappa^2\text{:}\kappa^2\text{-}SiH_6)(thf)_2]$ showed three bending modes at 1053, 1013, and 976 cm^{-1}, and three stretching modes at 1620, 1558, and 1503 cm^{-1}.[64]

The crystal structure of **64** features a triangular Sr_3 core with each metal bridged by a μ-H ligand, while an octahedral $[^n OctSiH_5]$ unit bridges all three metals *via* four equatorial hydrides and one terminal hydride (Fig. 8). ^{1}H NMR spectroscopy shows rapid hydride exchange at room temperature, giving a broad resonance at δ 5.66 ppm, which splits into a complex pattern of resonances at −80 °C. At −80 °C, a resonance at δ_{Si} 112.4 ppm was observed in a ^{29}Si–^{1}H HSQC experiment. The crystal structure of **63** contains a similar μ-H bridged triangular Sr_3 core to that in **64**, with the trigonal bipyramidal cluster capped by two μ_3-SiH_3 ligands.

Compound **61** acts as a masked equivalent of the elusive dimeric strontium hydride $[(Me_4TACD)_2Sr_2(\mu\text{-}H)_2(thf)_x]^{2+}$; reacting with Brønsted acid $[NEt_3H][B(C_6H_3\text{-}3,5\text{-}Me_2)_4]$, CO_2, or oxidant 1,3,5,7-cyclooctatetraene (COT), to eliminate SiH_4 and yield strontium hydride-based products (Scheme 25). Specifically, $[NEt_3H][B(C_6H_3\text{-}3,5\text{-}Me_2)_4]$ yielded the bis(borate) salt **58**, CO_2 provided the dimeric formate $[(Me_4TACD)_2Sr_2(\mu\text{-}OCHO)(thf)_2][B(C_6H_3\text{-}3,5\text{-}Me_2)_4]_2$ (**65**), and COT was reduced under loss of H_2 to form the dinuclear inverse sandwich compound $[(Me_4TACD)_2Sr_2(\mu\text{–}\eta^8\text{:}\eta^8\text{-}COT)][B(C_6H_3\text{-}3,5\text{-}Me_2)_4]_2$ (**66**).[63] Based on literature precedent for the formation of $[(BDI^{dipp})_2Ca_2COT]$,[85] **66** is most likely formed through an even-electron insertion–deprotonation sequence, rather than *via* two-fold single electron reduction of the conjugated tetraene. It is noteworthy that calcium hydride complex **42d** is unreactive towards COT; formation of $[(Me_4TACD)_2Ca_2(\mu\text{–}\eta^8\text{:}\eta^8\text{-}COT)][B(C_6H_3\text{-}3,5\text{-}Me_2)_4]_2$ (**67**) was instead achieved by *in situ* reduction with caesium metal and salt metathesis of iodide complex **50**.[42]

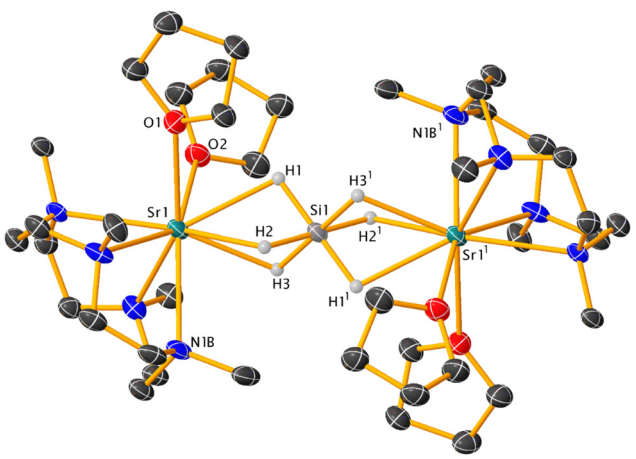

Fig. 7 The molecular structure of dication $[\mathbf{61b}]^{2+}$, with only silicon-bound hydrogen atoms.[54]

4.4. Barium

The molecular coordination chemistry of barium is far less studied than that of lighter group 2 elements, especially for organo- and hydridobarium complexes. The large size, extremely low electronegativity, and dominance of undirectional ionic bonding make isolating well-defined, low-nuclearity, and heteroleptic complexes a significant challenge.[86]

Neutral and cationic Me_4TACD barium benzyl complexes were prepared using a method similar to that of lighter homologues. Adding Me_4TACD to a THF-suspension of $[Ba(CH_2Ph)_2]$ yields a yellow solution from which the neutral dibenzyl complex $[(Me_4TACD)Ba(CH_2Ph)_2]$ (**68**) crystallised (Scheme 26).[87] Comparing its crystal structure to related calcium (**34**) and strontium (**56a**) complexes highlights differences in coordination. Whereas **34** contains a six-coordinate calcium centre and two η^1-benzyl ligands, the larger Sr^{2+} cation accommodates an additional THF molecule, with both benzyl ligands remaining η^1-bound. Whilst the still-larger Ba^{2+} is expected to adopt a yet-higher coordination number *via* ligation of additional solvent molecules, **68** is THF-free, and the coordination sphere is satisfied by slipped η^2 and η^3-bound benzyl ligands. This is consistent with the high lability of Ba-THF bonds and π-acidity of the softer metal cation.

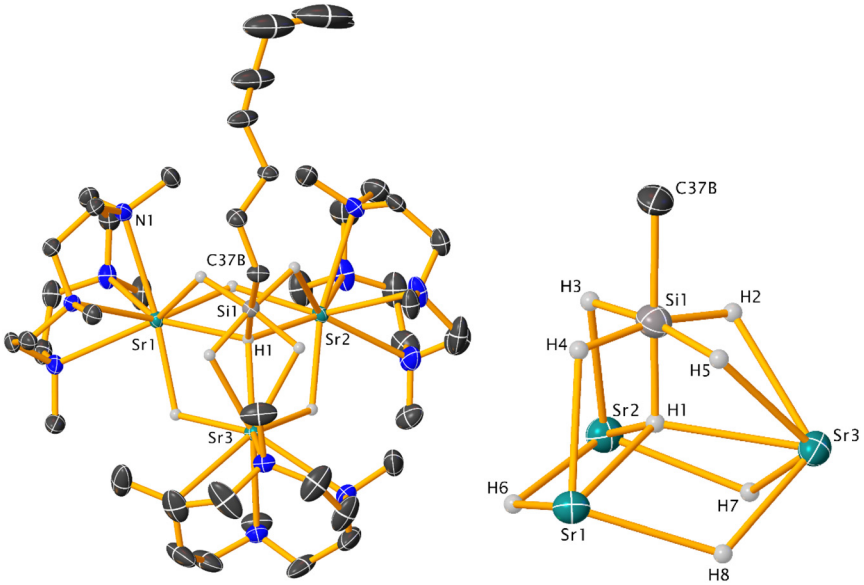

Fig. 8 Cationic part of the molecular structure of compound **64** with hydrogen atoms omitted except for hydride ligands (left); the $\{Sr_3H_3(RSiH_5)\}$ core of **64** without ligands and *n*-octyl chain (right).[54]

Protonolysis of **68** with $[NEt_3H][B(C_6H_3\text{-}3,5\text{-}Me_2)_4]$ provided the cationic benzyl complex $[(Me_4TACD)Ba(CH_2Ph)(thf)_x][B(C_6H_3\text{-}3,5\text{-}Me_2)_4]$ (**69**), which was not crystallographically characterised, but shows downfield shifted C*H*$_2$ resonance in the ^{1}H NMR, suggesting increased benzyl hapticity.

Hydrogenolysis of **68** resulted in the release of free Me_4TACD, toluene, and the precipitation of $[BaH_2]_n$ (Scheme 26). The *in situ* ^{1}H NMR spectrum displayed a broad resonance at δ 9.4 ppm, attributed to soluble oligomeric barium hydride clusters. Hydrogenolysis of **69** resulted in the formation of the THF insoluble dimeric dihydride cation $[(Me_4TACD)_2Ba_2(\mu\text{-}H)_2(thf)_4][B(C_6H_3\text{-}3,5\text{-}Me_2)_4]_2$ (**70**), which crystallised directly from the reaction mixture (Scheme 26). Complex **70** represents a rare crystallographically characterised molecular barium hydride. Heptanuclear and tetradecanuclear clusters $[Ba_7H_7(N(SiMe_3)_2)_7]\cdot 2C_6H_6$ and $[Ba_{14}H_{12}\{N(SiMe_3)_2\}_{12}\{(Me_3Si)(Me_2SiCH_2)N\}_4]$ were also structurally characterised.[88] The only other examples of dinuclear species are $[(Tp^{Ad,iPr})_2Ba_2(\mu\text{-}H)_2]$ ($Tp^{Ad,iPr}$ = hydrotris(3-adamantyl-5-isopropyl-pyrazolyl)borate)[89] and $[(\eta^5\text{-}C_5R_5)_2Ba_2(\mu\text{-}H)_2(DABCO)]$ (R = C_6H_3-3,5-^{i}Pr),[71] which are supported by extremely bulky 5-electron donor L_2X-type ligands. Although insolubility precluded characterisation of **70** by NMR spectroscopy, the crystal structure reveals the dicationic part to consist of two eight-coordinate barium centres each bound to the κ^4-Me_4TACD, two μ-hydrides, and two THF molecules (Fig. 9). The higher coordination number compared to that of the lighter metals in **60** and **42** reflects the large size of the Ba^{2+} cation and its tendency to adopt higher coordination geometries.

The isolation of the barium hydride **70** is notable given the extreme lability and inaccessibility of the putative strontium congener $[(Me_4TACD)_2Sr_2(\mu\text{-}H)_2(thf)_x]^{2+}$. Its isolation, likely aided by its insolubility, prevents ligand redistribution in solution. Given the success in employing the large 15-membered *NNNNN* macrocycle Me_5PACP to strontium,[52,53] and the often-higher activity of barium catalysts compared to the lighter group 2 elements,[58,71,76,77,86] soluble complexes with $[Ba_2H_2]^{2+}$ moiety supported by large aza-macrocycles may be of interest. Indeed, preliminary results suggest that a soluble molecular barium hydride can be accessed by hydrogenolysis of a benzyl barium cation supported by a very large 18-membered *NNNNNN* macrocycle, $[(Me_6HACO)Ba(CH_2Ph)][B(C_6H_3\text{-}3,5\text{-}Me_2)_4]$ (Me_6HACO = *N*,*N*′,*N*″,*N*‴,*N*⁗,*N*⁗′-hexamethyl-1,4,7,10,13,16-hexaazacyclooctadecane), although isolation and characterisation of the proposed hydride product remains unrealised.[90]

5. Group 12 metals

Although part of the d-block, zinc is considered a main-group element due to the stable closed-shell $3d^{10}$ electronic configuration. While zinc(II) shares some chemical similarities with magnesium(II), its higher electronegativity and increased covalent contributions lead to notable differences. Whilst no Me_4TACD complexes of highly toxic cadmium and mercury are known to date, the solution-state binding of Me_4TACD to Zn^{2+} and Cd^{2+} as aqueous nitrate salts has been studied alongside other aza-macrocyclic ligands.[91,92] The steric and coordinative demand of Me_4TACD on the relatively small Zn^{2+} cation (five-coordinate effective ionic radius 0.68 Å)[93] is such that the invariably five-coordinate metal centre is coordinatively oversaturated. The fifth coordination site is occupied by a Lewis-basic L-type ligand in a dicationic complex or by an X-type ligand (X = halide, hydride) in a monocationic complex. $[(Me_4TACD)ZnX][HBPh_3]$ salts are active catalysts in the hydro-

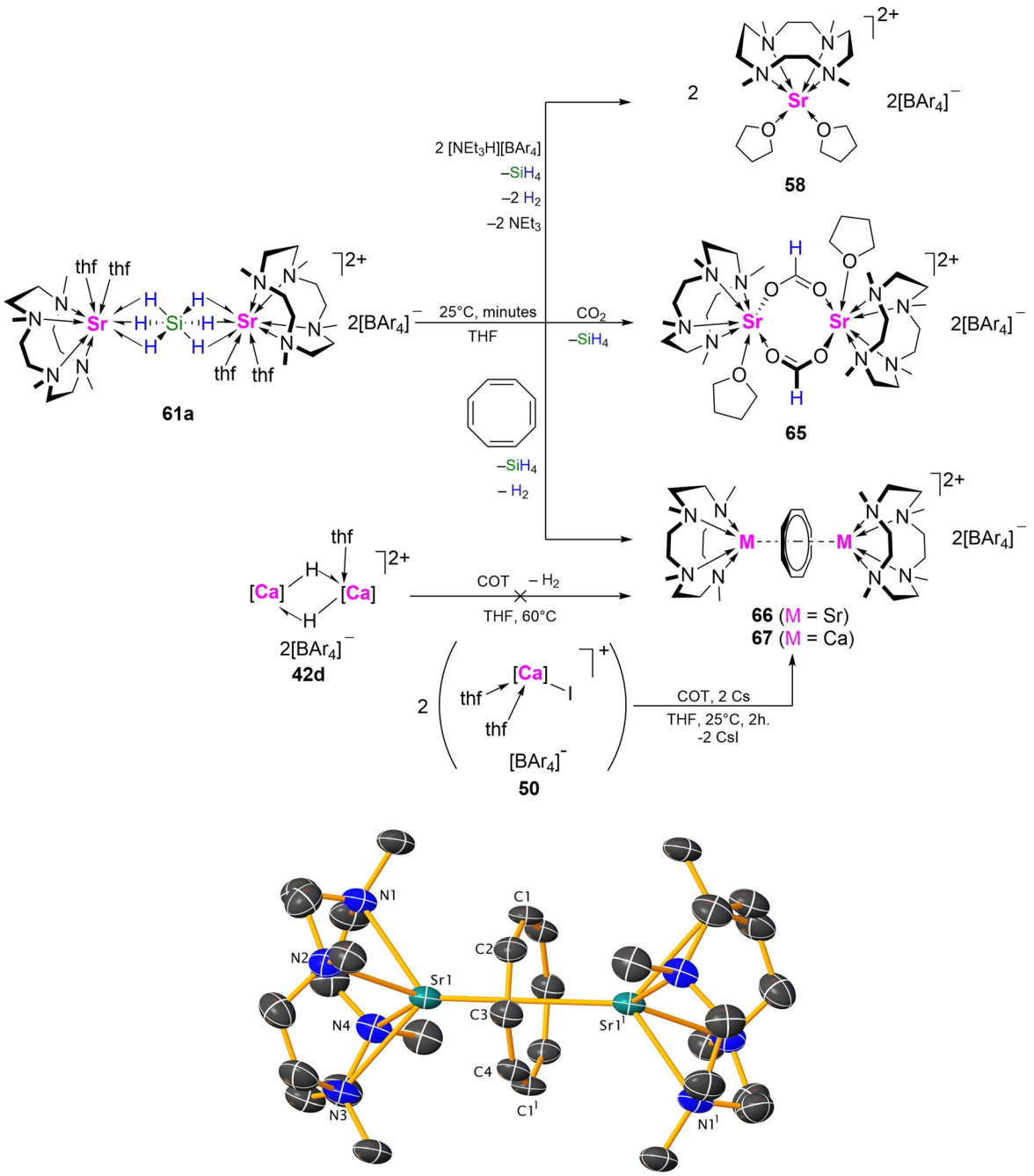

Scheme 25 Reactivity of hexahydridosilicate complex **61a** to give bis(borate) **58**, formate **65**, and cyclooctadienyl complex **66**. For comparison, calcium hydride **42d** is unreactive towards 1,3,5,7-cyclooctadiene; calcium cyclooctadienyl complex **67** is accessed from iodide **50** *via* caesium-mediated reduction and salt-metathesis. Dicationic part of the crystal structure of complex **66**. Ar = C_6H_6-3,5-Me_2.

boration and hydrosilylation of polar organic substrates, and the $[(Me_4TACD)ZnH]^+$ cation displays hydride-centred nucleophilicity towards electrophilic CO_2. The resolute coordinative saturation, however, restricts more complex metal-centred reactivity compared to heavier alkaline-earth derivatives or related $[L_nZnX]^+$ cations supported by di- and tridentate ligands. Me_4TACD has also recently been employed as a ligand for dizinc(I) complexes.

5.1. Zinc(II)

All crystallographically characterised Me_4TACD zinc complexes reported to date adopt a distorted square pyramidal geometry within a five-coordinate (di)cation structure. Complexation of zinc dihalides with Me_4TACD in THF leads to auto-ionisation, forming charge-separated salts $[(Me_4TACD)ZnX]X$ (**71a**, X = Cl; **71b**, X = Br; **71c**, X = I), in high yields (Scheme 27).[94] Anion

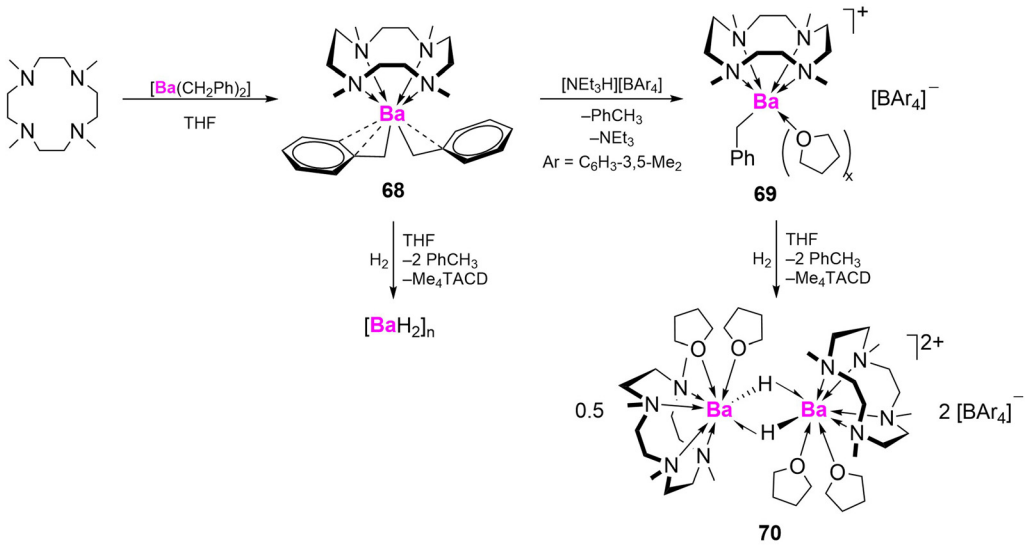

Scheme 26 Synthesis of barium benzyl complexes **68** and **69** and their respective hydrogenolysis to give BaH_2 and **70**. Ar = C_6H_6-3,5-Me_2.

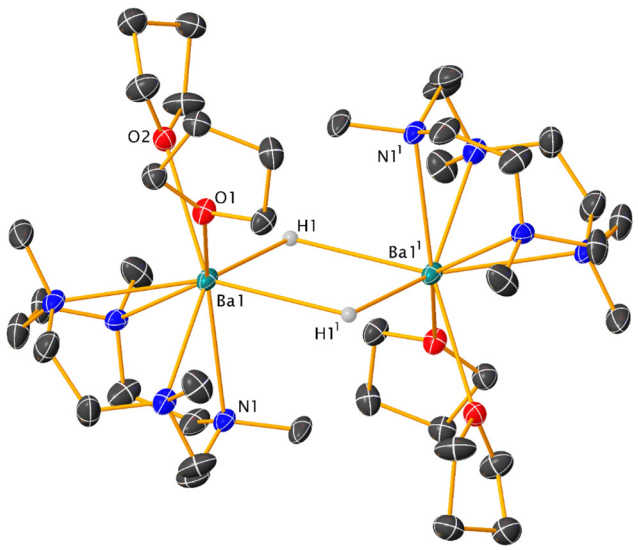

Fig. 9 Dicationic part of the crystal structure of barium hydride **70** with hydrogen atoms omitted except for barium-bound hydrides.[87]

exchange with Na[BPh_4] or K[$HBPh_3$] provided access to cationic halide complexes [(Me_4TACD)ZnX][$HBPh_3$] (**72a**, X = Cl; **72b**, X = Br; **72c**, X = I)[94] and [(Me_4TACD)ZnCl][BPh_4] (**73**)[95] in high yields (Scheme 27). A two-fold halide abstraction was carried out by reacting Me_4TACD with ZnI_2 and two equiv. Ag[BF_4] or Ag[PF_6] in one pot, yielding dicationic acetonitrile complexes [(Me_4TACD)Zn($NCCH_3$)][A]$_2$ (**74a**, [A] = BF_4; **74b**, [A] = PF_6; Scheme 27).[96] Compounds **73** and **74** were employed as diamagnetic diluents in magnetic relaxation studies of isostructural Cu(II) congeners.[95–97] Hydridotriphenylborate complexes **72a–c** react with CO_2 *via* insertion into the H–B bond to provide formatotriphenylborate salts [(Me_4TACD)ZnX][HCO_2BPh_3] (**75a**, X = Cl; **75b**, X = Br; **75c**, X = I; Scheme 27).[94]

Cationic amido zinc complex [(Me_4TACD)Zn($N(SiMe_2H)_2$)][$HBPh_3$] (**72d**) was prepared by BPh_3 mediated hydride abstraction of [$Zn(N(SiMe_2H)_2)_2$]$_2$ in the presence of Me_4TACD, with elimination of the cyclic silazane [$(Me_2HSiN)_2(SiMe_2)_2$] (Scheme 28).[94] Like its halide analogues, **72d** reacts with CO_2 through rapid insertion into the B–H bond, forming formatoborate salt [(Me_4TACD)Zn($N(SiMe_2H)_2$)][HCO_2BPh_3] (**75d**).

Zinc dihydride [ZnH_2]$_n$ does not react with Me_4TACD alone but reacts with Lewis acids in the presence of neutral *N*-donors to provide molecular complexes. Reaction of [ZnH_2]$_n$ with Me_4TACD in the presence of BPh_3 yields a five-coordinate zinc hydride cation [(Me_4TACD)ZnH][$HBPh_3$] (**76a**; Scheme 29).[98] A similar, four-coordinate charge-separated species [(PMDTA)ZnH][$HBPh_3$] was obtained using tridentate PMDTA, but bidentate *N*-donors provide four-coordinate dihydrides [(L)Zn(H)(μ_2-H)BPh_3], with a μ_2-hydride bridging the zinc and boron centres.[98] The cationic zinc hydride cation was also obtained as tetraarylborate salts, [(Me_4TACD)ZnH][BAr_4] (Ar = C_6H_3-3,5-Me_2 (**76b**), C_6H_3-3,5-$(CF_3)_2$ (**76c**)) by combining zinc dihydride with Brønsted acidic [(Me_4TACD)H][BAr_4] in THF.[99]

CO_2 rapidly inserts into both B–H and Zn–H bonds of **76a** to provide charge-separated zinc formate-formatoborate complex [(Me_4TACD)Zn(κ*O*-OCHO)][(OCHO)BPh_3] (**77a**),[98] or into the Zn–H bond of **76b** to form formatozinc cation [(Me_4TACD)Zn(κ*O*-OCHO)][BAr_4] (**77b**; Scheme 29).[99] The terminal formate ligand in **77a** and **77b** binds zinc in a κ*O* manner. The direct reaction of [ZnH_2]$_n$ with CO_2 in the presence of Me_4TACD yielded the charge-separated diformate [(Me_4TACD)Zn(κ*O*-OCHO)][OCHO] (**77c**), unlike acyclic bi- and tri-dentate polyamines, which form monomeric diformate complexes [(L_n)Zn$(OCHO)_2$] (L_n = TMEDA, TEEDA, TMPDA, PMDTA).[98]

Compound **76b** also reacts with BH_3·thf to form the mononuclear tetrahydridoborate [(Me_4TACD)Zn(μ-H)$_2BH_2$][BAr_4] (**78**, Ar = C_6H_3-3,5-Me_2).[99] The η^2 binding mode of the tetrahydrido-

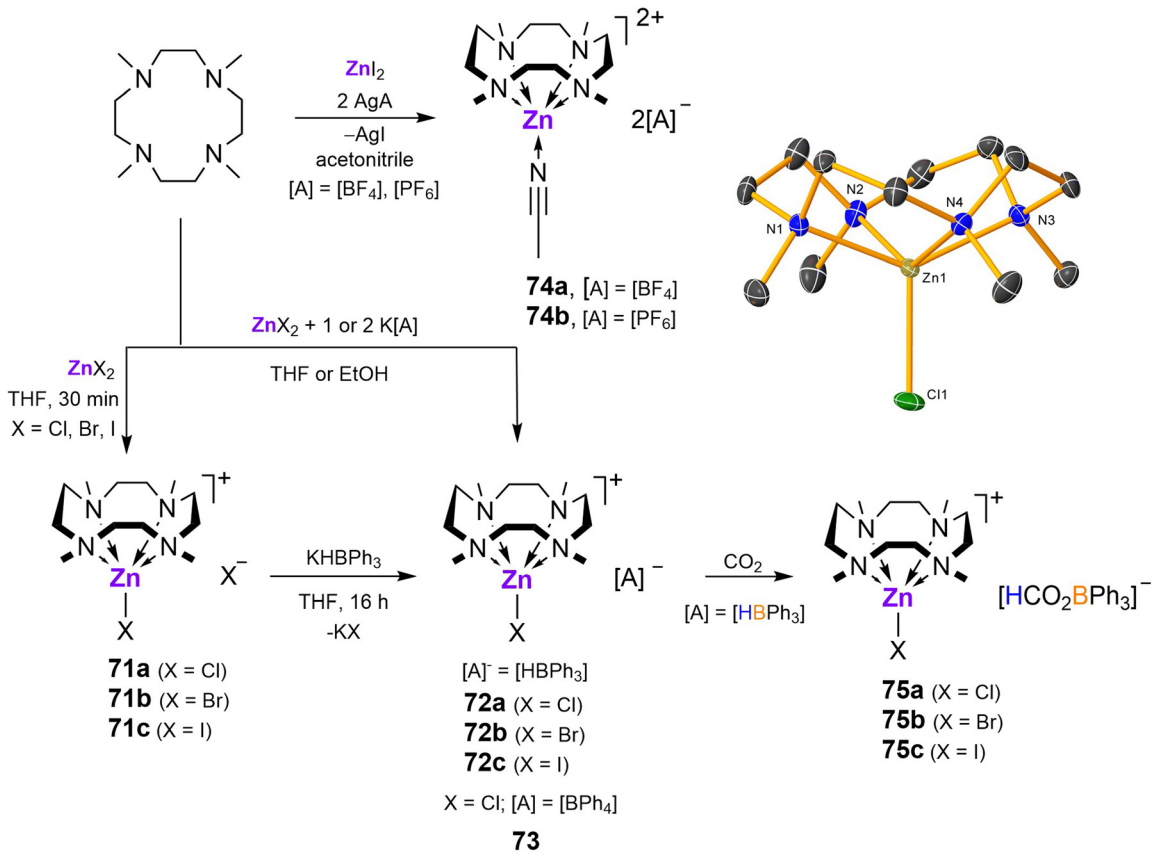

Scheme 27 Complexation of zinc dihalides by Me_4TACD, anion-exchange derivatives, and reactivity of hydridoborate derivatives towards CO_2. Cationic part of the crystal structure of compound **73** (H-atoms omitted).[94–96]

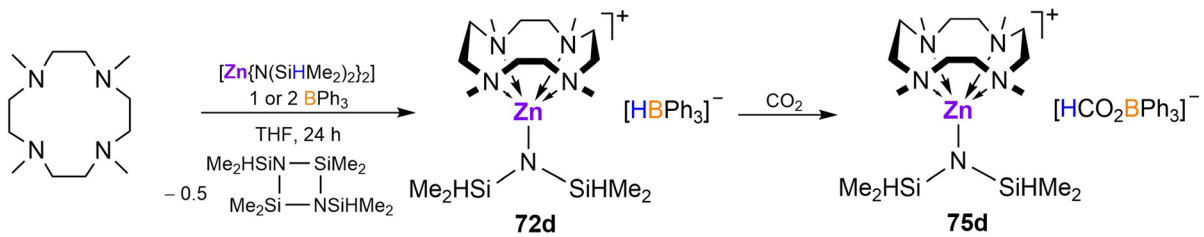

Scheme 28 Synthesis of amidozinc hydridoborate complex, and its reactivity towards CO_2.[94]

borate moiety in **78** contrasts to the η^3-coordinated tetrahydridoborate in the congeneric magnesium complex **24**.[47]

5.1.1. Catalysis mediated by [(Me_4TACD)ZnX][$HBPh_3$] complexes. Zinc $[HBPh_3]^-$ derivatives were employed as catalysts for hydrofunctionalisation of polar substrates (Table 1). Complexes **72a–d** were tested for hydroboration of ketones, imines, esters, amides, pyridine, and CO_2 using HBpin as hydride source.[94] The amide derivative **72d** exhibited the highest activity, readily hydroborating benzophenone, benzimine, and pyridine under mild conditions, although alkali- and alkaline-earth derivatives were more active.[36,100] CO_2 was reduced to MeOBpin and pinBOBpin in 16 h at 60 °C. Complex **76a** catalyses selective CO_2 hydrosilylation to formate using *n*-butyldimethylsilane as hydride source.[98] The silylformate was obtained in quantitative spectroscopic yields with 5 mol% **76a** at 70 °C under 1 bar CO_2 in 48 h. Although silane conversion occurred as quickly as with bi- and tri-dentate derivatives, methoxysilane formation was minimal for the tetradentate macrocycle due to the oversaturation of the five-coordinate zinc centre.

The tetraarylborate derivative **76b** is inactive in the hydrosilylation of CO_2. Crystals of the zinc formate-hydridoborate salt [(Me_4TACD)Zn(κ*O*-OCHO)][$HBPh_3$] (**77d**, Fig. 10) were obtained from a concentrated reaction solution of the hydrosilylation of CO_2 with *n*-butyldimethylsilane and catalyst **77a**, which may imply that the zinc formate cation is itself incap-

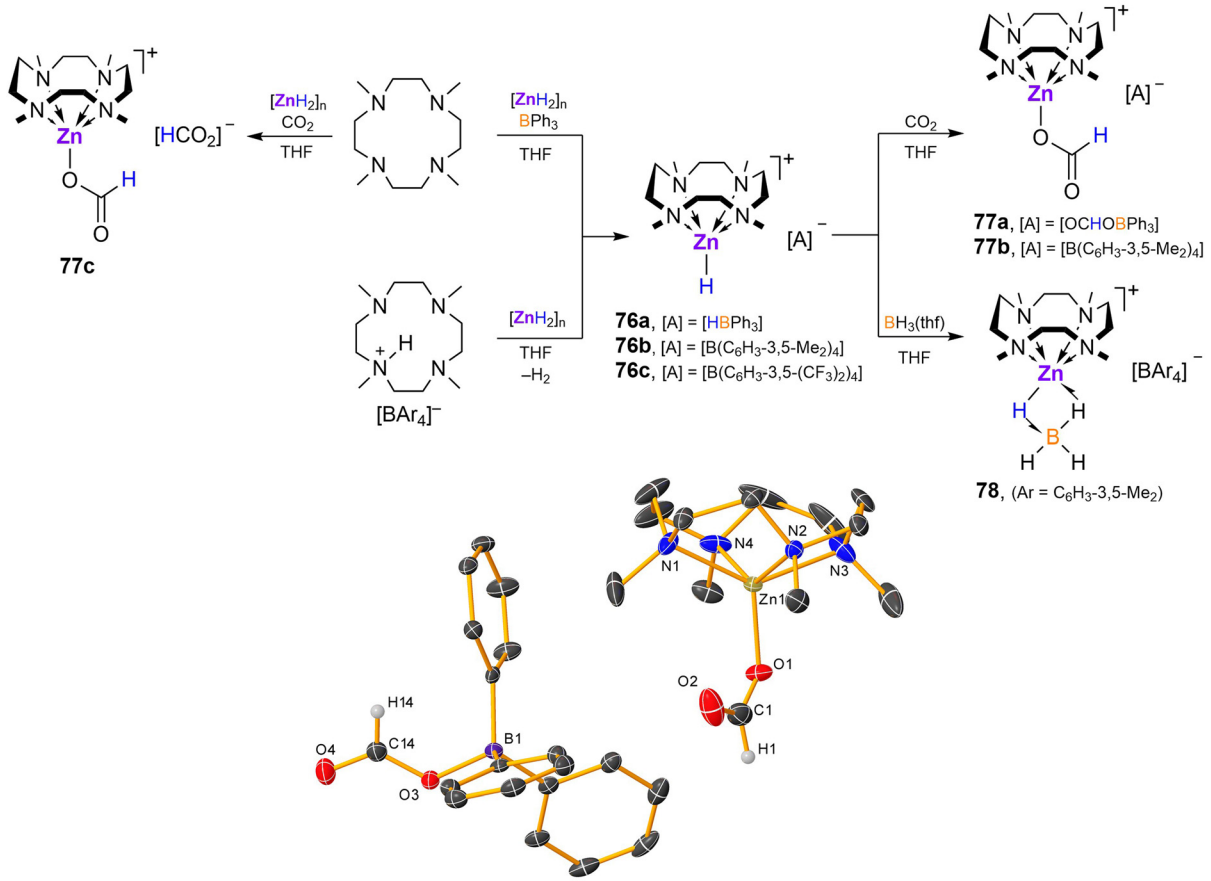

Scheme 29 Reaction of $[ZnH_2]_n$ with Me_4TACD in the presence of Lewis acids BPh_3 or CO_2, reaction of $[ZnH_2]_n$ with $[(Me_4TACD)H]^+$, and onward reactivity of hydridozinc cations toward CO_2 and BH_3·thf.[98,99] Crystal structure of compound **77a** (H-atoms omitted except for H1 and H14).[98]

able of turnover.[99] Notably, zinc hydride cations $[(L_n)ZnH][BAr_4]$ supported by acyclic ligands (L_n = TMEDA, TEEDA, PMDTA, Me_6TREN; Ar = C_6H_3-3,5-$(CF_3)_2$) are far more active in the catalytic hydrosilylation and hydroboration of CO_2.[101,102] Thus, combined hydricity and Lewis acidity is essential for active catalysis; the steric and coordinative demand of the strongly chelating Me_4TACD macrocycle quenches Lewis acidity and coordinative availability of the zinc centre and precludes zinc-mediated catalysis.

5.2 Zinc(I)

The unsymmetrical dizinc(I) cation $[Cp^*ZnZn(Me_4TACD)][BAr_4]$ (**79**; Ar = C_6H_3-3,5-Me_2), synthesised from $[Cp^*_2Zn_2]$ and $[(Me_4TACD)H][BAr_4]$ under elimination of Cp*H (Scheme 30),[103] is unreactive towards further equivalents of $[(Me_4TACD)H][BAr_4]$. The dizinc(I) dication $[(Me_4TACD)_2Zn_2]^{2+}$ was instead accessed by reacting **79** with HBpin, providing $[(Me_4TACD)_2Zn_2][BAr_4]$ (**80**) in 30% yield (Scheme 30).[103] The Zn–Zn bond in **79** is somewhat longer (2.3510(3) Å) compared to that in $[Zn_2Cp^*_2]$ (2.302(1) Å), whilst **80** shows an elongated Zn–Zn bond of 2.4860(6) Å, significantly longer than those in analogous $[Zn_2L_6]^{2+}$ dications (2.36–2.41 Å; L = THF, DMAP).[104,105]

Compound **79** mediates the heterolysis of activated C–H bonds in N≡CCH_3 and PhC≡CH in the presence of catalytic Me_4TACD (10 mol%) as a Brønsted base, providing organozinc (II) complexes $[(Me_4TACD)ZnR][BAr_4]$ (**81a, b**; R = $H_2CC{\equiv}N$, C≡CPh; Scheme 31).[103]

6. Group 13 metals

Protonolysis of organo- and hydrido-triel precursors with tetraaryl borate salts of $[(Me_4TACD)H]^+$ yielded (di)cationic hydride complexes $[(Me_4TACD)AlH_2]^+$ and $[(Me_4TACD)MH]^{2+}$ (M = Al, Ga), and univalent cations $[(Me_4TACD)M]^+$ (M = Ga, In, Tl). The small ionic radius of Al^{3+} and Ga^{3+} resulted in an unusual, folded ligand conformation for $[(Me_4TACD)AlH_2]^+$ and Brønsted acidic reactivity of the Ga–H bond for coordinatively saturated $[(Me_4TACD)GaH]^{2+}$. The acid–base chemistry of the Ga(I)–(III) couple was studied.

6.1. Aluminium

The dihydridoaluminium cation $[(Me_4TACD)AlH_2][BAr_4]$ (**82a**, Ar = C_6H_3-3,5-Me_2; **82b**, Ar = C_6H_3-3,5-$(CF_3)_2$) was synthesised in near quantitative yields by reacting $Et_3N{\cdot}AlH_3$ with $[(Me_4TACD)H][BAr_4]$ (Scheme 32).[28] The macrocyclic ligand in

Table 1 Hydroboration and hydrosilylation mediated by Me_4TACD-zinc hydridotriphenylborates[94,98]

Precatalyst (loading), reducing agent	Substrate	Products
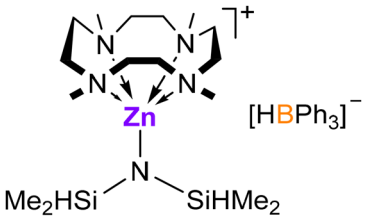 **72d** (10 mol%) 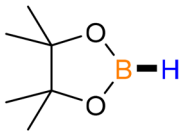	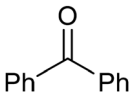	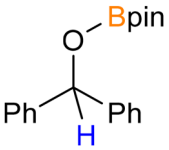
	CO_2	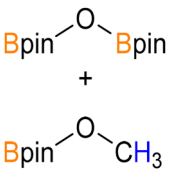
	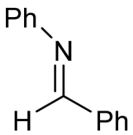	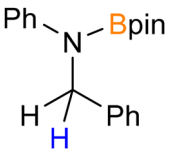
	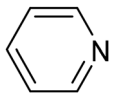	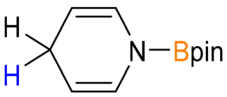
	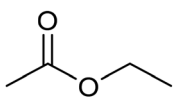	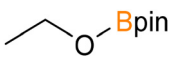
	CO_2	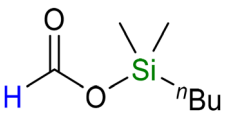
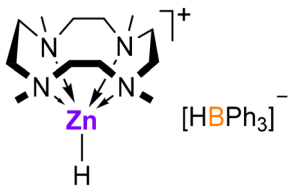 **76a** (5 mol%) 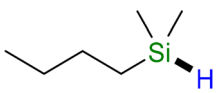		

82 adopts a rare *syn–syn–syn–anti* configuration in both solid and solution states, with one methyl group pointing towards the distal face of the complex, away from the metal centre.

The crystal structure of **82b** reveals a slightly distorted *mer*-octahedral geometry, with the two hydride ligands *cis* to one another (Fig. 11). Due to macrocyclic strain, the Al1–N1 distance (2.466(3) Å) is significantly longer than the other Al–N distances (2.091(3), 2.096(3), 2.145(3) Å), with NBO analysis indicating a low Wiberg Bond Index (WBI) for this Al–N interaction compared to the others. This folded conformation was previously observed only as a minor crystalline component in the solid-state structure of **27**, which exists in an exclusively all-*syn* conformation in solution.[27] Complex **82** represents the steric limit of the 12-membered macrocycle in chelating a small ion (effective ionic radius for six-coordinate aluminium, 0.535 Å)[93] whilst accommodating two hydride ligands. The related 14-membered macrocycle Me_4cyclam reacts with $Me_3N{\cdot}AlH_3$ by auto-ionization to form [(Me_4cyclam)AlH_2][AlH_4], which adopts an octahedral *trans*-dihydride motif with the larger macrocycle encircling the equatorial plane.[106] The folded ligand conformation of **82** is retained in solution up to 60 °C, as evidenced by ^{1}H NMR spectroscopy showing a

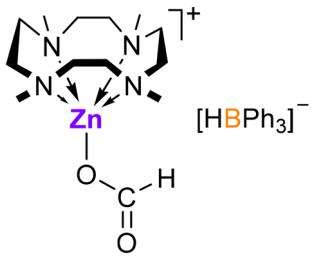

77d

Fig. 10 Zinc formate hydridotriphenylborate **77d**, isolated from the catalytic reaction mixture of CO_2 hydrosilylation by ^{n}BuMe$_2$SiH catalysed by **76a**.

complex array of multiplets corresponding to four pairs of magnetically inequivalent methylene protons, and three methyl environments in a 1 : 2 : 1 integral ratio.

Complex **82** reacts with the weak Brønsted acid [Et$_3$NH][BAr$_4$], yielding the dicationic hydride complexes [(Me$_4$TACD)AlH][BAr$_4$]$_2$ (**83a**, Ar = C$_6$H$_3$-3,5-Me$_2$; **83b**, Ar = C$_6$H$_3$-3,5-(CF$_3$)$_2$; Scheme 33).[28] ^{1}H NMR spectra confirmed that upon removal of one hydride, the macrocycle reverts to a time-averaged C_4-symmetric boat-like conformation. Depending on the counter-ion, the methylene environments in THF-d_8 appear either as a broad, unresolved signal (Ar = C$_6$H$_3$-3,5-Me$_2$), or a well-defined AA′XX′ multiplet (Ar = C$_6$H$_3$-3,5-(CF$_3$)$_2$), suggesting non-negligible ion pairing for the non-fluorinated anion. Compound **83** was also obtained *via* protonolysis of tetrameric aluminium(I) reagent [Cp*Al]$_4$ with [(Me$_4$TACD)H][BAr$_4$] at 70 °C (Scheme 33).[28] Due to the formation of a bis-borate salt, eight equivalents of conjugate acid were required to achieve quantitative conversion to an equimolar mixture of Me$_4$TACD, Cp*H, and **83**. Four equiv. of conjugate acid resulted in the incomplete conversion of the aluminium(I) reagent. The reaction of [(Me$_4$TACD)H][BAr$_4$] with [Cp*Al] leads to protonation of the Cp* ligand, forming Cp*H, and formal two-electron oxidation of Al(I) to Al(III) hydride dication. The reaction likely proceeds *via* protonation of transient [(Me$_4$TACD)Al]$^+$. Isolable mononuclear aluminium(I) cations remain elusive, but the related tetranuclear monovalent cluster cation [(κ^3-Me$_3$TACN)Al{κ^3-(AlCp*)$_3$}][Al(OR^F)$_4$] (OR^F = OC(CF$_3$)$_3$), has been reported.[107]

6.2. Gallium

Unlike Et$_3$N·AlH$_3$, protonolysis of Me$_3$N·GaH$_3$ with equimolar [(Me$_4$TACD)H][B(C$_6$H$_3$-3,5-(CF$_3$)$_2$)$_4$] yielded gallium(I) cation [(Me$_4$TACD)Ga][B(C$_6$H$_3$-3,5-(CF$_3$)$_2$)$_4$] (**84a**, Scheme 34),[28] which likely forms through spontaneous dehydrogenation of a short-lived gallium(III) dihydride cation [(Me$_4$TACD)GaH$_2$]$^+$. The spontaneous dehydrogenation of transient base-free [GaH$_2$]$^+$ has also been described.[108] Consistent with higher stability of the gallium(I) cation compared to its lighter congener, [(Me$_4$TACD)Ga][B(C$_6$H$_3$-3,5-Me$_2$)$_4$] (**84b**) was synthesised *via* protonolysis of [Cp*Ga] with [(Me$_4$TACD)H][B(C$_6$H$_3$-3,5-Me$_2$)$_4$] (Scheme 34).[28] Subsequent protonation of **84b** with [Et$_3$NH][B(C$_6$H$_3$-3,5-Me$_2$)$_4$] provided the dicationic hydride [(Me$_4$TACD)GaH][B(C$_6$H$_3$-3,5-Me$_2$)$_4$]$_2$ (**85**) after release of triethylamine (Scheme 34).[28] This

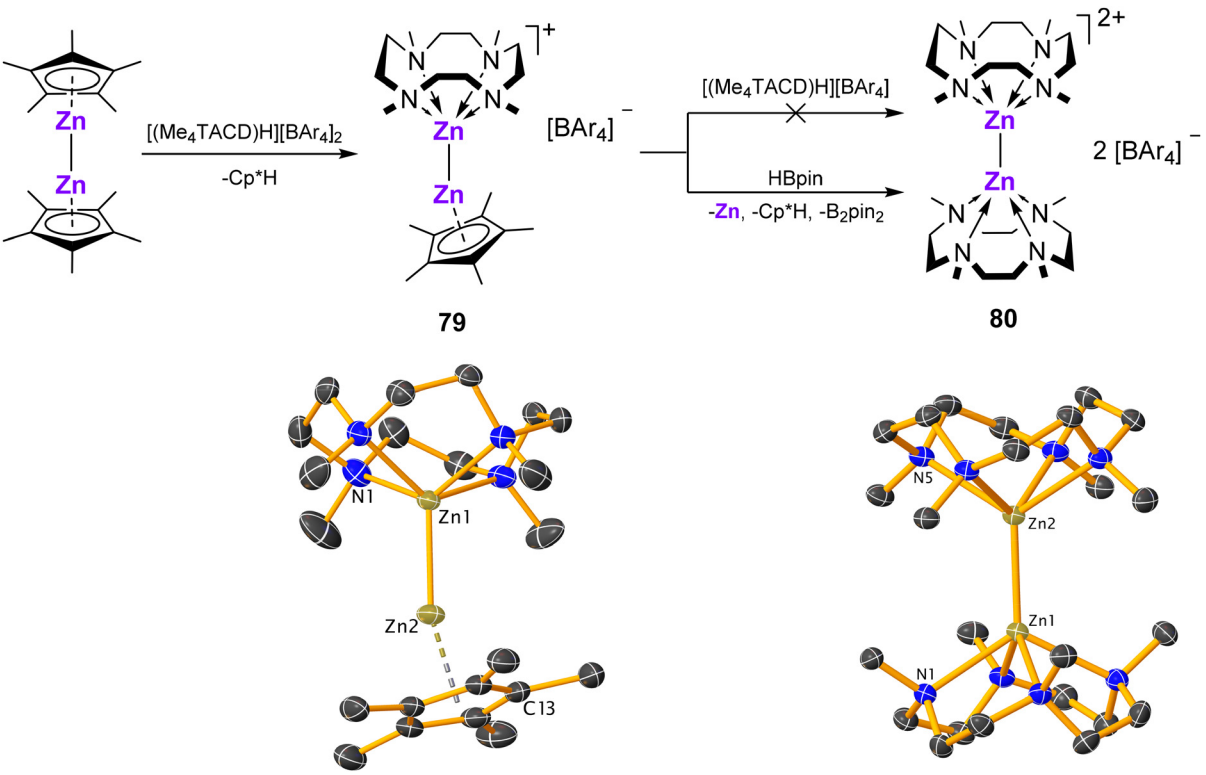

Scheme 30 Synthesis of dizinc(I) complexes **79** and **80** and the (di)cationic part of their crystal structures (H-atoms omitted).[103] Ar = C$_6$H$_3$-3,5-Me$_2$.

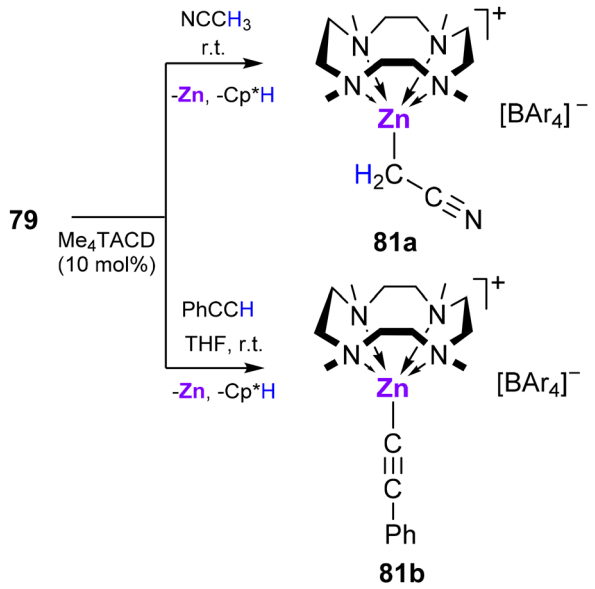

Scheme 31 Reaction of dizinc(I) compound **79** with acetonitrile and with phenylacetylene. Ar = C_6H_3-3,5-Me_2.

observation is consistent with the protonation of proposed $[(Me_4TACD)Al]^+$ in the synthesis of **83** from $[Cp^*Al]_4$. Similar protonation with oxidative addition of H–P bond to $[Ga]^+$ was reported in the reaction of $[(PhF)_nGa][Al(OR^F)_4]$ with $[HPPh_3][Al(OR^F)_4]$ in the presence of triphenylphosphine.[109]

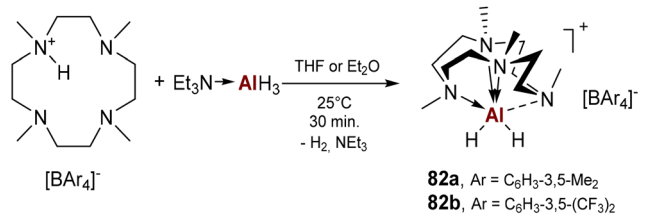

Scheme 32 Synthesis of aluminium hydrides **82a,b**.

The gallium(I) cation **84** forms a charge-separated ion-pair in the solid-state, with a four-coordinate gallium cation and a *pseudo* C_4-symmetric macrocyclic ligand (Fig. 12a).[28] The Ga–N distances are notably shorter than the Ga–O distances in the related $[(12\text{-crown-4})Ga][A]$ (A = $[GaCl_4]^-$, $[B(C_6F_5)_4]^-$)[110] and the metal centre projected less from the basal plane of the four donor atoms. **84** is formally isoelectronic to the germanium dication of $[(Me_4TACD)Ge]X_2$ (**90a**, X = $CF_3SO_3^-$; **90b**, X = $GeCl_3^-$) (*vide infra*), which displays significantly shorter M–N bonds due to the higher nuclear charge of the tetrel dication.[111] The ^{1}H NMR spectrum confirms stable macrocycle coordination, displaying a resolved methylene AA′XX′ spin system at room temperature. The ^{71}Ga NMR spectrum (122 MHz, 298 K) of **84** contains a broad signal at δ −173 ppm (**84b**, acetonitrile-d_3) or −188 ppm (**84a**, THF-d_8), significantly downfield-shifted compared to $Ga[Al(OR^F)_4]$ coordinated by arene or fluoroarene solvents (δ −756 ppm, C_6H_5F; −520 ppm, C_7H_8)[112] or ethers (δ −448 ppm, $Ga[Al(OR^F)_4]$ in THF;[112]

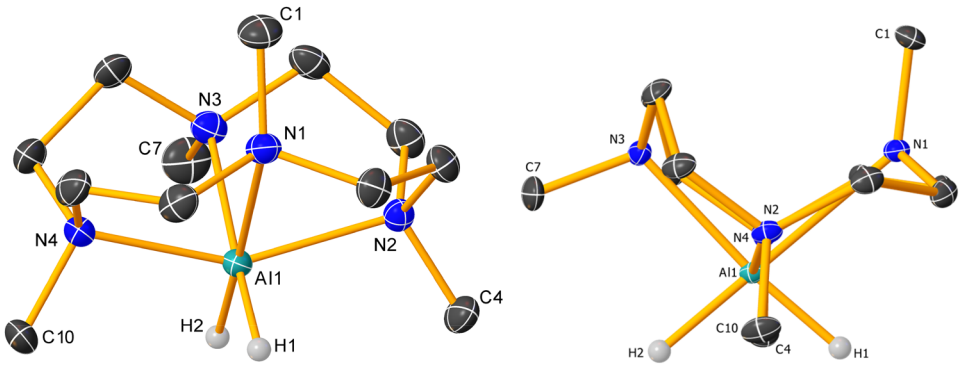

Fig. 11 Crystal structure (H-atoms omitted except H1 and H2) of the cationic part of the of **82b** in oblique (left) and side (right) views.[28]

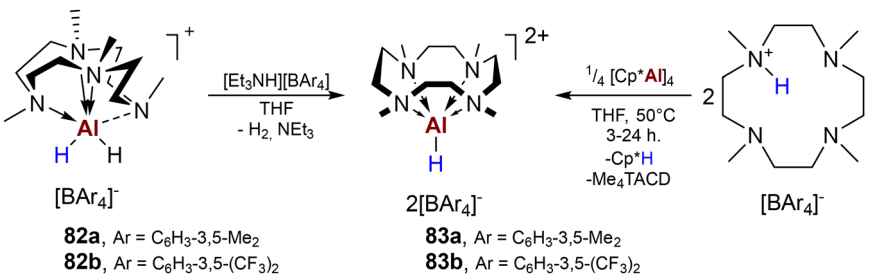

Scheme 33 Synthesis of aluminium hydride dication **83a,b** from protonolysis of **82a,b**, or protonolysis-protonation of $[Cp^*Al]_4$.

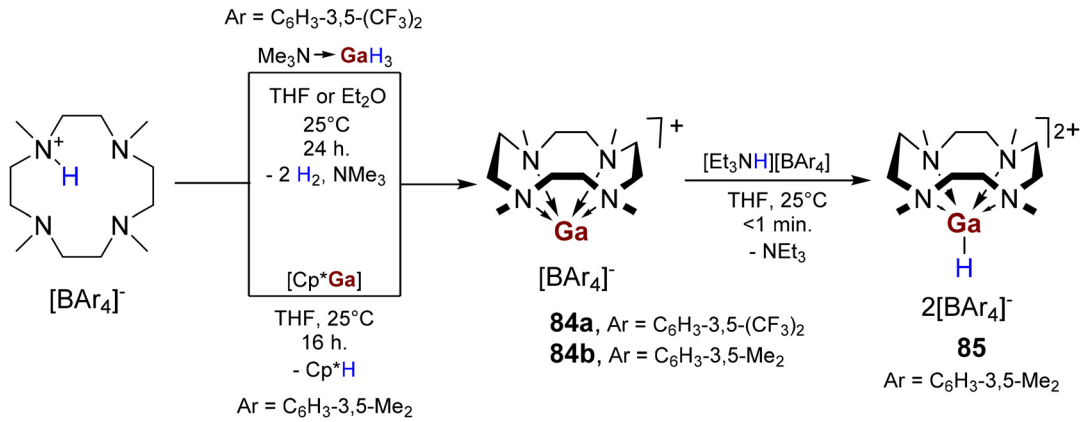

Scheme 34 Synthesis of gallium(I) complexes **84a,b** by protonolysis/dehydrogenation of $Me_3N{\cdot}GaH_3$ or protonolysis of [Cp*Ga]; synthesis of gallium(III) hydride dication **85**.

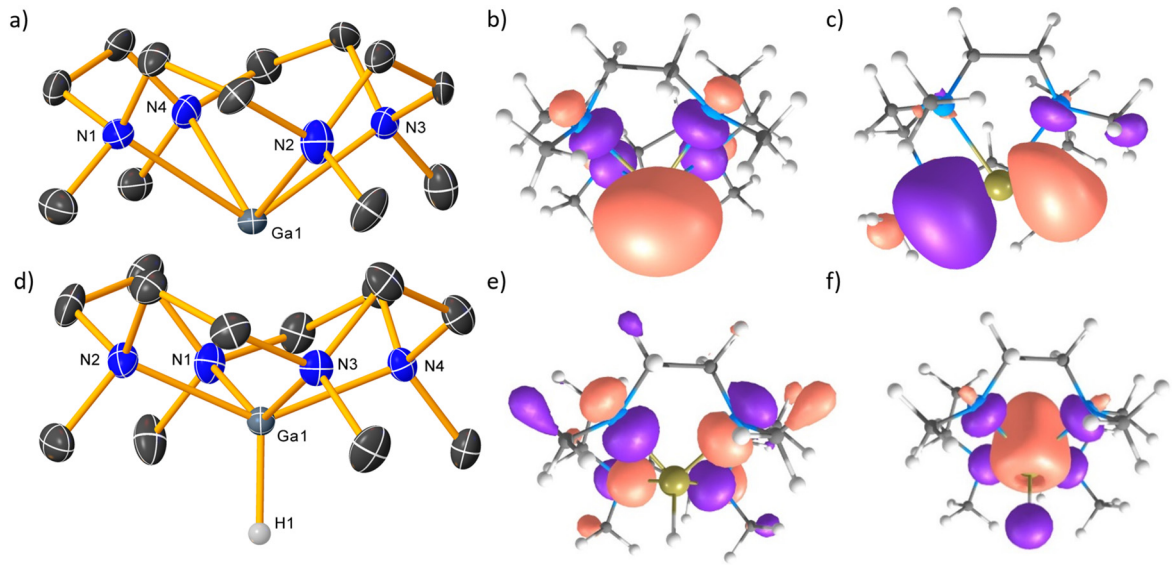

Fig. 12 Crystal structures (H-atoms omitted except for the gallium-bound hydride) of the (di)cationic parts from (a) **84b**; (d) **85**; (b) calculated HOMO, and (c) LUMO of $[(Me_4TACD)Ga]^+$; (e) calculated HOMO, and (f) LUMO of $[(Me_4TACD)GaH]^{2+}$.[28]

−471 ppm, [(12-crown-4)Ga][$GaCl_4$] in toluene).[110] Unlike **84**, the ^{1}H NMR spectrum of $[(Me_3TACN)Ga][Al(OR^F)_4]$[107] shows a single broad singlet for the methylene protons and no detectable ^{71}Ga resonance, suggesting ligand lability. In the crystal structure of **85** (Fig. 12d), the metal centre adopts a square pyramidal geometry (τ_5 = 0.03) with a terminal hydride in the apical position. Reflecting the higher formal oxidation state of +3, the Ga–N bonds are contracted by 0.33 Å, and the metal is pulled much closer to the basal N_4-plane compared to $[(Me_4TACD)Ga]^+$.

The macrocycle size and the nature of donor atoms significantly impact the frontier molecular orbitals of $[(L_n)Ga]^+$. NBO analysis of **84** revealed a HOMO comprising of an out-of-phase combination of a metal-localized lone pair and Ga–N σ-bonds, while the LUMO is an empty 4p orbital (Fig. 12b and c).[28] [(12-crown-4)Ga]$^+$ displayed a similar directional lone pair (HOMO) and p-like LUMO, but the weaker donor properties of the crown-ether resulted in a lower energy HOMO compared to **84**.[110] This suggests reduced reactivity, though no experimental studies have confirmed this effect. The 18-crown-6 complex cation $[(18\text{-crown-6})Ga]^+$ displays a non-directional lone-pair that is only slightly influenced by weakly bound axial solvent molecules, owing to near-coplanarity of the larger macrocycle and metal centre.[113–115] On account of a stabilised *ns*-orbital, "naked" Ga^+ and In^+ cations, ligated by weakly-bound solvent molecules and supported by weakly-coordinating anions react as oxidants and soft Lewis acids.[116–118] Coordination of σ-donor ligands raises the energy of the HOMO, leads to a directional lone-pair, and promotes reductive chemistry but often leads to disproportionation into zero- and trivalent products.[109,110,119–123] The Me_4TACD ligand leads to activation of the 4s orbital, leading to Brønsted basic reactiv-

ity towards $[Et_3NH]^+$ whilst imparting remarkable kinetic stability to the monovalent cation; **84b** is stable up to at least 60 °C in THF. No oxidation event could be determined for **84b** by cyclic voltammetry up to +1.1 V (*vs.* Fc/Fc^+ in acetonitrile), but an irreversible reduction at −2.5 V was tentatively ascribed to the Ga^I/Ga^0 couple.[124] $[Ga(o\text{-}C_6H_4F_2)_n][Al(OR^F)_4]$ gives a scan-rate dependent, partially reversible event at about +3.0 V (Ga^I/Ga^0 *vs.* Fc/Fc^+ in $o\text{-}C_6H_4F_2$).[116]

NBO analysis of **85** showed that its HOMO (Fig. 12e) is primarily composed of Ga–N bonding orbitals, while the LUMO is dominated by the Ga–H σ* antibonding orbital (Fig. 12f).[28] Accordingly, **85** is readily deprotonated at room temperature by IMe_4 (1,3,4,5-tetramethyl-imidazol-ylidene) to return to **84b** and eliminate the imidazolium salt $[IMe_4H][B(3,5\text{-}Me_2\text{-}C_6H_3)_4]$ (Table 2). Treating **85** with equimolar DBU (1,8-diazabicyclo [5.4.0]undec-7-ene, $pK_a(CH_3CN)$ = 24.3) resulted in an equilibrium mixture of conjugate acid–base pairs, which allows estimation of the Brønsted acidity of the gallium hydride as $pK_a(CH_3CN)$ = 24.5 using NMR spectroscopy. Brønsted acidity is appreciable for heavier tetravalent group 14 hydrides,[4,125,126] but the reactivity of group 13 hydrides is normally characterised by strong Brønsted basicity and nucleophilicity. Brønsted acidity is more reminiscent of late-transition metal hydrides.

Unlike isoelectronic $[(Me_4TACD)ZnH]^+$ (**76a,b**), which rapidly inserts CO_2 to give $[(Me_4TACD)Zn(OCHO)]^+$ (**77a,b**), **85** is inert towards CO_2 under ambient conditions. However, **84b** reacts with CO_2 (1 bar) in THF or acetonitrile solution to provide the cationic carbonate complex $[(Me_4TACD)Ga(\kappa_2\text{-}O_2CO)][B(C_6H_3\text{-}3,5\text{-}Me_2)_4]$ (**86**) with CO extrusion (Scheme 35). This reaction likely proceeds *via* a putative oxido gallium cation $[(Me_4TACD)GaO]^+$ through CO extrusion from a transient CO_2 complex $[(Me_4TACD)Ga(CO_2)]^+$. Although $[(Me_4TACD)GaO]^+$ remained elusive, oxidation of **84b** with N_2O in the presence of BPh_3 produces $[(Me_4TACD)GaO{\cdot}BPh_3][B(C_6H_3\text{-}3,5\text{-}Me_2)]$ (**87**), which itself reacts with CO_2 to form a gallium carbonate. **84b** acts as a pre-catalyst for the CO_2 hydroboration to form pinBOC(H)O using HBpin. Although the mechanistic details remain obscure, the formation of a Me_4TACD-containing intermediate with a ^1H NMR typical for gallium(III) (downfield shifted AA′XX′ multiplet) and CO during catalyst activation suggests initial oxidation of **84b** by CO_2.[124]

6.3. Indium and thallium

Similar to the synthesis of **84b**, the heavier monovalent cations $[(Me_4TACD)M][B(C_6H_3\text{-}3,5\text{-}Me_2)_4]$ (**8** M = In; **89**, M = Tl) were prepared by protonolysis of $[Cp^*M]_n$ (M = In, n = 6; M = Tl, n = ∞) with $[(Me_4TACD)H][B(C_6H_3\text{-}3,5\text{-}Me_2)_4]$ (Scheme 36).

The compounds **84**, **88**, and **89** are structurally similar, with metal centre moving further from the basal N_4-plane with increasing atomic number (1.3007(15) Å, **84**; 1.501(2)/1.521(2) Å, **88**; 1.616(5) Å, **89**), with a larger increase in difference between Ga and In (*ca.* 0.2 Å) than between In and Tl (0.1 Å) due to the lanthanide contraction. The crystal structure of **88** is shown in Fig. 13a. Calculated Wiberg Bond Indices (WBIs) for the M–N bonds decreased down group 13, reflecting increased size- and hard–soft mismatch between ligand and metal. Alternative polydentate ligands with softer sulphur, phosphorus, and arsenic donors have been explored for the heavier group 14 elements,[127] and may be well-suited to heavy univalent group 13 cations. Indeed, acyclic monodentate and chelating phosphines have already been employed for univalent gallium and indium cations.[128–132]

The ^1H NMR spectra of **88** and **89** resemble that of **84b** but lack a resolved methylene spin system. Similar signal broadening was observed for increasingly heavy alkali metal silanides, but this was attributed to the lability of the macrocycle.[41] Ligand resonances in the ^1H NMR spectrum of $[(Me_3TACN)Tl][Al(OR^F)_4]$ shift on addition of excess Me_3TACN,[107] indicating labile coordination to soft Tl(I) cation. However, for **88** and **89**, persistent coordination is observed at elevated tempera-

Table 2 Acid–base chemistry of compounds **84a** and **85**. Ar = C_6H_3-3,5-Me_2[28]

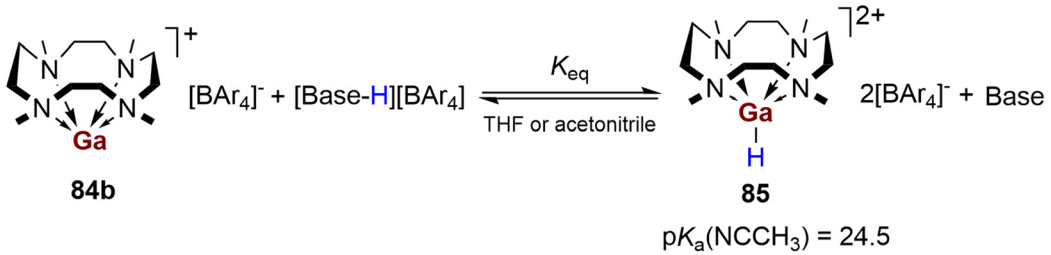

Base	K_{eq}	Solvent
NEt_3	≫1 (quantitative protonation)	THF
	0.77	Acetonitrile
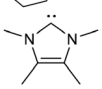	0 (quantitative deprotonation)	THF

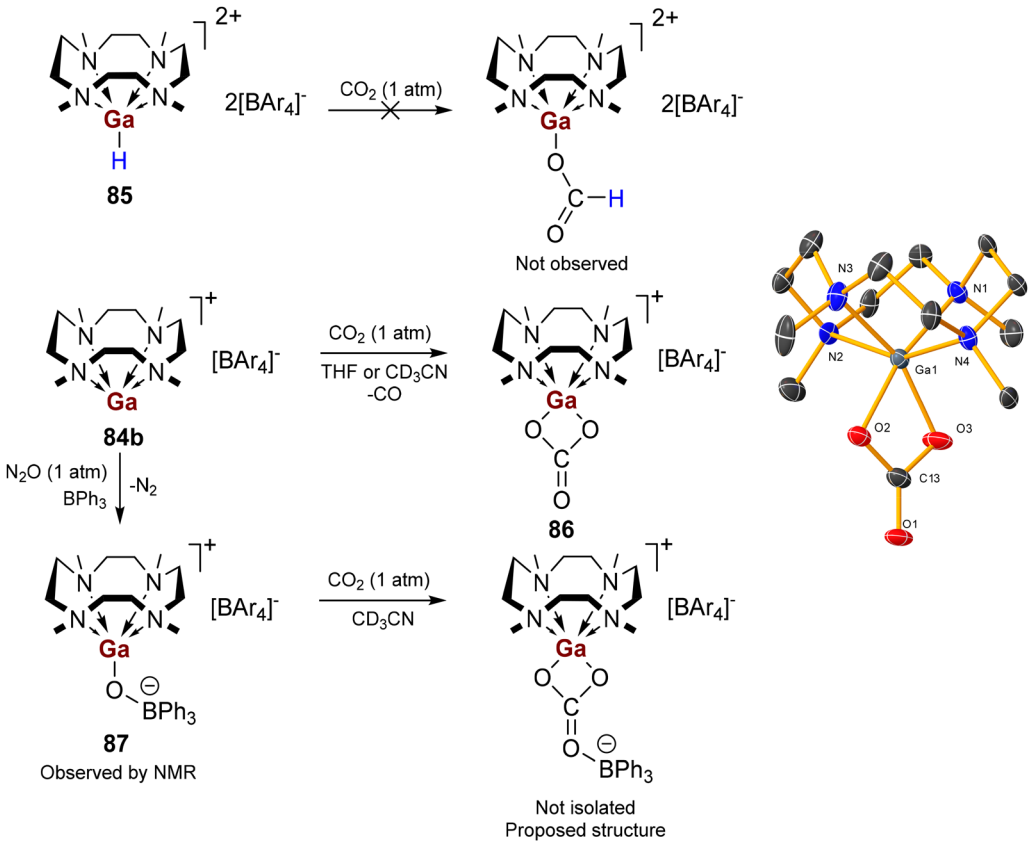

Scheme 35 Reactivity of **84b** and **85** towards CO_2 and N_2O (Ar = C_6H_3-3,5-Me_2). Cationic part of the crystal structure of **86** (H-atoms omitted).[124]

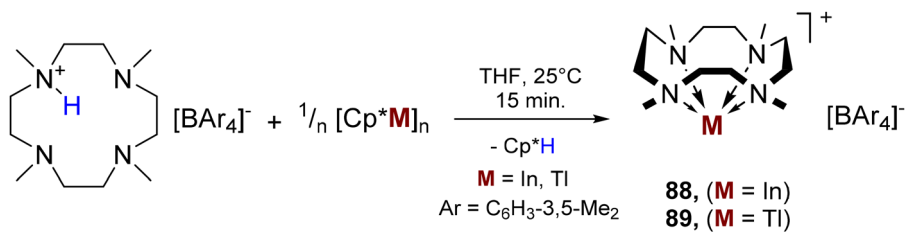

Scheme 36 Synthesis of compounds **88** and **89**.

tures as their methylene resonances split into two unresolved multiplets. At low temperatures, the time-averaged ring-twisting motion is "frozen-out", as indicated by ^{1}H and ^{13}C NMR spectroscopy showing four inequivalent C$\underline{H}_2$ (ABMX spin system) and two inequivalent $\underline{C}H_2$ resonances indicative of a static C_4-symmetric structure (Fig. 13b). The methyl resonances in the ^{1}H and $^{13}C\{^1H\}$ NMR spectra of **89** appeared as doublets at room temperature, due to temperature-dependent *J*-coupling to the ^{205}Tl nucleus (S = 1/2), although the corresponding ^{205}Tl NMR spectrum was not recorded.

Neither **88** nor **89** react with [Et_3NH][B(C_6H_3-3,5-Me_2)$_4$], suggesting that the putative conjugate acids [(Me_4TACD)MH]$^{2+}$ have a pK_a(CH_3CN) ≫ 18.83 and that the univalent cations are less basic than NEt_3. The lone pairs (HOMO) of **88** and **89** were calculated to reside −3.1 kcal mol^{-1} and −23.1 kcal mol^{-1} lower in energy than that of **84**, suggesting [(Me_4TACD)InH]$^{2+}$ to be a synthetically viable target.[28]

7. Group 14 metals

Me_4TACD supported germanium dications [Ge(Me_4TACD)]X_2 (**90a**, X = $CF_3SO_3^-$; **90b**, X = $GeCl_3^-$) were isolated as colourless solids by reacting $GeCl_2$(dioxane) with Me_4TACD in 1 : 1 and 1 : 3 ratios, respectively, in the presence of $Me_3SiO_3SCF_3$ for the former compound (Fig. 14).[111] Both compounds exist as charge-separated ion pairs in the solid state, with no significant cation–anion interactions. Whilst computational studies show that the HOMO of cryptand encapsulated Ge^{2+} dication [(222-crypt)Ge][O_3SCF_3]$_2$ and related [12]-crown-4 sandwich dication [([12]-

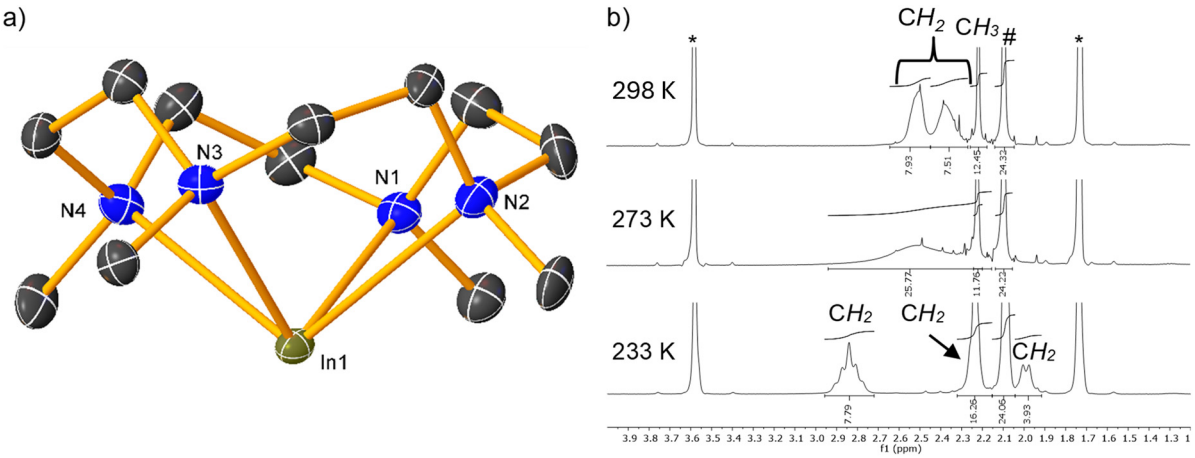

Fig. 13 (a) The crystal structure of the cationic part of **88** (30% level, H-atoms excluded); (b) stacked ^{1}H NMR spectra (400 MHz, THF-d_8 (*)) of **88** at different temperatures (# borate anion).[28]

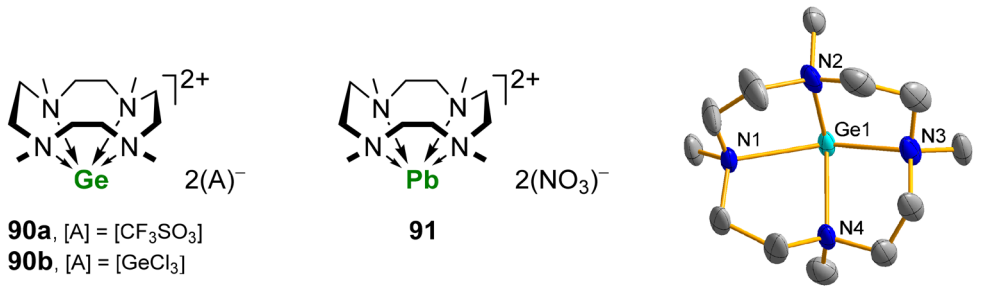

90a, [A] = [CF_3SO_3]
90b, [A] = [$GeCl_3$]
91

Fig. 14 Me_4TACD supported germanium and lead cations **90a,b**, and **91** and the molecular structure of the cationic part of **90a**.[111]

crown-4)$_2$Ge][A]$_2$ ([A] = $GeCl_3$, O_3SCF_3) is an essentially non-directional 4s orbital,[133–135] the stronger coordinating ability of the aza-macrocycle and 'half-sandwich' structure of **90a** and **90b** likely induces some directionality to the 4s lone pair. This effect has been computationally demonstrated for thia-macrocycle complexes of Ge(II),[136] as well as formally isoelectronic **84** and [(12-crown-4)Ga]$^+$.[28,110] Similar to **90**, the 14-membered macrocycle Me_4cyclam provides a charge-separated Ge^{2+} complex [(Me_4cyclam)Ge][$GeCl_3$]$_2$,[134] whilst 12-membered Me_3TACN permits closer interaction with triflate and chloride anions, though bromide remains fully charge separated.[111,134]

The aqueous coordination chemistry of $Pb(NO_3)_2$ has been studied for several aza-macrocyclic ligands, including Me_4TACD, although the resulting lead complex **91** was not structurally characterised.[91,92]

8. Conclusions

The macrocycle Me_4TACD is a versatile neutral ligand that has been employed to stabilise low-nuclearity molecular complexes of various main group metals. Compared to crown ethers, it offers greater robustness against degradation by nucleophilically induced ring-opening and stronger coordination due to the superior σ-donating properties of its amine functionality. Its inherent flexibility allows it to accommodate main group metal centres with remarkably varying ionic radii and reactive bonds such as terminal hydride.[138]

Me_4TACD efficiently encapsulates small metal cations like Li^+, Mg^{2+}, Zn^{2+}, Al^{3+}, and Ga^{3+}, leading to coordinative saturation and limiting reactivity. For example, complexes such as [(Me_4TACD)ZnH]$^+$ (ref. 98) or [(Me_4TACD)$_2$Mg$_2$(μ-H)$_2$]$^{2+}$ (ref. 47) react only with highly activated polar electrophiles, but not with apolar substrates such as H_2 or alkenes. On the other hand, blocking access to the metal can induce unusual chemical reactivity, such as Brønsted acidity of the gallium(III) hydride dication [(Me_4TACD)GaH]$^{2+}$.[28]

Predominantly electrostatic interactions with the larger and less-well encapsulated group 1 cations K–Cs lead to labile coordination of the macrocycle, as indicated by NMR spectra of the triphenylsilanide series [(Me_4TACD)MSiPh$_3$] (M = Li–Cs).[41] Heavier monovalent group 13 cations Ga–Tl are more strongly coordinated, such that the macrocycle engenders a degree of basic and reducing reactivity to the otherwise low-lying 4s lone-pair of Ga^+.[28] The tuning of frontier molecular orbital energies is important in developing transition-metal-like reactivity in low-valent p-block chemistry.

Me_4TACD effectively stabilizes cationic calcium hydride complexes,[137] where it strikes a balance between suppressing aggregation and ligand redistribution (Schlenk equilibria), and

allowing facile access of substrates to the coordinatively unsaturated metal centre. Dimeric calcium hydrides salts $[(Me_4TACD)_2Ca_2(\mu\text{-}H)_2(thf)_x]^{2+}$ and $[(Me_4TACD)_2Ca_2(\mu\text{-}H)_3]^{+}$ serve as active catalysts for alkene hydrogenation and hydrosilylation. However, its ability to stabilise analogous complexes of strontium instead leads to trinuclear hydride $[(Me_4TACD)_3Sr_3(\mu\text{-}H)_4(thf)]^{2+}$ (ref. 80) and di- or trinuclear hydridosilicate species. Dimeric strontium complexes are better stabilised by the larger 15-membered *NNNNN* macrocycle Me_5PACP. Whilst a dimeric barium dihydride dication $[(Me_4TACD)_2Ba_2(\mu\text{-}H)_2(thf)_4]^{2+}$ has been crystallographically characterised, its solution-state chemistry remains unexplored.[87]

Although the elaboration of reaction chemistry and catalysis for very small or very large main group metals may be limited by respective coordinative saturation and lability, as a supporting ligand for reactive cations, Me_4TACD has the potential to offer significant opportunities in the future development of s-block mediated catalysis and low-valent p-block chemistry alongside its more widely established cousins such as Me_3TACN, crown-ethers and acyclic polyamines. We hope this review stimulates future research activity in this regard.

Author contributions

P. G., L. M. and J. O. conceptualised and wrote the manuscript.

Data availability

No primary research results, software or code have been included and no new data were generated or analysed as part of this review.

Conflicts of interest

There are no conflicts to declare.

Acknowledgements

J. O. acknowledges the Deutsche Forschungsgemeinschaft for financial support and all the former coworkers for their hard work. Professor Shigehiro Yamaguchi, Nagoya University, kindly provided facilities at the Research Center for Material Science to complete this manuscript.

References

1 C. M. Cui, H. W. Roesky, H. G. Schmidt, M. Noltemeyer, H. J. Hao and F. Cimpoesu, *Angew. Chem., Int. Ed.*, 2000, **39**, 4274–4276.
2 T. J. Hadlington, M. Hermann, J. Li, G. Frenking and C. Jones, *Angew. Chem., Int. Ed.*, 2013, **52**, 10199–10203.
3 A. S. S. Wilson, M. S. Hill, M. F. Mahon, C. Dinoi and L. Maron, *Science*, 2017, **358**, 1168–1171.
4 S. Wang, T. J. Sherbow, L. A. Berben and P. P. Power, *J. Am. Chem. Soc.*, 2018, **140**, 590–593.
5 J. Hicks, P. Vasko, J. M. Goicoechea and S. Aldridge, *Nature*, 2018, **557**, 92–95.
6 J. Hicks, P. Vasko, J. M. Goicoechea and S. Aldridge, *Angew. Chem., Int. Ed.*, 2021, **60**, 1702–1713.
7 P. M. Chapple, S. Kahlal, J. Cartron, T. Roisnel, V. Dorcet, M. Cordier, J.-Y. Saillard, J.-F. Carpentier and Y. Sarazin, *Angew. Chem., Int. Ed.*, 2020, **59**, 9120–9126.
8 B. Rosch, T. X. Gentner, J. Eyselein, J. Langer, H. Elsen and S. Harder, *Nature*, 2021, **592**, 717–721.
9 R. Mondal, M. J. Evans, T. Rajeshkumar, L. Maron and C. Jones, *Angew. Chem., Int. Ed.*, 2023, **62**, e202308347.
10 F. Dankert, J. Messelberger, U. Authesserre, A. Swain, D. Scheschkewitz, B. Morgenstern and D. Munz, *J. Am. Chem. Soc.*, 2024, **146**, 29630–29636.
11 V. Nesterov, D. Reiter, P. Bag, P. Frisch, R. Holzner, A. Porzelt and S. Inoue, *Chem. Rev.*, 2018, **118**, 9678–9842.
12 M. Arrowsmith, H. Braunschweig, M. A. Celik, T. Dellermann, R. D. Dewhurst, W. C. Ewing, K. Hammond, T. Kramer, I. Krummenacher, J. Mies, K. Radacki and J. K. Schuster, *Nat. Chem.*, 2016, **8**, 890–894.
13 M.-A. Légaré, G. Bélanger-Chabot, R. D. Dewhurst, E. Welz, I. Krummenacher, B. Engels and H. Braunschweig, *Science*, 2018, **359**, 896–900.
14 P. Bag, A. Porzelt, P. J. Altmann and S. Inoue, *J. Am. Chem. Soc.*, 2017, **139**, 14384–14387.
15 Y. Wang and G. H. Robinson, *J. Am. Chem. Soc.*, 2023, **145**, 5592–5612.
16 J. L. Dye, *Philos. Trans. R. Soc., A*, 2015, **373**, 20140174.
17 S. D. Robertson, M. Uzelac and R. E. Mulvey, *Chem. Rev.*, 2019, **119**, 8332–8405.
18 N. Davison, P. G. Waddell and E. Lu, *J. Am. Chem. Soc.*, 2023, **145**, 17007–17012.
19 D. E. Anderson, A. Tortajada and E. Hevia, *Angew. Chem., Int. Ed.*, 2023, **62**, e202218498.
20 D. E. Anderson, A. Tortajada and E. Hevia, *Angew. Chem., Int. Ed.*, 2024, **63**, e202313556.
21 J. Coates, D. Hadi and S. Lincoln, *Aust. J. Chem.*, 1982, **35**, 903–909.
22 J. Cho, R. Sarangi and W. Nam, *Acc. Chem. Res.*, 2012, **45**, 1321–1330.
23 J. E. Richman and T. J. Atkins, *J. Am. Chem. Soc.*, 1974, **96**, 2268–2270.
24 T. J. Atkins, J. E. Richman and W. F. Oettle, *Org. Synth.*, 1978, **58**, 86.
25 J. F. Desreux, E. Merciny and M. F. Loncin, *Inorg. Chem.*, 1981, **20**, 987–991.
26 G. R. Weisman and D. P. Reed, *J. Org. Chem.*, 1996, **61**, 5186–5187.

27 L. E. Lemmerz, D. Mukherjee, T. P. Spaniol, A. Wong, G. Menard, L. Maron and J. Okuda, *Chem. Commun.*, 2019, **55**, 3199–3202.
28 L. J. Morris, P. Ghana, T. Rajeshkumar, A. Carpentier, L. Maron and J. Okuda, *Angew. Chem., Int. Ed.*, 2022, **61**, e202114629.
29 R. Riedel, A. G. Seel, D. Malko, D. P. Miller, B. T. Sperling, H. Choi, T. F. Headen, E. Zurek, A. Porch, A. Kucernak, N. C. Pyper, P. P. Edwards and A. G. M. Barrett, *J. Am. Chem. Soc.*, 2021, **143**, 3934–3943.
30 T. X. Gentner and R. E. Mulvey, *Angew. Chem., Int. Ed.*, 2021, **60**, 9247–9262.
31 D. E. Anderson, A. Tortajada and E. Hevia, *Angew. Chem., Int. Ed.*, 2023, **62**, e202308766.
32 S. Schade and G. Boche, *J. Organomet. Chem.*, 1998, **550**, 359–379.
33 J. Dyke, W. Levason, M. E. Light, D. Pugh, G. Reid, H. Bhakhoa, P. Ramasami and L. Rhyman, *Dalton Trans.*, 2015, **44**, 13853–13866.
34 H. Bhakhoa, L. Rhyman, E. P. Lee, D. K. W. Mok, P. Ramasami and J. M. Dyke, *Dalton Trans.*, 2017, **46**, 15301–15310.
35 H. Osseili, D. Mukherjee, T. P. Spaniol and J. Okuda, *Chem. – Eur. J.*, 2017, **23**, 14292–14298.
36 D. Mukherjee, H. Osseili, T. P. Spaniol and J. Okuda, *J. Am. Chem. Soc.*, 2016, **138**, 10790–10793.
37 R. Janot, W. S. Tang, D. Clémençon and J. N. Chotard, *J. Mater. Chem.*, 2016, **4**, 19045–19052.
38 W. S. Tang, J.-N. Chotard, P. Raybaud and R. Janot, *J. Phys. Chem. C*, 2014, **118**, 3409–3419.
39 W. S. Tang, J.-N. Chotard, P. Raybaud and R. Janot, *Phys. Chem. Chem. Phys.*, 2012, **14**, 13319–13324.
40 J.-N. Chotard, W. S. Tang, P. Raybaud and R. Janot, *Chem. – Eur. J.*, 2011, **17**, 12302–12309.
41 D. Schuhknecht, V. Leich, T. P. Spaniol, I. Douair, L. Maron and J. Okuda, *Chem. – Eur. J.*, 2020, **26**, 2821–2825.
42 D. Schuhknecht, Doctoral Thesis, RWTH Aachen University, 2020.
43 H. Osseili, K.-N. Truong, T. P. Spaniol, D. Mukherjee, U. Englert and J. Okuda, *Chem. – Eur. J.*, 2017, **23**, 17213–17216.
44 D. Schuhknecht, K.-N. Truong, T. P. Spaniol, L. Maron and J. Okuda, *Chem. Commun.*, 2018, **54**, 11280–11283.
45 S. Arndt, M. U. Kramer, W. Fegler, Y. Nakajima, I. Del Rosal, R. Poteau, T. P. Spaniol, L. Maron and J. Okuda, *Organometallics*, 2015, **34**, 3739–3747.
46 W. Fegler, A. Venugopal, T. P. Spaniol, L. Maron and J. Okuda, *Angew. Chem., Int. Ed.*, 2013, **52**, 7976–7980.
47 L. E. Lemmerz, D. Mukherjee, T. P. Spaniol, A. Wong, G. Ménard, L. Maron and J. Okuda, *Chem. Commun.*, 2019, **55**, 3199–3202.
48 L. E. Lemmerz, A. Wong, G. Ménard, T. P. Spaniol and J. Okuda, *Polyhedron*, 2020, **178**, 114331.
49 D. Schuhknecht, C. Lhotzky, T. P. Spaniol, L. Maron and J. Okuda, *Angew. Chem., Int. Ed.*, 2017, **56**, 12367–12371.
50 V. Leich, T. P. Spaniol, L. Maron and J. Okuda, *Angew. Chem., Int. Ed.*, 2016, **55**, 4794–4797.
51 S. Harder, S. Müller and E. Hübner, *Organometallics*, 2004, **23**, 178–183.
52 T. Höllerhage, T. P. Spaniol, A. Carpentier, L. Maron and J. Okuda, *Inorg. Chem.*, 2022, **61**, 3309–3316.
53 T. Höllerhage, D. Schuhknecht, A. Mistry, T. P. Spaniol, Y. Yang, L. Maron and J. Okuda, *Chem. – Eur. J.*, 2021, **27**, 3002–3007.
54 D. Schuhknecht, T. P. Spaniol, L. Maron and J. Okuda, *Angew. Chem., Int. Ed.*, 2020, **59**, 310–314.
55 D. Schuhknecht, T. P. Spaniol, I. Douair, L. Maron and J. Okuda, *Chem. Commun.*, 2019, **55**, 14837–14839.
56 J. Martin, J. Eyselein, J. Langer, H. Elsen and S. Harder, *Chem. Commun.*, 2020, **56**, 9178–9181.
57 B. Maitland, M. Wiesinger, J. Langer, G. Ballmann, J. Pahl, H. Elsen, C. Färber and S. Harder, *Angew. Chem., Int. Ed.*, 2017, **56**, 11880–11884.
58 J. Martin, C. Knüpfer, J. Eyselein, C. Färber, S. Grams, J. Langer, K. Thum, M. Wiesinger and S. Harder, *Angew. Chem., Int. Ed.*, 2020, **59**, 9102–9112.
59 H. Bauer, M. Alonso, C. Fischer, B. Rösch, H. Elsen and S. Harder, *Angew. Chem., Int. Ed.*, 2018, **57**, 15177–15182.
60 E. Le Coz, Z. Zhang, T. Roisnel, L. Cavallo, L. Falivene, J.-F. Carpentier and Y. Sarazin, *Chem. – Eur. J.*, 2020, **26**, 3535–3544.
61 C. Bellini, V. Dorcet, J.-F. Carpentier, S. Tobisch and Y. Sarazin, *Chem. – Eur. J.*, 2016, **22**, 4564–4583.
62 C. Bellini, J.-F. Carpentier, S. Tobisch and Y. Sarazin, *Angew. Chem., Int. Ed.*, 2015, **54**, 7679–7683.
63 T. Höllerhage, P. Ghana, T. P. Spaniol, A. Carpentier, L. Maron, U. Englert and J. Okuda, *Angew. Chem., Int. Ed.*, 2022, **61**, e202115379.
64 R. Huo, A. J. Armstrong, G. R. Nelmes, D. J. Lawes, A. J. Edwards, C. L. McMullin and J. Hicks, *Chem. – Eur. J.*, 2024, **30**, e202400662.
65 D. Schuhknecht, T. P. Spaniol, Y. Yang, L. Maron and J. Okuda, *Inorg. Chem.*, 2020, **59**, 9406–9415.
66 R. Lalrempuia, C. E. Kefalidis, S. J. Bonyhady, B. Schwarze, L. Maron, A. Stasch and C. Jones, *J. Am. Chem. Soc.*, 2015, **137**, 8944–8947.
67 M. D. Anker, C. E. Kefalidis, Y. Yang, J. Fang, M. S. Hill, M. F. Mahon and L. Maron, *J. Am. Chem. Soc.*, 2017, **139**, 10036–10054.
68 M. D. Anker, M. S. Hill, J. P. Lowe and M. F. Mahon, *Angew. Chem., Int. Ed.*, 2015, **54**, 10009–10011.
69 B. Rösch, T. X. Gentner, H. Elsen, C. A. Fischer, J. Langer, M. Wiesinger and S. Harder, *Angew. Chem., Int. Ed.*, 2019, **58**, 5396–5401.
70 Z.-W. Qu, H. Zhu and S. Grimme, *Chem. – Eur. J.*, 2023, **29**, e202202602.
71 X. Shi, G. Qin, Y. Wang, L. Zhao, Z. Liu and J. Cheng, *Angew. Chem., Int. Ed.*, 2019, **58**, 4356–4360.
72 Y. Liang, U. K. Das, J. Luo, Y. Diskin-Posner, L. Avram and D. Milstein, *J. Am. Chem. Soc.*, 2022, **144**, 19115–19126.
73 Y. Liang, I. Efremenko, Y. Diskin-Posner, L. Avram and D. Milstein, *Angew. Chem., Int. Ed.*, 2024, **63**, e202401702.

74 J. Spielmann, F. Buch and S. Harder, *Angew. Chem., Int. Ed.*, 2008, **47**, 9434–9438.
75 A. S. S. Wilson, C. Dinoi, M. S. Hill, M. F. Mahon and L. Maron, *Angew. Chem., Int. Ed.*, 2018, **57**, 15500–15504.
76 H. Bauer, K. Thum, M. Alonso, C. Fischer and S. Harder, *Angew. Chem., Int. Ed.*, 2019, **58**, 4248–4253.
77 H. Bauer, M. Alonso, C. Färber, H. Elsen, J. Pahl, A. Causero, G. Ballmann, F. De Proft and S. Harder, *Nat. Catal.*, 2018, **1**, 40–47.
78 A. S. S. Wilson, M. S. Hill and M. F. Mahon, *Organometallics*, 2019, **38**, 351–360.
79 L. Garcia, C. Dinoi, M. F. Mahon, L. Maron and M. S. Hill, *Chem. Sci.*, 2019, **10**, 8108–8118.
80 T. Höllerhage, A. Carpentier, T. P. Spaniol, L. Maron, U. Englert and J. Okuda, *Chem. Commun.*, 2021, **57**, 6316–6319.
81 C. N. de Bruin-Dickason, T. Sutcliffe, C. Alvarez Lamsfus, G. B. Deacon, L. Maron and C. Jones, *Chem. Commun.*, 2018, **54**, 786–789.
82 D. Mukherjee, T. Höllerhage, V. Leich, T. P. Spaniol, U. Englert, L. Maron and J. Okuda, *J. Am. Chem. Soc.*, 2018, **140**, 3403–3411.
83 X. Sun and A. Hinz, *Inorg. Chem.*, 2023, **62**, 10249–10255.
84 M. C. Lipke and T. D. Tilley, *Angew. Chem., Int. Ed.*, 2012, **51**, 11115–11121.
85 M. S. Hill, M. F. Mahon, A. S. S. Wilson, C. Dinoi, L. Maron and E. Richards, *Chem. Commun.*, 2019, **55**, 5732–5735.
86 P. M. Chapple and Y. Sarazin, *Eur. J. Inorg. Chem.*, 2020, 3321–3346.
87 T. Höllerhage, T. P. Spaniol, U. Englert and J. Okuda, *Z. Anorg. Allg. Chem.*, 2023, **649**, e202200315.
88 M. Wiesinger, B. Maitland, C. Färber, G. Ballmann, C. Fischer, H. Elsen and S. Harder, *Angew. Chem., Int. Ed.*, 2017, **56**, 16654–16659.
89 X. Shi, C. Hou, C. Zhou, Y. Song and J. Cheng, *Angew. Chem., Int. Ed.*, 2017, **56**, 16650–16653.
90 T. Höllerhage, T. P. Spaniol, U. Englert and J. Okuda, *Inorg. Chim. Acta*, 2022, **543**, 121198.
91 R. D. Hancock, P. W. Wade, M. P. Ngwenya, A. S. De Sousa and K. V. Damu, *Inorg. Chem.*, 1990, **29**, 1968–1974.
92 M. T. S. Amorim, S. Chaves, R. Delgado and J. J. R. F. da Silva, *J. Chem. Soc., Dalton Trans.*, 1991, 3065–3072.
93 R. D. Shannon, *Acta Crystallogr., Sect. A: Found. Adv.*, 1976, **32**, 751–767.
94 D. Mukherjee, A. K. Wiegand, T. P. Spaniol and J. Okuda, *Dalton Trans.*, 2017, **46**, 6183–6186.
95 H. H. Cui, W. Lv, W. Tong, X. T. Chen and Z. L. Xue, *Eur. J. Inorg. Chem.*, 2019, 4653–4659.
96 H. H. Cui, J. Wang, X. T. Chen and Z. L. Xue, *Chem. Commun.*, 2017, **53**, 9304–9307.
97 M. X. Xu, Z. Liu, B. W. Dong, H. H. Cui, Y. X. Wang, J. Su, Z. X. Wang, Y. Song, X. T. Chen, S. D. Jiang and S. Gao, *Inorg. Chem.*, 2019, **58**, 2330–2335.
98 F. Ritter, L. J. Morris, K. N. McCabe, T. P. Spaniol, L. Maron and J. Okuda, *Inorg. Chem.*, 2021, **60**, 15583–15592.
99 F. Ritter, Doctoral Thesis, RWTH Aachen University, 2021.
100 D. Mukherjee, S. Shirase, T. P. Spaniol, K. Mashima and J. Okuda, *Chem. Commun.*, 2016, **52**, 13155–13158.
101 F. Ritter, T. P. Spaniol, I. Douair, L. Maron and J. Okuda, *Angew. Chem., Int. Ed.*, 2020, **59**, 23335–23342.
102 R. Chambenahalli, R. M. Bhargav, K. N. McCabe, A. P. Andrews, F. Ritter, J. Okuda, L. Maron and A. Venugopal, *Chem. – Eur. J.*, 2021, **27**, 7391–7401.
103 P. Mahawar, T. Rajeshkumar, T. P. Spaniol, L. Maron and J. Okuda, *Chem. Commun.*, 2024, **60**, 11359–11362.
104 S. Schulz, D. Schuchmann, I. Krossing, D. Himmel, D. Bläser and R. Boese, *Angew. Chem., Int. Ed.*, 2009, **48**, 5748–5751.
105 H. Banh, C. Gemel, R. W. Seidel and R. A. Fischer, *Chem. Commun.*, 2015, **51**, 2170–2172.
106 J. L. Atwood, K. D. Robinson, C. Jones and C. L. Raston, *J. Chem. Soc., Chem. Commun.*, 1991, 1697–1699.
107 P. Dabringhaus and I. Krossing, *Chem. Sci.*, 2022, **13**, 12078–12086.
108 R. J. Wehmschulte, R. Peverati and D. R. Powell, *Inorg. Chem.*, 2019, **58**, 12441–12445.
109 M. Schorpp, R. Tamim and I. Krossing, *Dalton Trans.*, 2021, **50**, 15103–15110.
110 J. L. Bourque, R. A. Nanni, M. C. Biesinger and K. M. Baines, *Inorg. Chem.*, 2021, **60**, 14713–14720.
111 M. Everett, A. Jolleys, W. Levason, M. E. Light, D. Pugh and G. Reid, *Dalton Trans.*, 2015, **44**, 20898–20905.
112 J. M. Slattery, A. Higelin, T. Bayer and I. Krossing, *Angew. Chem., Int. Ed.*, 2010, **49**, 3228–3231.
113 J. T. Boronski, M. P. Stevens, B. van Ijzendoorn, A. C. Whitwood and J. M. Slattery, *Angew. Chem., Int. Ed.*, 2021, **60**, 1567–1572.
114 C. G. Andrews and C. L. B. Macdonald, *Angew. Chem., Int. Ed.*, 2005, **44**, 7453–7456.
115 A. Higelin, C. Haber, S. Meier and I. Krossing, *Dalton Trans.*, 2012, **41**, 12011–12015.
116 A. Barthelemy, K. Glootz, H. Scherer, A. Hanske and I. Krossing, *Chem. Sci.*, 2022, **13**, 439–453.
117 Z. L. Li, G. Thiery, M. R. Lichtenthaler, R. Guillot, I. Krossing, V. Gandon and C. Bour, *Adv. Synth. Catal.*, 2018, **360**, 544–549.
118 Z. L. Li, S. W. Yang, G. Thiery, V. Gandon and C. Bour, *J. Org. Chem.*, 2020, **85**, 12947–12959.
119 P. Dabringhaus, A. Barthelemy and I. Krossing, *Z. Anorg. Allg. Chem.*, 2021, **647**, 1660–1673.
120 K. Glootz, D. Kratzert, D. Himmel, A. Kastro, Z. Yassine, T. Findeisen and I. Krossing, *Angew. Chem., Int. Ed.*, 2018, **57**, 14203–14206.
121 M. R. Lichtenthaler, F. Stahl, D. Kratzert, L. Heidinger, E. Schleicher, J. Hamann, D. Himmel, S. Weber and I. Krossing, *Nat. Commun.*, 2015, **6**, 8288.
122 C. Dohmeier, D. Loos and H. Schnockel, *Angew. Chem., Int. Ed. Engl.*, 1996, **35**, 129–149.
123 J. C. Beamish, A. Boardman and I. J. Worrall, *Polyhedron*, 1991, **10**, 95–99.
124 L. J. Morris, P. Mahawar and J. Okuda, *J. Org. Chem.*, 2022, **80**, 5090–5096.

125 M. Auer, F. Diab, K. Eichele, H. Schubert and L. Wesemann, *Dalton Trans.*, 2022, **51**, 5950–5961.
126 J. J. Maudrich, F. Diab, S. Weiss, M. Widemann, T. Dema, H. Schubert, K. M. Krebs, K. Eichele and L. Wesemann, *Inorg. Chem.*, 2019, **58**, 15758–15768.
127 K. R. Cairns, R. P. King, R. D. Bannister, W. Levason and G. Reid, *Dalton Trans.*, 2023, **52**, 2293–2308.
128 A. Higelin, U. Sachs, S. Keller and I. Krossing, *Chem. – Eur. J.*, 2012, **18**, 10029–10034.
129 A. Barthélemy, H. Scherer, H. Weller and I. Krossing, *Chem. Commun.*, 2023, **59**, 1353–1356.
130 A. Barthélemy, H. Scherer, M. Daub, A. Bugnet and I. Krossing, *Angew. Chem., Int. Ed.*, 2023, **62**, e202311648.
131 A. Barthélemy, H. Scherer and I. Krossing, *Chem. – Eur. J.*, 2022, **28**, e202201369.
132 P. Dabringhaus, H. Scherer and I. Krossing, *Nat. Synth.*, 2024, **3**, 732–743.
133 P. A. Rupar, V. N. Staroverov and K. M. Baines, *Science*, 2008, **322**, 1360–1363.
134 F. Cheng, A. L. Hector, W. Levason, G. Reid, M. Webster and W. Zhang, *Angew. Chem., Int. Ed.*, 2009, **48**, 5152–5154.
135 P. A. Rupar, R. Bandyopadhyay, B. F. T. Cooper, M. R. Stinchcombe, P. J. Ragogna, C. L. B. Macdonald and K. M. Baines, *Angew. Chem., Int. Ed.*, 2009, **48**, 5155–5158.
136 R. P. King, J. M. Herniman, W. Levason and G. Reid, *Inorg. Chem.*, 2023, **62**, 853–862.
137 D. Mukherjee, D. Schuhknecht and J. Okuda, *Angew. Chem., Int. Ed.*, 2018, **57**, 9590–9602.
138 M. M. D. Roy, A. A. Omana, A. A. S. Wilson, M. S. Hill, S. Aldridge and E. Rivard, *Chem. Rev.*, 2021, **121**, 12784–12965.